Online Voltage Stability Prediction and Control Using Computational Intelligence Technique

by

Qun Debbie Zhou

A thesis submitted to the Faculty of Graduate Studies of

in partial fulfillment of the requirements of the degree of

Doctor of Philosophy

The Department of Electrical and Computer Engineering

The University of Manitoba

Winnipeg, Manitoba, Canada

To my daughter and parents.

Abstract

Voltage instability has been reported as the main cause for many blackouts and become a major concern in power systems. This thesis deals with two specific areas of voltage stability in on-line power system security assessment: small-disturbance (long-term) and large-disturbance (short-term) voltage stability assessment. For each category of voltage stability, both voltage stability analysis and controls are studied. The overall objective is to use the learning capabilities of computational intelligence technology to build up the comprehensive on-line power system security assessment and control strategy as well as to enhance the speed and efficiency of the process with minimal human intervention.

The voltage stability problems are quantified by voltage stability indices which measure the system for the closeness of current operating point to voltage instability. The indices are different for small-disturbance and large-disturbance voltage stability assessment. Conventional approaches, such as continuation power flow or time-domain simulation, can be used to obtain voltage stability indices. However, these conventional approaches are limited by computation time that is significant for on-line computation. The Artificial Neural Network (ANN) approach is proposed to compute voltage stability indices as an alternative to the conventional approaches. The proposed ANN algorithm is used to estimate voltage stability indices under both normal and contingency operating conditions.

The input variables of ANN are obtained in real-time by an on-line measurement system, i.e. Phasor Measurement Units (PMU). This thesis will propose a suboptimal approach for seeking the best locations for PMUs from a voltage stability viewpoint.

The ANN-based method is not limited to compute voltage stability indices but can also be extended to determine suitable control actions. In this thesis, it is demonstrated that long-term voltage stability can be improved by re-scheduling real power generation based on the sensitivity of the ANN approach.

Load shedding is one of the most effective approaches against short-term voltage instability under large disturbances. The basic requirement of load shedding for recovering voltage stability is to seek an optimal solution for when, where, and how much load should be shed. Two simulation based approaches are proposed for load shedding to prevent voltage instability or collapse. In the first approach, a particle swarm optimization (PSO) algorithm is implemented which performs an efficient search for a global optimization. In the second approach, a sensitivity based algorithm is conducted through the sensitivity index of the load shedding buses. The proposed approaches are presented using the New England 39-bus test system. The second approach is found to be significantly faster than the first one and results in considerable savings in computer resources for the test system with which the methods were compared.

Acknowledgements

The successful completion of this research would not have been possible without the consistent guidance of my supervisor, Dr. Udaya D. Annakkage. His perpetual energy and enthusiasm for my work motivated me throughout the course of this work. I also thank Dr. Athula D. Rajapakse, a member of the supervisory committee, who provided valuable advices and was always accessible and willing to help with my research.

I greatly appreciate the team work environment for the project "Application of Wide Area Measurements for Protection and Control". Dr. Ioni Fernando and Mr. Todd E. Buchholzer from Manitoba Hydro, my external contacts, provided thoughtful suggestions and their professional experience broadened my perspective on the practical aspects in the power industry. I also thank student team members Francisco Gomez Lezama, Kasun Nanayakkara and Jeffery Zimmer for their contributed efforts to the project. This team inspired me throughout the Ph.D research program. I would like to acknowledge Manitoba Hydro, Canada and Natural Sciences and Engineering Research Council of Canada (NSERC) for the financial support they provided for my research.

My most sincere thanks to the technical staff at the Department of Electrical and Computer Engineering, especially Mr. Erwin Dirks who always offered timely software and computer resource assistance. I would also like to express my special gratitude to Dr. Lei Wang and Xi Lin from Power Tech Labs, British Columbia for their swift response for technical support of the software $DSATools^{TM}$.

A very special word of gratitude to Dr. Yi Zhang who has been a constant source of

encouragement during my Ph.D study. I also wish to thank Dr. Bathiya Jayasekara, Dr. Chandana Karawita, Yuefeng Liang, Shan Jiang, Hui Ding for sharing literature, as well as for their emotional support, invaluable assistance, and caring.

Last but not least, my deepest love and gratitude to my beloved daughter and parents. Whenever I encountered difficulties with my research, my daughter's lovely smile and joyful voice were the best comfort. My parents provided support, patience, and encouragement. It is to them I dedicate this thesis for their endless and unconditional love.

Qun Debbie Zhou

December 2009

Table of Contents

List of Figures

List of Tables

Chapter 1

Introduction

This chapter briefly reviews some concepts of power systems and background introduction that are related to this thesis. The content includes the structure of on-line power system security assessment, operating states, power system stability and control, on-line measurement, and computational intelligence techniques. In addition, the motivation, objectives for the research, and the organization of the thesis are also presented.

1.1 On-line Power System Security Assessment

Power systems often encompass large geographical areas. The interconnected power networks are therefore very large, with tens of thousands of nodes, branches and generating units. Facing with such a complex system whose operating point changes frequently, system operation has become ever more challenging. Although a power system is designed to operate safely under various circumstances, it is inevitable that the system will experience insecure states. Recently, there have been a number of to-

tal and partial blackouts in many countries around the world [1, 2, 3, 4]. These events have highlighted the importance of the secure and reliable operation of power systems.

Traditionally, system operators have depended heavily on the results of operational planning studies conducted off-line to guide them through day-to-day operations [5]. In today's complex systems, total reliance on this off-line approach has become impractical. This has raised the requirement for on-line approaches in power system security assessments. The real-time assessment of the system's security and reliability levels, especially under unforeseen contingencies, is known as on-line power system security assessment [6]. In order to quantify the impact of various contingencies on the security of a given power system and execute preventive and corrective control actions, the on-line approaches require the data from a centralized control center. SCADA system complemented with PMU wide area measurement system can provide these necessary data. Figure 1.1 illustrates an example of the on-line power system security assessment architecture [5].

The basic functions of an on-line dynamic security assessment system include the following parts:

1. Take a snapshot of the power system operating point using an on-line measuring system. This information includes instant breaker status.

2. Using the above information, assemble the system model relevant to the present status.

3. Perform the security assessment.

4. Report and visualize the result of assessment.

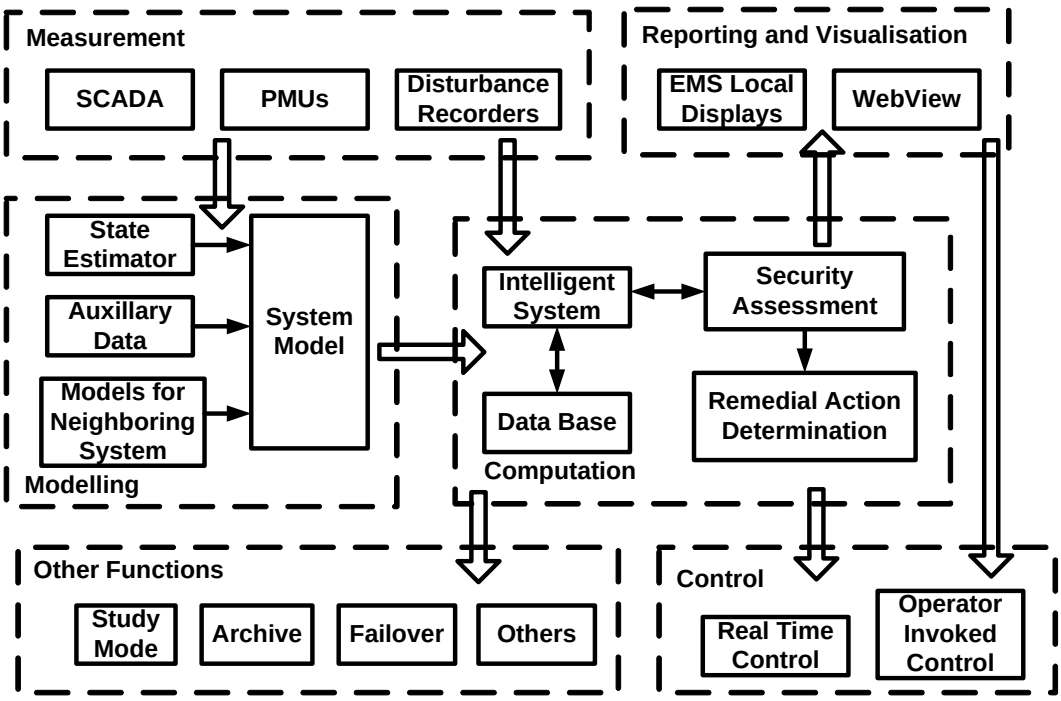

Figure 1.1: Components of on-line dynamic security assessment

5. Raise alarms when security issues are detected.

6. Identify security issues and make recommendations on control actions to alleviate them.

The main components are denoted by boxes drawn with dashed lines in Figure 1.1. Four main components are considered and studied in this thesis: measurement, modelling, computation, and control. The key parts of the main research focus of this thesis are computation and control.

1.2 Power System Operating States

Power system security assessment is an analysis performed to determine whether, and to what extent, a power system is reasonably safe from serious interference to its

operation [7]. In the basic framework of security established in 1967 by DyLiacco [8], the concept of system operating states was defined into three states: normal , emergency, and restorative states. In 1978 Fink and Carlsen [9] extended the classification of states to: normal, alert, emergency, in extremis, and restorative. Figure 1.2 shows the five-state classification of power system operating states [10].

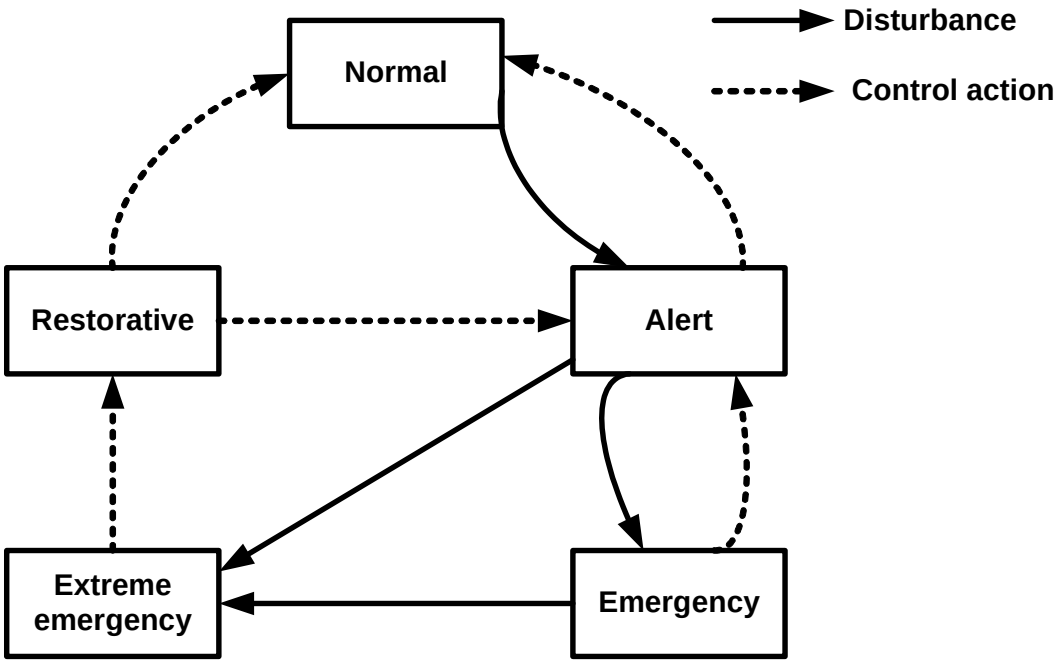

Figure 1.2: Power system operating states

In the normal state, a power system operates with an adequate security margin after being subjected to the contingencies. All the important quantities for power system operation are within their normal range.

The alert state arises when the security level falls below a certain limit of adequacy. In this state all the constraints are still satisfied; however, system security has weakened, so that a further increase in demand or another contingency may threaten the

power system operation and transit alert to a state of emergency or of extreme emergency. When the system is in the alert state, preventive actions, such as generation rescheduling or increased reserve, can be undertaken to restore the system to its normal state.

In the emergency state, the power system is still intact but the violation of constraints is more severe. The emergency state usually follows the alert state when preventive actions have not been undertaken or have not been successful. When a system is in the emergency state, it is necessary to undertake effective protective and corrective actions to restore it to the alert state or normal state. Some typical protective and corrective actions are fault clearing, excitation control, generation tripping, and load curtailment.

A power system can transit to the extreme emergency state from the emergency state if the above control actions are not applied or are ineffective. In this state, the operating constraints are violated and the system security does not exist. Control actions, such as load shedding, are aimed at saving as much of the system as possible from a widespread blackout.

To return a power system from an extreme emergency state to an alert or normal state, a restorative state is necessary in which power system operators perform control actions in order to reconnect all the facilities and restore system loads. The system can reach either the normal or the alter state, depending on the conditions.

1.3 Power System Stability Classification

An important part of power system security is the system's ability to withstand the effects of contingencies. Hence, power system stability has been acknowledged as an important problem in electric power system operation. Historically, transient instability has been the dominant stability problem on most systems, and has been the focus of much of the industry's attention concerning system stability. Due to the declining investments in new generation and transmission facilities, the power system has become stressed. In addition, new technologies and controls are used in highly stressed operating conditions, and different forms of system instability have emerged [11]. Figure 1.3, reproduced from [11], gives an overall picture of the power system stability problem.

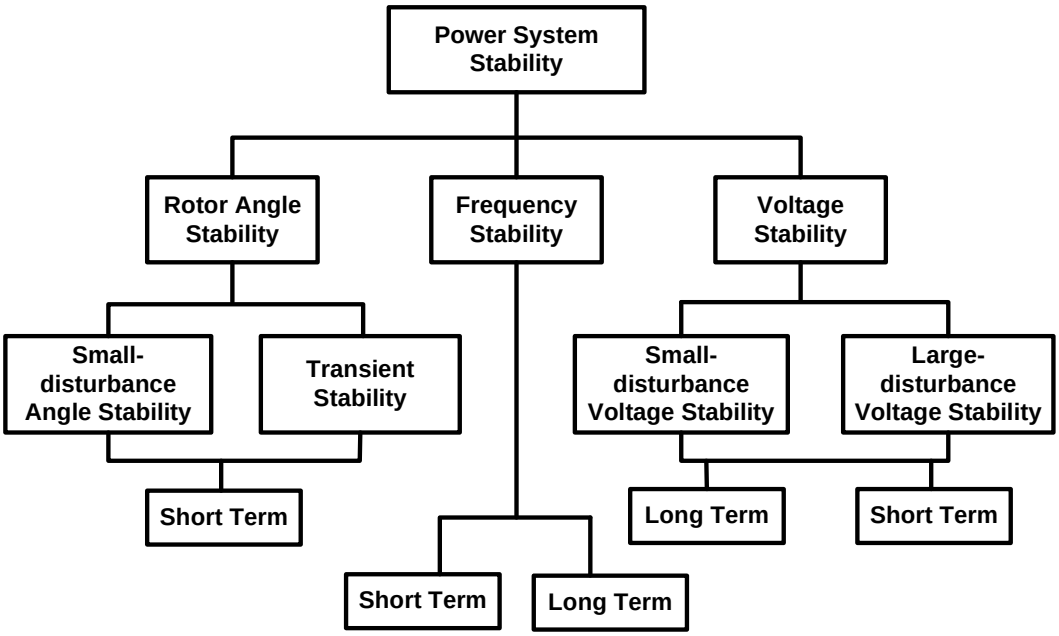

Figure 1.3: Classification of power system stability

Power system stability is a comprehensive and complex subject. This thesis will focus

on voltage stability categories and its subcategories. A number of such voltage instability incidents have been experienced around the world. Many of them are described in [2]. When the system is moving towards voltage instability, protection and controls are required to mitigate this situation and finally restore the system to normal operation [10]. As a consequence, voltage stability analysis and control in a power system has become a major concern for power system planning and operation [12].

1.3.1 Small-disturbance Voltage Stability

According to the definition in [11], small-disturbance voltage stability refers to the system's ability to maintain steady voltages when subjected to small perturbations such as incremental changes in system load. This form of stability is influenced by the slower acting equipment such as tap-changing transformers, thermostatically controlled loads, and generator current limiters. As this happens relatively slowly, it is also called as long-term, or steady-state voltage stability. Instability is due to the loss of long-term operating equilibrium, or a lack of attraction toward the stable post-disturbance equilibrium when a remedial action is applied too late [12]. With appropriate assumptions, system equations can be linearized for analysis, thereby allowing the computation of valuable sensitivity information useful in identifying factors influencing stability [11].

1.3.2 Large-disturbance Voltage Stability

According to the definition in [11], large-disturbance voltage stability refers to the system's ability to maintain steady voltages following large disturbances such as sys-

tem faults, loss of generation, or circuit contingencies. The time frame of interest for this kind of voltage stability is in the order of several seconds; it is sometimes called short-term voltage stability. This kind of voltage stability analysis requires the solution of appropriate system differential equations that need time domain simulation solutions of nonlinear response of the system after being subjected to a large disturbance.

When using a simulation tool for large disturbance voltage stability analysis, an appropriate portion of the load are represented by the dynamic load model (i.e. induction motors) since dynamic modelling of loads is often essential to assess voltage stability. In addition, generators, excitation system, governors, reactive compensation or diverse control devices, and disturbances need to be appropriately represented in their detailed dynamic models spanning the study period of time.

1.4 Preventive and Corrective Control

From the viewpoint of security assessment, the first task is to analyze the security of the current operating point. If the power system is in a normal state, the assessment should report how close the system is to an insecure state to give the operator an idea of what might happen. If the system moves to an alert state or to an emergency state, the assessment should pass the information on to the remedial control component [13]. This component assists the operator in executing remedial actions to improve security of the power system operation. The remedial actions are commonly classified into two categories: preventive actions and corrective actions [10].

Preventive actions are designed to put the system in a state such that the occurrence of a credible disturbance does not make the system unstable. In practice, this means operating the system prior to the contingency. A series of potential contingencies with reasonable probability of occurrence are selected by contingency screening methods, and preventive control actions are taken for those critical contingencies based on stability indices. Preventive controls thus usually require operating the system to a higher cost. Generation rescheduling, reactive compensation switching, using emergency back-up reactive power reserve provided by synchronous generators, and load reduction are some examples for preventive control actions. This thesis investigates generation rescheduling to enhance the steady state voltage stability margin.

Corrective actions are intended to moderate the consequences of a disturbance and are carried out only if this disturbance occurs. When an abnormal condition develops, some corrective actions must be taken to restore the system to normal operation. System protection may contribute to stabilize the system in post-contingency first. Then, the corrective actions, such as compensation switching, secondary voltage control, generation trip, or load shedding, may be taken into account in post-contingency control. Load shedding is normally a "last resort" option but is the most effective alternative to eliminate the detected fault and return the system to an acceptable condition. The advantage of corrective control over preventive control is that it reduces the operating cost by acting only when the contingency occurs.

1.5 Computational Intelligence - CI

Computational intelligence (CI) is an offshoot of artificial intelligence [14]. Intelligence is the capability of a system to adapt its behavior to meet its goals in a range of environments. It is a property of all purpose-driven decision-makers [15]. Computational intelligence is a methodology involving computing that provides a system with an ability to learn and/or to deal with new situations, such that the system is perceived to possesses one or more attributes of reason, such as generalization, discovery, association, and abstraction [16]. The IEEE computational intelligence society categorizes computational intelligence into three broad subjects:

- Neural Networks
- Fuzzy Systems
- Evolutionary computation, which includes
  - Evolutionary Algorithms
  - Swarm Intelligence

This thesis utilizes two main computational intelligence techniques: artificial neural network and particle swarm optimization.

1.5.1 Artificial Neural Network - ANN

An artificial neural network (ANN), sometimes called "neural network" (NN), is a non-linear mathematical model or computational model that tries to simulate the structure and functional aspects of biological neural networks. A major advantage of the ANN approach is that the domain knowledge is distributed in the neurons,

and information processing is carried out in a parallel distributed manner [17]. This approach has many desirable properties and capabilities such as:

1. Nonlinearity. An ANN has been conceived as a method of figuring out the nonlinear relationship between input and output variables. A neural network is made up of interconnected neurons that are presented by proper nonlinear function and weights. It simulates the highly interconnected, parallel computational structure with many relatively simple individual processing elements [16]. Power system includes many kinds of nonlinear devices and controls. Therefore, the nonlinear computation capability of ANN is desirable in applications in power systems.

2. Learning ability. ANN is an adaptive system that is able to learn these complex relationships based on external or internal information that flows through the network during the training phase. It adapts by altering the weight of connections in the network with an amount proportional to the difference between the desired output and the actual output. Therefore, they can be used to model complex relationships between inputs and outputs as well as to find patterns in data.

3. Generalization. Generalization is an important characteristic of human cognition. A neural network should be able to perform this function. Generalization in this case refers to the neural network sufficiently abstracting what it learns in training and extending this to produce reasonable outputs for those inputs not encountered during training.

4. Real Time Operation. Using current state-of-the-art solutions, the technical feasibility of a neural network application in a real-time operation seems to depend

on the appropriate understanding of the learning process to the problems. A trained ANN can be used for on-line prediction because of its fast response and very low computational times at the expense of comprehensive off-line studies. The time spent on training the ANN is spent prior to the real time. Therefore, the advantage of the time spend on training is available in real time. Having spent the time to train the ANN, the trained ANN is then capable of estimating the stability margin of an unseen system state. If an analytical method is used, it has to acquire the present system state and execute the algorithm pertaining to the analytical method. In this case, computing time is spent in real time.

These are the properties of neural networks that are most desirable for solving the problem in this thesis. On the other hand, artificial neural networks also have some disadvantages:

1. Black Box. Artificial neural networks act like " Black Box Models " with little or no prior knowledge of the function included in itself [18]. The "Black Box" nature of artificial neural networks makes it is difficult to determine how the ANN will optimize weights between neurons to make a decision. Consequently, it is hard to know which of the input features are important for the output results. When applying neural networks to voltage stability analysis, this disadvantage makes it impossible to seek the most important features to output through the hidden ANN structure and weights. We have to develop other algorithms to solve the problem.

2. Large Sample Size. Neural networks are data-driven techniques. Therefore, data preparation is a critical step in building a successful neural network model.

Without a good, adequate, and representative data set, it is impossible to develop a useful, predictive ANN model. Thus, the reliability of ANN models depends to a large extent on the quality of data [19]. Generally, a larger sample provides a better chance for ANN to adequately approximate the underlying data structure. However, superfluous sample data can bring in noisy data which causes estimation error. Therefore, obtaining sufficiently large sample size is a challenge for a practical problem.

3. No On-line Training. The training of ANN requires a great deal of computational effort and is usually an off-line process.

The number of artificial neural network applications to electric power system problems has increased dramatically in the last few years as have its successes in a variety of disciplines. [20] provides a comprehensive bibliographical survey in this field. In this thesis, the terms artificial neural network, neural network and ANN are used interchangeably.

1.5.2 Particle Swarm Optimization - PSO

Particle Swarm Optimization (PSO) is a population based stochastic optimization technique developed by James Kennedy and Russell C. Eberhart in 1995 [21], inspired by the social behavior of bird flocking or fish schooling. PSO belongs to the categories of swarm intelligence techniques and evolutionary algorithms for optimization.

The particle swarm optimization algorithm models the movement of a swarm, in which individuals are called “particles”, that finds a solution to an optimization problem in

a search space. The position of a particle represents a candidate solution to the optimization problem at hand. Each particle searches for better positions in the search space by changing its velocity according to rules originally inspired by behavioral models of bird flocking. A better position is determined by personal best position of each particle, so that potentially good solutions can be used to guide the construction of the new solutions. Additionally, at swarm level, the best overall positions among all particles is also recorded, and this position upon termination of the algorithm may serve as the answer.

Particle swarm optimization has been used extensively in many fields, including function optimization, neutral network and system control. [22] provides a review of the PSO technique, the basic concepts and different structures and variants, as well as its applications to different optimization problems in power systems. Particle swarm optimization technique has been verified to be robust for solving problems featuring non-linearity, non-differentiability, multiple objective optimization, and high dimensionality through adaptation [23]. A particle swarm approach is applied in this thesis to seek for a load shedding scheme that serves as a control action actuated after a contingency to restore the voltage stability. The PSO algorithm searches a problem space of candidate load shedding locations and finds the optimal load shedding places and associated amount.

1.6 On-line Measurement

On-line measurement takes a snapshot of power system conditions and acquires data. Until now, critical nodes in transmission grids have usually been monitored using

static or quasi-dynamic data based on rms measurements. Supervisory control and data acquisition (SCADA) systems usually collect measurements of real and reactive power in network branches, busbar voltages, and frequency at a few locations in the system [13]. The power system is a highly interconnected system with generators and loads that may be hundreds of miles away. A wide area protection and control (WAPaC) system is an advanced measurement technology to collect information not available from contemporary SCADA technology [24, 25]. Wide area protection and control systems measure wide-area or global signals and are essentially based on new data acquisition technology called Phasor Measurement Unit (PMU). Figure 1.4 demonstrates a wide area measurement system that consists of phasor measurement units deployed at geographically dispersed locations in the system [26].

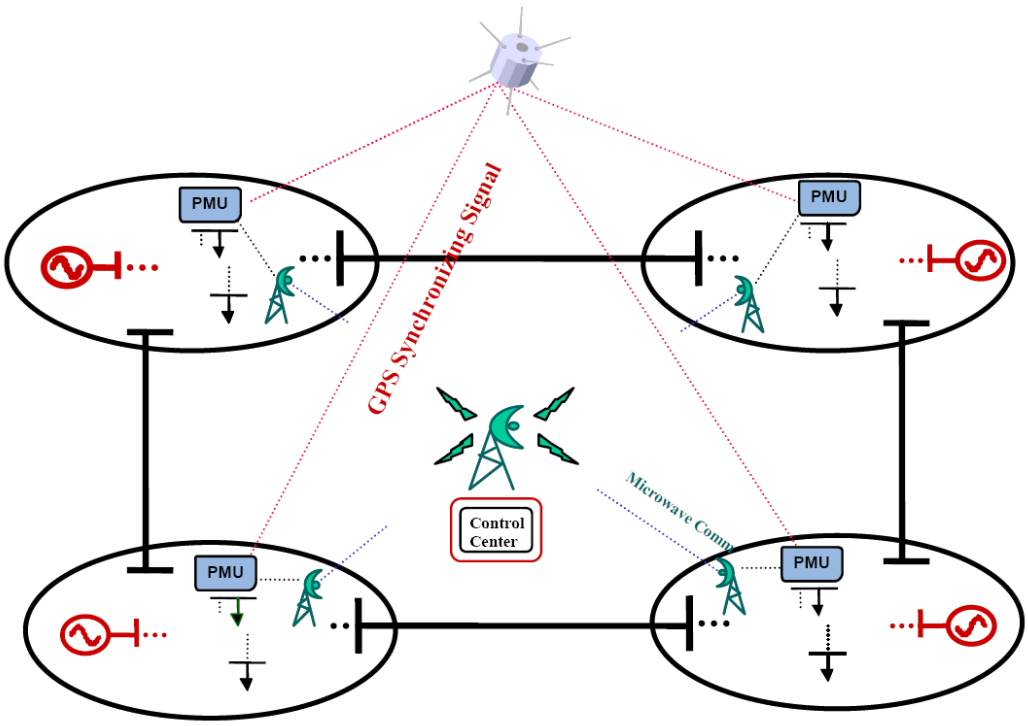

Figure 1.4: A wide area measurement system

The Phasor Measurement Units (PMU) is considered to be one of the most important measuring devices in the future power systems. Figure 1.5 demonstrates the phasor measurement capability at two remote locations due to GPS (Global Positioning System) synchronization. Phasor is a quantity with magnitude and phase angle with respect to a reference that is used to represent a sinusoidal signal. The sinusoidal signal can be bus voltage or line current. The phase angle of any node is displayed as the phase angle measured by the PMU minus the phase of a specified reference at a time, such as time = 0. The phase angle differences between two sets of phasor measurements (i.e. δ_1-δ_2) is independent of the reference. The reference can be one of the phasor measurements.

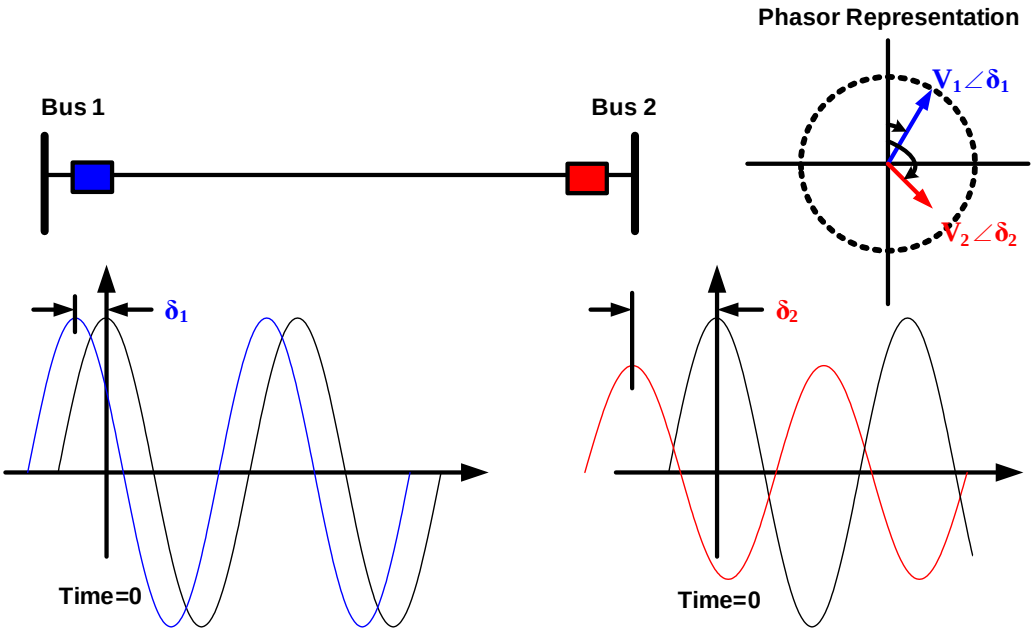

Figure 1.5: Synchronized phasor measurements at remote locations

Introduction of Phasor Measurement Units (PMU) has opened up new opportunities to implement more effective special protective and correction methods [27]. The

distinction for PMU comes from its unique ability to monitor both magnitudes and synchronized phase angles of voltages and currents from widely dispersed locations in addition to more conventional quantities [28]. The synchronized phase angles were once immeasurable but they provide vital information for stability analysis, to detect, predict and mitigate voltage instability in large power networks [29].

1.7 Research Motivation

The operation of power systems has become more difficult in recent times. Power systems are operated closer to security limits, environmental and economical constraints restrict the expansion of transmission network, and the need for long distance power transfer has increased significantly. Voltage instability has become a major concern in many power systems. Many blackouts due to voltage instability have been reported in [2]. This has resulted in a continually increasing interest and study into voltage stability or voltage security assessment.

When disturbances occur in a large power network, both local and system-wide conditions influence voltage stability problems. Under abnormal conditions, it is challenging for operators to deal with large volumes of data, and then initiate the most appropriate remedial actions. Therefore these security assessments should be done on-line to get an accurate measure of the power system operating state and lead operators to make informed decisions on executing proper control actions when necessary.

A typical on-line security assessment (Figure 1.1) takes snapshots of the power system variables. As not all the power system variables are measured, it is important

to determine the most probable power flow state by using the state estimation for the on-line stability calculation. The phase angle, which is the estimated value on the state estimation, can be measured with precise time-synchronization by PMUs (Phasor Measurement Units). PMU information can be integrated into the conventional state estimation to improve the accuracy of measurement. We intend to use new measured data provided by PMUs for on-line security assessment.

Off-line tools for the voltage security assessment consist of: 1. power flow based static tools, such as the VSAT [30], CPFlow [31], 2. Quasi-Dynamic (Fast Time Domain) simulation programs [32], 3. time-domain simulation (dynamic) tools, such as PSS/E [33], TSAT [34]. However, these conventional approaches are limited by computation time that is significant for on-line computation. This requires an intelligent system that greatly improves security assessment computations. An intelligent system is able to learn from situations previously encountered and employ this knowledge to new situations rapidly. We intend to use intelligent techniques, such as ANN, to be an integral part of on-line voltage security assessment.

The fundamental motivation of this research is to build up a comprehensive on-line strategy for voltage stability analysis, voltage stability preventive and corrective control. The strategy will do the following:

1. Apply the computational intelligence techniques to quickly and effectively estimate voltage security;

2. Investigate how to employ new on-line measurement techniques, i.e., Phasor Measurement Units, in intelligence based voltage security assessment;

3. Provide solutions of control actions to maintain or restore the voltage stability according to operating states.

1.8 Research Objectives

The objectives of this on-line voltage stability analysis and control strategy are to:

1. Investigate existing literature relating to voltage stability analysis methods. This revealed that mainly two voltage stability categories should be considered (Figure 1.3). Therefore, the research is focused on both small-disturbance voltage stability and large-disturbance voltage stability.

2. Identify the performance indices or voltage stability criteria that predicts the proximity to voltage instability problems. These indices could be used either on-line or off-line to help operators determine how far the system is to collapse. As a result, voltage stability margin is used for long-term voltage stability analysis under small disturbances and transit voltage dip is used for short-term voltage stability analysis under large disturbances.

3. Investigate computation tools relating to voltage stability analysis methods. Among the methods of estimating the voltage stability margin, the continuation power flow method is selected for the on-line voltage stability application. On the other hand, for large-disturbance voltage stability, it is important to recognize that the voltage stability and rotor angle stability are coupled with each other under contingencies [11]. The general structure of the system model for voltage stability analysis is similar to that for transient stability analysis. A time-domain simulation is an essential tool for this because the large-disturbance

voltage stability is determined by the dynamic characteristics of generators, loads, etc..

4. Develop a continuation power flow program to calculate the long-term voltage stability margin. In addition to the conventional power flow, the program considers continuation techniques to overcome the singularity of the Jacobian matrix when the system approaches stressful conditions. The program should also include various types of constraints, static load models and tap changing transformers that can have a significant impact on the small-disturbance voltage stability phenomenon.

5. Develop a framework for combining the continuation power flow program with an artificial neural network that involves the initial system operating points measured by PMUs to calculate the voltage stability margin. Some important aspects of ANN application need to be understood, such as: input feature selection, sample data size, overfitting or underfitting, computation speed, and accuracy measure.

6. Develop the ANN based approach and test it on a study system. Then, implement the approach on a practical power system to evaluate the feasibility and reliability of the proposed approach for a real and large size system.

7. Apply the ANN based approach into the different contingency scenario (N-1 contingency scanning). According to the output of evaluation of voltage stability under N-1 contingency, the proper preventive control, such as generation reschedule, needs to be employed to enhance voltage stability.

8. Develop a framework for combining time-domain simulation program with an artificial neural network to determine the transient voltage dip under large dis-

turbances. The transient voltage dip serves as short-term voltage instability index.

9. Develop a load shedding scheme as a corrective action against short-term voltage instability under large disturbances. As a result, an optimal load shedding solution makes an intelligent decision about: (i) where the most effective locations are for load shedding, and (ii) what is the minimal amount of load to be shed for those selected shedding locations.

1.9 Organization of the Thesis

In Chapter 2, a Continuation Power Flow (CPF) program is developed. CPF can be efficiently computed through parameterization techniques of continuation methods [35]. It uses an iterative predictor-corrector scheme to find the solution path and to determine the small-disturbance voltage stability limit for a certain load increase pattern (loading direction). The program can handle various types of constraints and models that can have a significant impact on the voltage stability phenomenon.

In Chapter 3, the developed CPF program is combined with the ANN approach to calculate the voltage stability margin that serves as a voltage stability index. Bus voltage magnitude and phase angle for individual buses are gathered from a power flow program. The operating points data can also be obtained from on-line Phasor Measurement Unit (PMU) devices. All the generating data is fed to an ANN to train the neural network and to form the trained ANN that can be effectively applied to on-line voltage stability assessment. Some important aspects of ANN application, such as input feature selection, sample data size, overfitting or underfitting, com-

putation speed and accuracy measure, are discussed using the 39-bus New England study system. The proposed approach is also tested for a power system of practical size.

In Chapter 4, several extended applications of the proposed ANN approach for small-disturbance voltage stability and control are presented. They are optimal choice of PMU locations, N-1 contingency scanning, and generation rescheduling. It is not economic to install PMUs at all buses in a power system. When only a limited number of PMUs are used, it is important to locate them at the most effective positions in the network. Thus, the optimal method of choosing PMU location is proposed in this chapter. Since disturbances are inevitable in power systems, it is particularly important for the proposed ANN approach to be able to estimate the voltage stability margin after a contingency. Applying the ANN approach for various contingencies is covered in this chapter. Moreover, the plan of generation rescheduling as a preventive action to enhance voltage stability margin is also presented.

In Chapter 5, the ANN based algorithm is applied to predict short-term voltage stability under large disturbances. The main difference is that the ANN approach is combined with a commercial time-domain simulation program to calculate transient voltage dip which serves as the short-term voltage stability index under large disturbances.

If the system is facing the risk of voltage instability or voltage collapse, some corrective actions must be carried out. Load shedding as a effective corrective action needs to be developed in order to avoid risks of voltage instability. In Chapter 6, two

simulation based approaches are proposed for load shedding to prevent voltage instability or collapse. The proposed approaches seek an optimization solution to make a decision about where the most effective locations are for load shedding and how much the minimal amount of loads is to be shed for those selected shedding locations. This proposed algorithms are based on time domain simulation, with the dynamic devices including voltage-dependant loads properly modelled.

Chapter 7 concludes the work carried out, main contributions, and suggestions for future research in the area of power systems security assessment and control.

References used for conducting the research together with related literature are listed under the Bibliography. The test systems data and some details of mathematical derivation are presented in the Appendices.

Chapter 2

Small-disturbance Voltage Stability

Small-disturbance, or steady-state (static), voltage stability is concerned with the ability of a power system to maintain acceptable voltage following small perturbations, such as gradual changes in load and generation. This chapter will start by reviewing basic concepts of steady-state voltage stability in a simple radial system. Then, the concept is extended to an interconnected power system. Continuation Power Flow (CPF) is developed for the steady-state voltage stability solution of a network with various static models of system components. The algorithm, procedures, and results of the CPF program are presented in detail.

2.1 Basic Concepts in Power Flow

Power flow calculation is required for the analysis of steady state as well as dynamic performance of power systems [10]. Such calculations involve voltage magnitude V, voltage phase angle θ, line active power P, and line reactive power Q, in the power network for specific terminal operation conditions.

There are three basic types of buses (nodes):

1. Slack bus: Voltage and phase angle are specified, and its angle serves as reference for the angles of all other bus voltages. A slack bus is usually selected as the bus with the largest generation capability.

2. Voltage controlled (PV) bus: Active power and voltage magnitude are specified. For example, generators, synchronous condensers, and static var compensators can be set as PV bus.

3. Load (PQ) bus: Active power and reactive power are specified. For example, all the buses except the PV buses and slack bus can be set this kind.

The network equations in terms of node admittance matrix at bus i can be given in polar coordinates as below:

$$\begin{aligned} P_i &= V_i^2 G_{ii} + V_i \sum_{i \neq k} V_k (G_{ik} cos\theta_{ik} + B_{ik} sin\theta_{ik}) \\ Q_i &= -V_i^2 B_{ii} + V_i \sum_{i \neq k} V_k (G_{ik} cos\theta_{ik} - B_{ik} sin\theta_{ik}) \end{aligned} \tag{2.1}$$

Where $Y_{ik} = G_{ik} + jB_{ik}$ is the ik^{th} element of node admittance matrix Y, $V_i(cos\theta_i + jsin\theta_i)$ is the complex voltage at Bus i, $\theta_{ik} = \theta_i - \theta_k$ is the voltage angle difference of the conjoint buses, and $S_i = P_i + jQ_i$ is complex power.

When the Newton Raphson method is applied to solve the set of nonlinear equations (2.1), we have a linearized model around the given operating point which can be expressed as equation (2.2).

$$\begin{bmatrix} \Delta P \\ \Delta Q \end{bmatrix} = \begin{bmatrix} \frac{\partial P}{\partial \theta} & \frac{\partial P}{\partial V} \\ \frac{\partial Q}{\partial \theta} & \frac{\partial Q}{\partial V} \end{bmatrix} \begin{bmatrix} \Delta \theta \\ \Delta V \end{bmatrix} = [J] \begin{bmatrix} \Delta \theta \\ \Delta V \end{bmatrix} \tag{2.2}$$

Where J is Jacobian matrix which is a linear transformation of space of $[\Delta\theta \ \ \Delta V]$ into space of $[\Delta P \ \ \Delta Q]$. ΔP, ΔQ, ΔV and $\Delta\theta$ represent incremental changes in bus active power, reactive power, voltage magnitude and phase angle respectively.

2.2 Voltage Stability in a Simple Radial Network

To indicate voltage collapse phenomena and its corresponding physics mechanism as well as some basic concepts, a simple radial network needs to be considered. This radial network shown in Figure 2.1 has a constant voltage source, which represents a synchronous machine with sufficient exciter support, a transmission line and an On-load Tap Changing transformer (OLTC) to supply a load.

2.2.1 Relationship of Voltage, Current and Active Power to Load Impedance

The voltage of the source is E_s, the off-normal ratio of the transformer is k, the impedance of the transmission line is $Z_L\angle\theta$, load impedance is $Z_D\angle\phi$. Appendix D describes the derived equations of current, voltage and transmitted active power to the load. The relationships, the normalized current I/I_s, the normalized receiving end voltage V_r/E_s, and the normalized power supplied to the load $P_r/P_{r,max}$ as a function Z_L/Z_D, are shown in Figure 2.2. The plots in the figure are obtained by setting $\tan\theta = 10.0$, $\cos\phi = 0.95$, and $k = 0.9, 1.0, 1.1$.

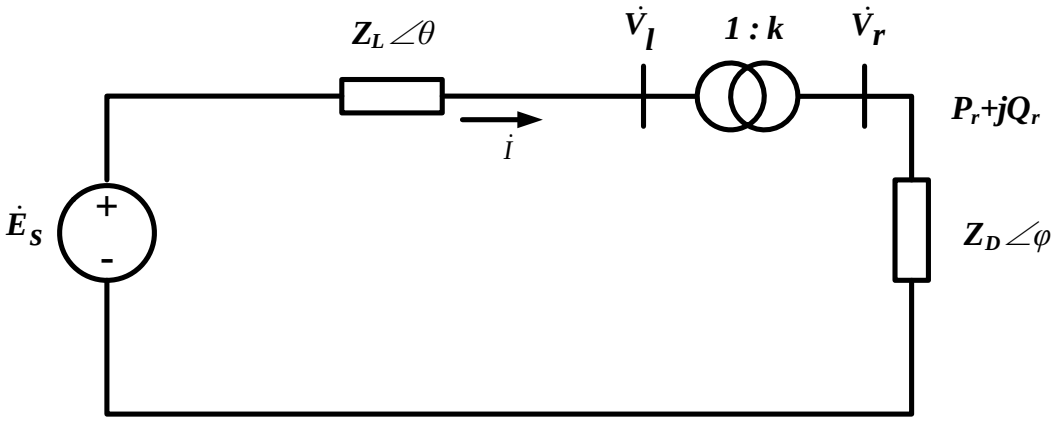

Figure 2.1: A simple radial network with transformer

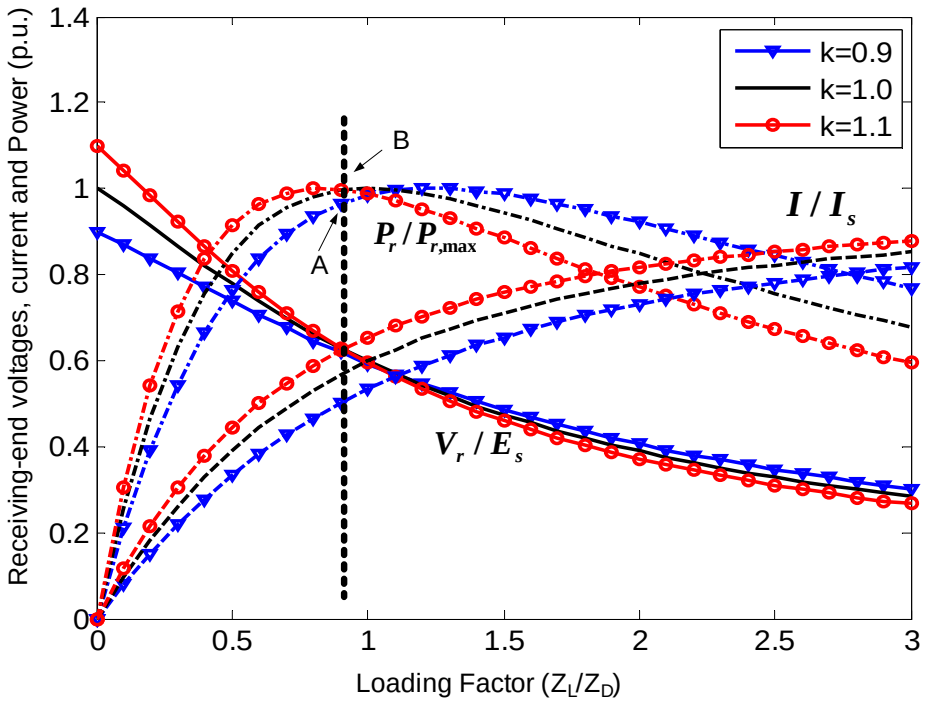

Figure 2.2: Relationship of I/I_s, V_r/E_s, $P_r/P_{r,max}$ to Z_L/Z_D at $\tan\theta = 10.0$, $\cos\phi = 0.95$

The following voltage stability phenomena and mechanism can be inferred from Figure 2.2:

1. When the load demand increases (effectively Z_L/Z_D increases) P_r increases rapidly at first and then slowly before reaching a maximum, and finally decreases. This is thus a maximum value of active power that can be transmitted through an impedance from a constant voltage source. The load voltage decreases and current increases with the load demand.

2. The operating points before the maximum value of power transmitted are normal (stable) operation conditions. In order to meet the increasing load demand (effectively Z_L/Z_D increases), voltage source has to provide more power. After passing the power transmitting peak ($P_{r,max}$), it goes into abnormal (unstable) operation conditions. In this region the increasing load demand only results in less power transmitted and the voltage tends to decrease to zero.

3. When the load is supplied by a transformer with OLTC, the tap-changer action may lead to an unexpected voltage control. For a certain load demand, raising the transformer ratio k has reduced the effective Z_D seen from system side and increased the effective Z_L/Z_D. This moves the operating point closer to the power transmitting peak. Once the load demand is higher than the one corresponding to maximum power, control of power by varying load would be unstable. If load demand is fixed, the operation point jumps from A to B if ratio k changes from 0.9 to 1.1 as shown in Figure 2.2. At $P_r/P_{r,max}$ line where A (k=0.9) is in stable region; but where B (k=1.1) is passed the peak point and go into the unstable region. Therefore, though raising k obtains temporarily higher load voltage it finally leads the system to voltage collapse.

4. The maximum transmitted power $P_{r,max}$ can be increased by increasing the source voltage E_s. In a real power system, the source voltage E_s is not always constant. When the limits of excitation system are reached, voltage source E_s drops. A shortage of voltage source limits the power transmitting when load has high demand; hence, it can cause voltage instability.

5. The maximum transmitted power $P_{r,max}$ can also be increased by increasing load power factor (ϕ decrease). Therefore, the load characteristic has influence on the maximum transmitted power. If the reactive compensating device is used at load side that is equivalent to increase receiving end power factor and thereby helps prevent voltage collapse in many situations.

2.2.2 $P-V$ Curve of a Simple System

A more traditional method of illustrating the voltage stability phenomenon is to plot the relationship between V_r and P_r ($P-V$ curve). For the simple radial network in Figure 2.1, the relationship of voltage and active power is expressed in the following equation (2.3). The detailed derivation can be found in Appendix D.

$$V^2 = \frac{1}{2} - \left(\frac{1}{\tan\theta} + \tan\phi \right) P \pm \sqrt{\frac{1}{4} - \left(\frac{1}{\tan\theta} + \tan\phi \right) P - \left(1 - \frac{\tan\phi}{\tan\theta} \right)^2 P^2} \tag{2.3}$$

Where V is the receiving end voltage, P is the transmitted real power at the receiving end. θ is the transmission line impedance angle and ϕ is the load power factor angle.

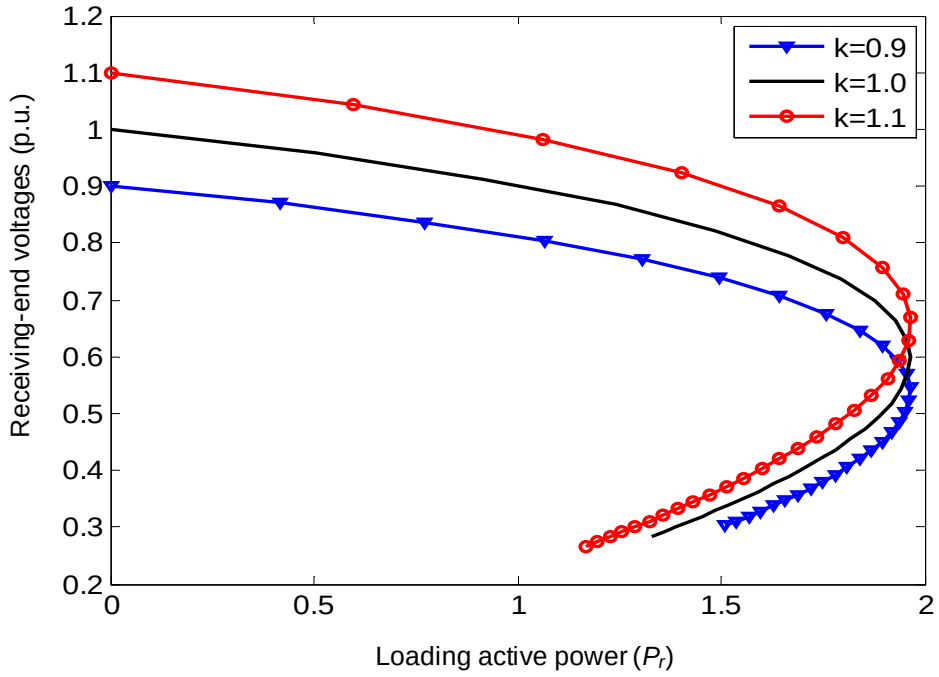

Figure 2.3: The $P_r - V_r$ characteristics of the simple radial system

Observing Figure 2.3, there are two equilibrium solutions corresponding to the same active power at the low loading. One is a high voltage solution and the other is a low voltage solution. When the loading increases, the two solutions approach each other and finally become one nose point.

Out of the two solutions, the higher voltage operating point is stable and the lower voltage operating point is unstable. The power system can only operate on the upper-half of $P-V$ curve where the system dynamics act to restore the state to the operating point when it is perturbed. On the other hand, any slight disturbances from the low voltage operating point on the lower-half of $P-V$ curve result in the operating state moving away from the operating point towards the origin.

The nose point of the $P-V$ curve is named as the voltage stability limit.

2.3 Voltage Stability Index

For small-disturbance voltage stability, there are a number of voltage stability indices that can assess the degree of voltage security and measure the severity of the voltage stability problem. These indices are used to determine the closeness of an operating point to the critical point [36]. Some proposed methods of calculating these indices include singular vector [37, 38], saddle-node bifurcation [39], optimization method [40] and continuation load flow [35, 31, 41], sensitivity factors [42], second order performance index [43], the energy function method [44], modal analysis [45], voltage stability L indicator [46], and $V-Q$ curve [47].

Among these indices, the voltage stability margin is a quite straightforward and easily understood index for the system operators. The operators can know how additional real power can be safely and reliably transferred across the system, or how much power can be transferred from one area to another over all transmission lines or paths between those areas under specified system conditions. In utilities, this concept is used as an indicator for the operator to know how far the stability limit is from the current operating point in terms of megawatts [48]. The concept can be described directly based on the construction of a $P-V$ curve. Similar to the simple radial system presented in Section 2.2.2, large interconnected power system has similar $P-V$ relationship.

Figure 2.4 illustrates a $P-V$ curve of a load bus. As explained in Section 2.2.2, the upper part of the $P-V$ curve is stable while the lower part is unstable under steady state conditions. Consequently, normal operation is restricted to the upper part of the curve. In Figure 2.4, the point A is an initial operating point. The point B, which corresponds to the maximum real power delivered (nose point), is defined as voltage stability limit. The distance between point A and B (in MW) is defined as the voltage stability margin and serves as a voltage stability index. The voltage stability index is expressed as below:

$$P_{margin} = P_{max} - P_0 \tag{2.4}$$

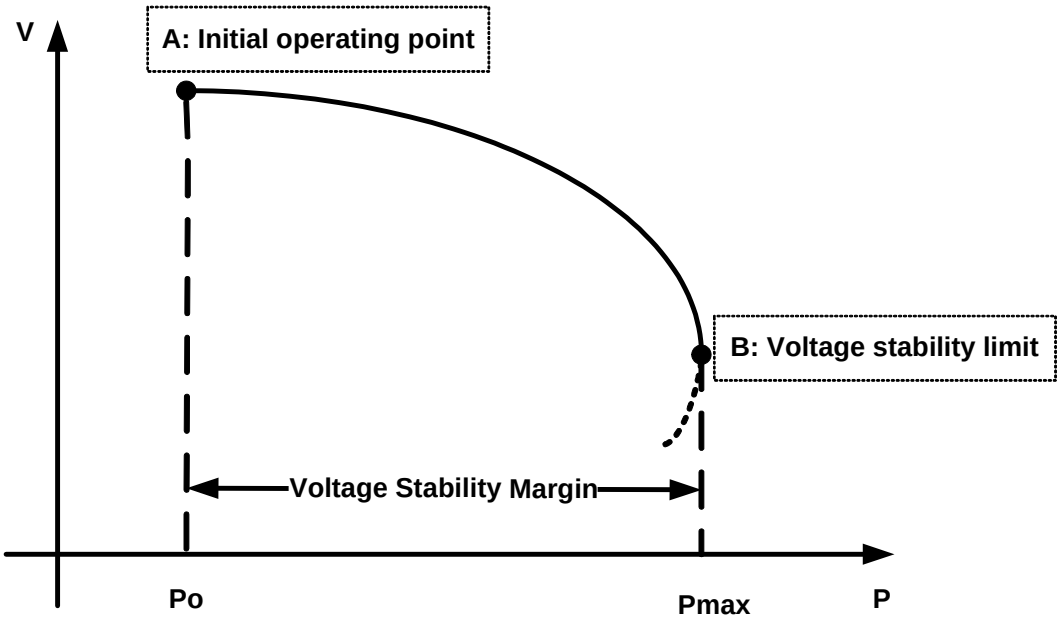

Figure 2.4: $P-V$ curve and voltage stability margin

With respect to the delivered active power (P) variations, various power flow cases

are computed to trace the $P-V$ curve. If the conventional power flow model is used for tracing the $P-V$ curve, the operating point is incremented along the $P-V$ curve. However, the Jacobian matrix of equation (2.2) becomes singular close to the voltage stability limit. Therefore, the voltage stability limit cannot be obtained using conventional power flow programs due to convergence difficulties. The continuation method is a mathematical path-following methodology used to solve systems of non-linear equations. The continuation power flow algorithm modifies the conventional power flow equations (2.2) to overcome the singularity of the Jacobian matrix. Consequently, continuation power flow algorithms are able to obtain the voltage stability margin when the system is moving toward a stressful condition [10]. This makes the continuation method quite attractive in approximations of the critical point in a power system [49].

2.4 Direction of Load and Generation

The general principle behind the continuation power flow is that by introducing a load parameter into the conventional power flow equations, it is possible to apply a locally parameterized continuation technique to the power flow problem [31, 35]. The parameterized power flow equation takes the form given in equation (2.5).

$$F(V, \theta, \lambda) = 0 \tag{2.5}$$

where V represents a vector of bus voltage magnitudes, and θ represents a vector of bus voltage angles. λ represents the parameter of load change.

The goal of tracing $P-V$ curve is to determine the extent to which the power system can be loaded before reaching the voltage stability limit. For this problem, we can increase the load step by step until the limit is reached. The load parameter λ is used to increase the load.

The change of load with the parameter λ can be described by any one of the following ways:

1. The real and reactive power of only one PQ load increase while other loads remain constant.
2. The real and reactive power of PQ loads increase in a particular area while other loads remain constant.
3. The real and reactive power of PQ loads increase in area A, the real and reactive power of PQ loads decrease in area B, and the rest of the loads remain constant.
4. The real and reactive power of all PQ loads increase.

When the load is increased, the generation must be increased to meet the increased demand. This can be done in many different ways. Generation dispatch with the variation of load parameter λ can respond with one of the following methods.

1. Real power at only the slack bus increases with λ.
2. Real power at selected generator buses increases with λ.
3. Real power generated by all generators increases with λ.

The voltage stability margin depends on how the loads and generation are increased. Generally, the loads on all nodes in a power system do not increase at the same rate.

In practice, the load variation is estimated using load forecasting programs. In order to accommodate the increased load, the power output of the generators also needs to be increased. This uneven increase in the loading and generation can be modeled by:

$$\begin{aligned} \mathbf{P_g} &= \mathbf{P_{g0}} + \lambda \mathbf{P_{gd}} \\ \mathbf{P_l} &= \mathbf{P_{l0}} + \lambda \mathbf{P_{ld}} \\ \mathbf{Q_l} &= \mathbf{Q_{l0}} + \lambda \mathbf{Q_{ld}} \end{aligned} \tag{2.6}$$

Where $\mathbf{P_g}$ is a vector of active power generated by the generators excluding the slack bus, $\mathbf{P_l}$ is a vector of active power delivered to the loads, and $\mathbf{Q_l}$ is a vector of reactive power delivered to the loads. $\mathbf{P_{g0}}$, $\mathbf{P_{l0}}$, and $\mathbf{Q_{l0}}$ represent the corresponding quantities at the current operating point. The vectors $\mathbf{P_{gd}}$, $\mathbf{P_{ld}}$, and $\mathbf{Q_{ld}}$ define the direction of power change. λ is a parameter that defines the magnitude of loading along the direction of load/generation increase.

The load forecast can be used to determine the loading direction ($\mathbf{P_{ld}}$) for the active power P. The reactive power forecasts are generally not available. In the absence of a reactive power forecast, a constant power factor can be used to obtain the reactive power direction ($\mathbf{Q_{ld}}$). The direction of generator power increase ($\mathbf{P_{gd}}$) can be obtained from the generation dispatch.

2.5 Continuation Power Flow

Generally, to get power flow the network equation (2.1) needs to be solved. There are different types of nodes in a power network. For the PQ nodes, P and Q are specified (known); and for the PV nodes, P and the magnitude V are specified (known). The boundary conditions imposed by different types of nodes make the problem non-linear and therefore power flow equations (2.1) are solved iteratively using techniques such as the Gauss-Seidel or Newton-Raphson method [10]. The iterations begin with guessed values of the voltage magnitudes and angles at all load buses, and of the voltage angles at all generator buses. Conventional power flow algorithms based on Newton-Raphson or Gauss-Seidel techniques fail to converge when the operating point approaches the nose point of the $P-V$ curve. Numerically stable algorithms known as Continuation Power Flow (CPF) technique have been proposed in [31, 35] to overcome this problem.

The basic principle of continuation power flow is to use an iterative predictor-corrector scheme to trace the operating point on the $P-V$ curve for a specified load increase pattern [35]. As shown in Figure 2.5, starting at a normal load, the load parameter λ can be increased by a tangent predictor to estimate an approximate solution. The correction step then determines the exact solution for a conventional power flow.

2.5.1 Prediction Step

The prediction step plays a key role in determining a possible solution to be used for the initial value of the power flow computation in the next step. The prediction step estimates an approximately sized predictor along the tangent direction to the solution path. The first task in the prediction step is to find out the tangent vector through a process of differentiation of equation (2.5) to obtain equation (2.7).

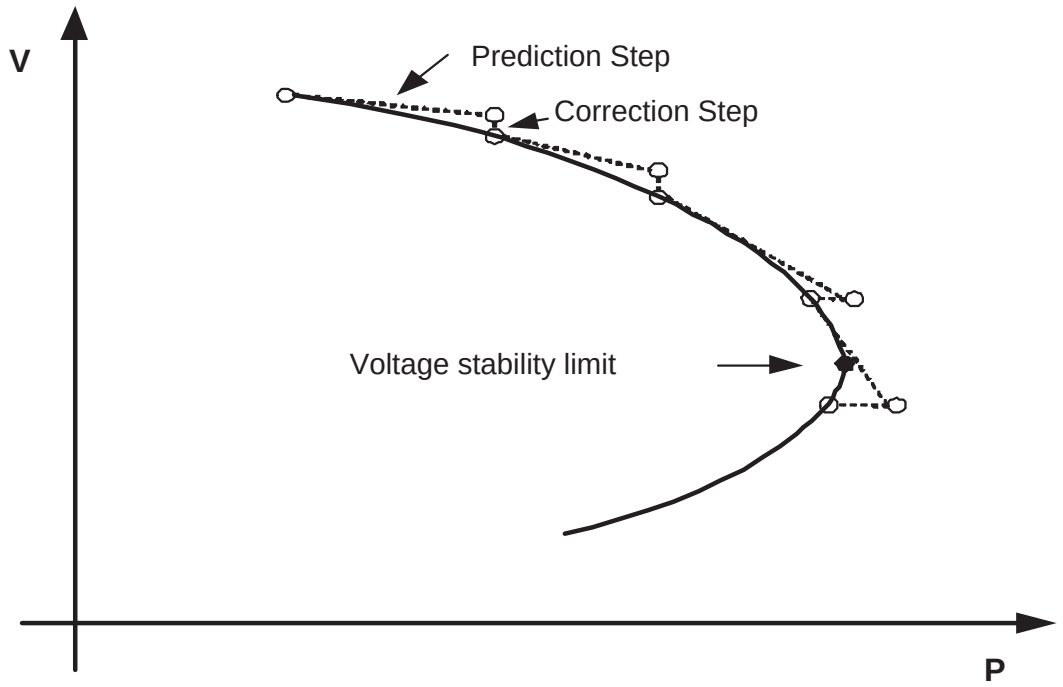

Figure 2.5: The predictor-corrector scheme of Continuation Power Flow

$$d[F(V,\theta,\lambda)] = [F_v \;\; F_\theta \;\; F_\lambda] \cdot \begin{bmatrix} dV \\ d\theta \\ d\lambda \end{bmatrix} = 0 \tag{2.7}$$

In observing the above equation, there are n equations with $n+1$ variables. Thus one more equation is needed. This results in equation (2.8).

$$\begin{bmatrix} F_v \;\; F_\theta \;\; F_\lambda \\ e_k \end{bmatrix} \cdot \begin{bmatrix} dV \\ d\theta \\ d\lambda \end{bmatrix} = \begin{bmatrix} 0 \\ \pm 1 \end{bmatrix} \tag{2.8}$$

Where e_k is a row vector with the only nonzero entry in the k^{th} element which equals one. If the k^{th} element is positive, the tangent direction is increasing and a '+1' should be used. If the k^{th} element is negative, the tangent direction is decreasing and

a '-1' should be used.

The predictor can be found by solving equation (2.8) and find the new value for the next step:

$$\begin{bmatrix} V^* \\ \theta^* \\ \lambda^* \end{bmatrix} = \begin{bmatrix} V \\ \theta \\ \lambda \end{bmatrix} + \sigma \cdot \begin{bmatrix} dV \\ d\theta \\ d\lambda \end{bmatrix} \tag{2.9}$$

Here σ is a scale to determine the step size. A constant value of σ is used in this thesis.

2.5.2 Correction Step

Using the predictor as an initial value of power flow, the correction step conducts computation using the expanded parameterized power flow equations.

let

$$x = \begin{bmatrix} V \\ \theta \\ \lambda \end{bmatrix}, \qquad x \in R^{n+1} \tag{2.10}$$

Here, x is a $(n+1)$-dimensional vector in the space of real variables (R^{n+1}).

In the correction step, a set of $n+1$ equations is solved, as follows,

$$\begin{bmatrix} F(V,\theta,\lambda) \\ x_k - x_k^* \end{bmatrix} = [0] \tag{2.11}$$

2.5.3 How to Select k

The index k appears in both prediction step and correction step. Mathematically, it should correspond to the state variable that has the largest tangent vector component. So, k is selected as,

$$x_k : \begin{bmatrix} \dot{x_k} \end{bmatrix} = max\{\begin{bmatrix} \dot{x_1}, \dot{x_2}, \cdots, \dot{x_{n+1}} \end{bmatrix}\} \tag{2.12}$$

2.5.4 Flowchart of CPF Program

The continuation power flow method adopted in this thesis is a combination of the repeated power flow and predictor-corrector continuation method. It starts with conventional power flow program and continues until non-convergence is encountered. Then, it switches to continuation power flow to trace the $P-V$ curve to the nose point. A brief summary in the form of a flow chart is shown in Figure 2.6.

2.6 Factors that Impact Voltage Stability

Voltage stability problems normally occur in heavily stressed systems. In addition to the strength of transmission network and power transfer level, the main factors contributing to voltage collapse are [10]:

- Generator reactive power capability limits
- Undesired transformer tap changing

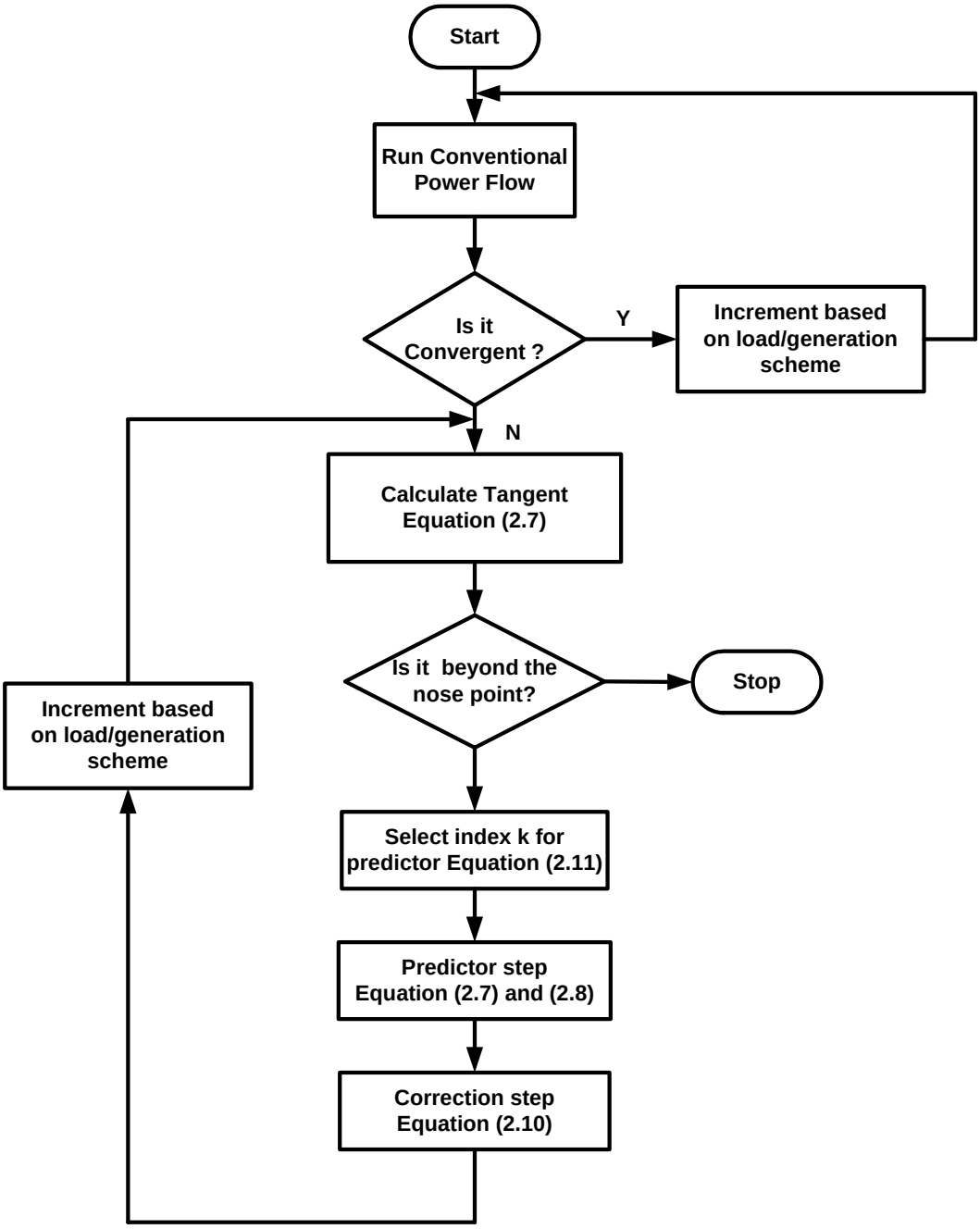

Figure 2.6: The flow chart of Continuation Power Flow

- Load characteristics
- Characteristics of reactive power compensating devices

The practical power system does not have infinite reactive power sources. Generator reactive power capability limits have a very significant effect on voltage stability. If the limitation on generator reactive power is reached, imposed mainly by maximum excitation limiters, the generator will lose the capability of reactive power control. In the continuation power flow program, the generator bus turns from PV bus to PQ bus. Without considering the generator reactive power limit, the results would be overly optimistic.

On-Load Tap Changers (OLTC) are widely used for voltage regulation in electricity networks and their tap changing action should be included in continuation power flow. Following some disturbances, transformer OLTCs try to restore their secondary voltages. With each tap change operation, the resulting increment in load would increase the MWs, the MVARs, and the losses, which sometimes causes a significant voltage reduction at the high voltage side. The process eventually may lead to voltage collapse. As a result, tap-changing operations should be frozen in some situations to avoid the voltage instability.

Voltage stability is largely determined by load characteristics. It is necessary to study load characteristics of different types of load when the system operates at different voltage levels and especially at low voltage levels.

Voltage instability is essentially a local phenomenon. The starting point of some power system blackouts is a local shortage of reactive power. Therefore, reactive

power compensation is often the most effective way to prevent a voltage collapse. Reactive compensation can include a mixture of shunt/serial capacitor banks, and/or Static Var Compensation (SVC) and so on.

High-voltage direct-current (HVDC) transmission has advantages over AC transmission in special situations. HVDC systems have the capability to rapidly control the transmitted power. Therefore, they have a significant impact on the stability of the associated AC power systems. An understanding of the characteristics of the HVDC systems is essential for the study of stability of the power system [10].

In performing comprehensive voltage stability studies, the following components have been included in the system modelling of the developed continuation power flow program.

- Generator Reactive Power Capability Limits
- OLTC Tap Transformers
- Static Loads
- Reactive Compensation Devices
- HVDC converters

2.7 Case Study

2.7.1 Validation of CPF Program

A commercial power flow program PSAT was used to validate the accuracy of the CPF program which is written in MATLAB. PSAT is one of the components included

in the Dynamic Security Assessment Software $DSATools^{TM}$ [50], a toolset for power system planning and operational studies, designed by Powertech Lab Inc. PSAT is a fully featured yet conventional power flow program.

A 12-bus system [51] was used for comparison and its network and data are given in Appendix A. PSAT was run repeatedly by increasing all the load in steps of 1% ($\lambda = 0.01$). The discrete points were obtained along the $P - V$ curve after several computations by PSAT. When the load increased by 13% of the initial load (i.e. λ was equal to 0.13), the power flow could not converge and computation stops. In Figure 2.7, the star mark points are the results of PSAT.

Therefore, when the power flow of PSAT is getting close to the nose point, it is divergent. The comparison between PSAT and CPF can only be done up to this point of the power flow. The results obtained with both CPF and PSAT are presented in Figure 2.7. The results show that the developed CPF program has identical points to PSAT. Moreover, the CPF program enlarges the region of convergence leading to the nose point of the $P - V$ curve.

2.7.2 Generator Reactive Power Capability Limit

The developed continuation power flow program was applied on the New England 39-bus system to find the solution path along the $P - V$ curve for a specified direction of load increase. The detailed data of the 39-bus system are given in Appendix B. This case study was used to compute the voltage stability margin of a base case. It was assumed that a uniform percentage load increase for all the loads and all the

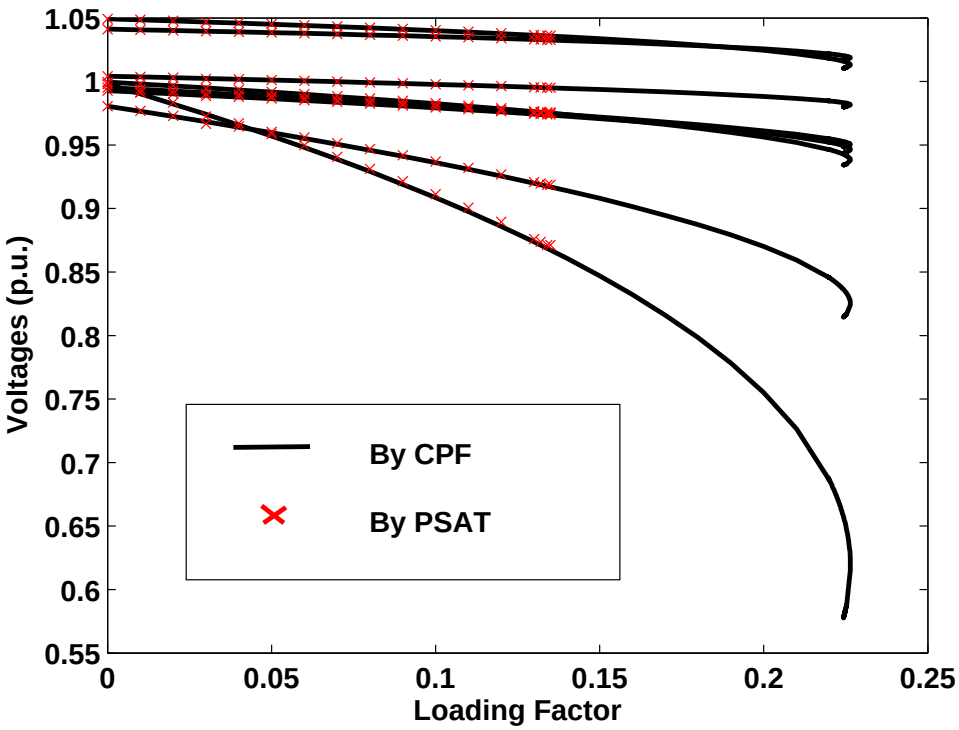

Figure 2.7: Comparison between CPF and PSAT

generators increase their real power output by the same percentage. Further, the computation took into account the generator reactive power limits. Figure 2.8 shows $P - V$ curves for some selected buses.

In Figure 2.8, the curves labeled 'Bus 37' and labeled 'Bus 30' are generator buses. At the beginning of load increase period, the generator buses maintain constant voltage at their reference setting level. When the load increases by 50% ($\lambda = 0.5$), the generator 'Bus 37' reaches its reactive power limit. After this point, its voltage decreases and does not keep constant as before. Soon, another generator labeled 'Bus 30' reaches its reactive power limit at $\lambda = 0.65$. Then the voltages of all buses drop rapidly and lead to eventual voltage collapse. At initial operating point ($\lambda = 0$), the base load is 6472.5MW. At the critical point, ($\lambda = 0.68$), the maximum load is 10873.8MW. Therefore, for this initial operating point, the voltage stability margin is 4401.3MW, with regard to the considered direction of load increase.

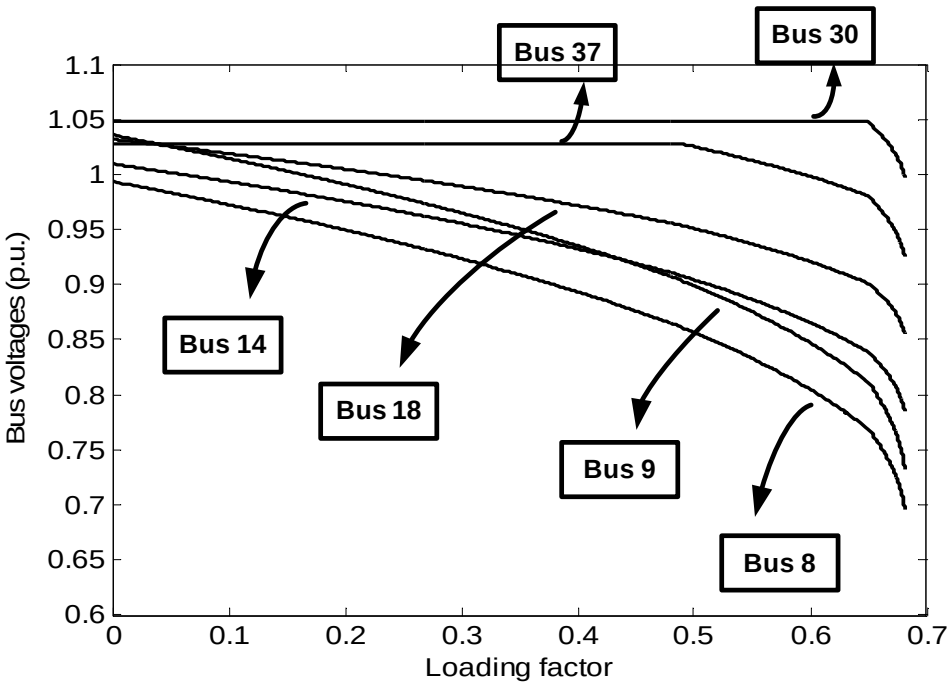

Figure 2.8: $P - V$ curve of base case in 39-bus system

Chapter 3

Predicting Voltage Stability Margin Using ANN

This chapter combines ANN with the continuation power flow program in small-disturbance voltage stability analysis to predict voltage stability margin. It has been found that the bus voltage magnitudes and phase angles, which could be obtained through the synchronized Phasor Measurement Units (PMUs), are the most appropriate input features to train a neural network. Two methods, comparison tests and analytical method, are used to verify that voltage magnitudes and phase angles are good inputs of ANN. Some additional aspects of ANN computation, such as sample data size, overfitting or underfitting, computation speed, and accuracy measure are discussed. The proposed approach is also tested for a power system of practical size.

3.1 Framework of ANN Strategy

Continuation power flow can successfully compute voltage stability margin. However, the approach is limited by computation time which is significant for on-line computation. The heavy and time-consuming computational workload is the main disadvantage of the continuation power flow and makes it unsuitable for on-line usage [52]. This calls up the computational intelligence technology which has attracted the attention of researchers in a wide range of disciplines including computer science, engineering, medicine, and business. Computational intelligence has the ability to learn from the situations previously seen and apply this knowledge to unseen situations rapidly. The Artificial Neural Network (ANN) is one of the most commonly applied computation intelligence techniques.

In order for an ANN to imitate the function of continuation power flow, it is essential to understand the process of how continuation power flow computes voltage stability margin. The procedure involved in the determination of voltage stability margin is shown in Figure 3.1.

The solution of the conventional power flow gives voltage magnitude V_0, voltage angle θ_0, real power P_0, and reactive power Q_0, at the initial operating point for all nodes in the network. In an on-line application, the above quantities are available from the measurements. The continuation power flow program, starting from an initial operating point, traces the $P-V$ curve to the nose point. The corresponding nose point is specified by V_{crit}, θ_{crit}, and λ. After that, the network equations calculate the power P_{max} and Q_{max}. Then the voltage stability margin is computed using (2.4).

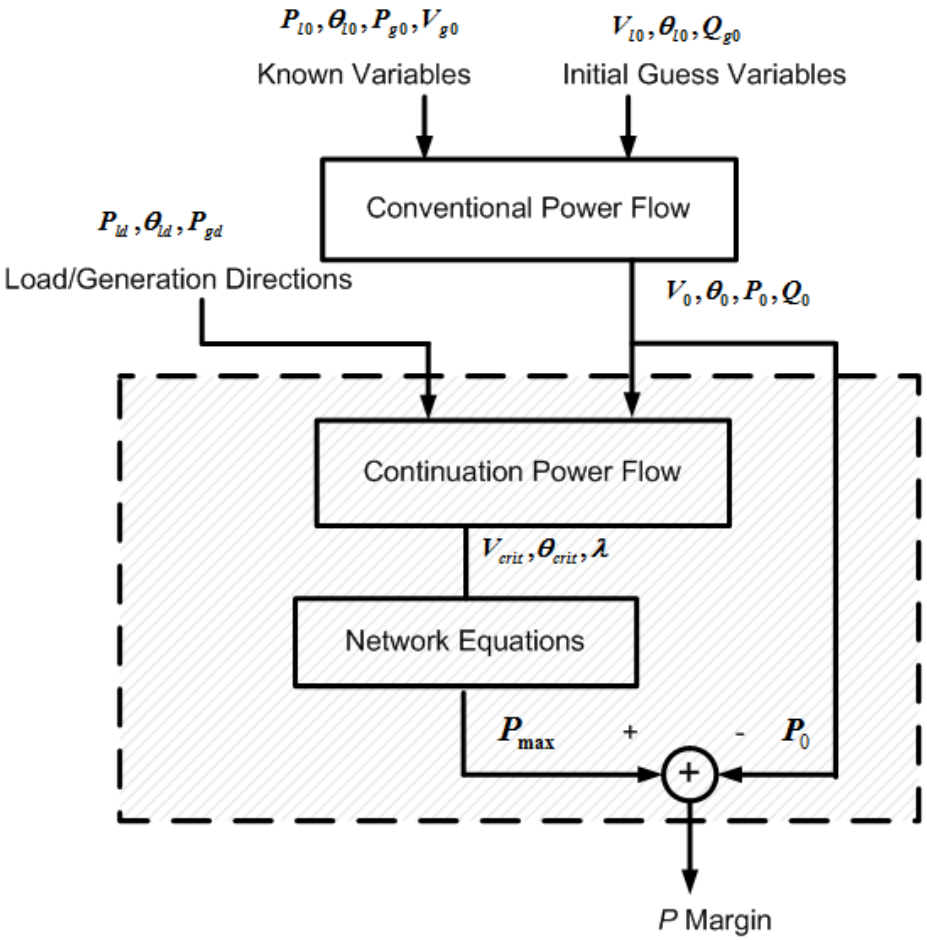

Figure 3.1: Process of computing voltage stability margin

When applying the ANN approach to estimate the voltage stability margin, ANN replaces the computations shown in the shaded area in Figure 3.1 after having been trained. An ANN can learn the mapping between the input quantities (V_0, θ_0,P_0, and Q_0) and the output (voltage stability margin) from numerous sample mapping data generated offline by the CPF program.

For a system with n buses, (2.1) can be expressed in vector format. Furthermore, using the subscript 0 to denote the initial condition, equation (2.1) is expressed in

vector format:

$$\begin{aligned} \mathbf{P_0} &= f(\mathbf{V_0}, \theta_\mathbf{0}) \\ \mathbf{Q_0} &= g(\mathbf{V_0}, \theta_\mathbf{0}) \end{aligned} \tag{3.1}$$

Equation (3.1) shows that once any two variables are known, the other two variables can be obtained. Thus any two variables of $\mathbf{V_0}$, $\theta_\mathbf{0}$, $\mathbf{P_0}$, and $\mathbf{Q_0}$ are sufficient to define the operating point. This suggests that all four variables ($\mathbf{V_0}$, $\theta_\mathbf{0}$, $\mathbf{P_0}$, and $\mathbf{Q_0}$) are not required as inputs to the ANN. Since it is desirable to minimize the number of inputs to ANN, the set of input variables that have the strongest relationship with the output should be selected. Generally, the heuristic understanding of the problem is used to select the best inputs. In the absence of such a priori knowledge, a systematic study need to be done to select the best combination of input features.

3.2 Design of ANN

3.2.1 Multilayer Perceptron Network

Among the numerous artificial neural networks which have been proposed, the most widely used type of neural network is the Multilayer Perceptron (MLP) Networks, also known as the multilayer feed-forward network [53]. A feed-forward neural network provides a general framework for representing non-linear functional mappings between a set of input variables and a set of output variables. This is achieved by representing the non-linear function of many variables in terms of compositions of non-linear functions of a single variable, called activation functions [54].

The architecture of a feed-forward neural network is shown in Figure 3.2. The ANN consists of successive layers including an input layer, hidden layers and an output layer of neurons. A circle represents a neuron. The line between two neurons represents the weight relationships. The connections only run from every neuron in one layer to every neuron in the next layer, but with no other connections permitted. The activation function is applied on each neuron of hidden layers. In this thesis the activation function used is the Sigmoidal function which is shown in equation (E.3) in Appendix E. The output layer is compared to a target and the derivatives of the error is applied in a backpropagation process to adjust the weights [54].

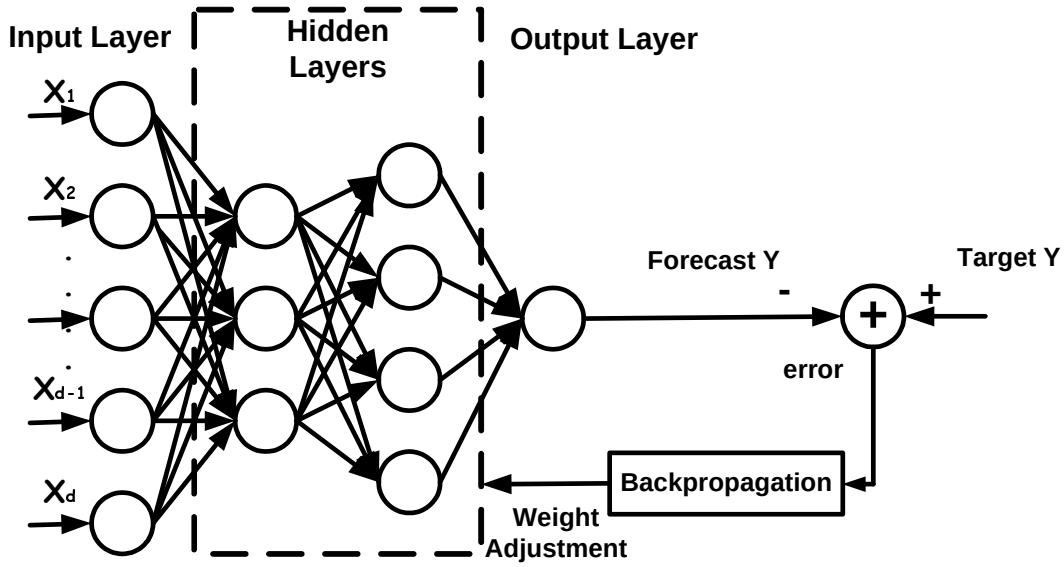

Figure 3.2: Multilayer Perceptron (MLP) Network structure and learning process

3.2.2 ANN Training Scheme

Figure 3.3 illustrates the complete process of designing an ANN based voltage stability margin estimator. The three main steps of training the ANN are as follows:

1. A large number of cases with different load/generation levels is randomly created. The random cases are gathered through a conventional power flow program to ensure that only the acceptable cases pass into the next step. This process is used to generate sufficient training patterns for ANN training algorithm.

2. A CPF program is used to generate the voltage stability margin which serves as a voltage stability index for each input data. This is the target output of the ANN to be trained.

3. The input features and output index are fed into the ANN training algorithm.

During the testing process, the trained ANN can be used to predict the voltage stability index for cases unseen by the ANN.

3.2.3 Preparation of Training Data

In order to generate random operating points under normal operation of the power system, random disturbances were added to the base case active and reactive power of the loads and generators. Furthermore, small random disturbances were added to the base case generator voltages magnitudes. The following model is used to generate these random input data for the power flow [55]:

- For Load Buses

$$P_L^i(k) = P_{L0}^i \left(1 + 2\Delta_{PL} \left[0.5 - \varepsilon_{PL}^i(k) \right] \right) \tag{3.2}$$

$$Q_L^i(k) = Q_{L0}^i \left(1 + 2\Delta_{QL} \left[0.5 - \varepsilon_{QL}^i(k) \right] \right) \tag{3.3}$$

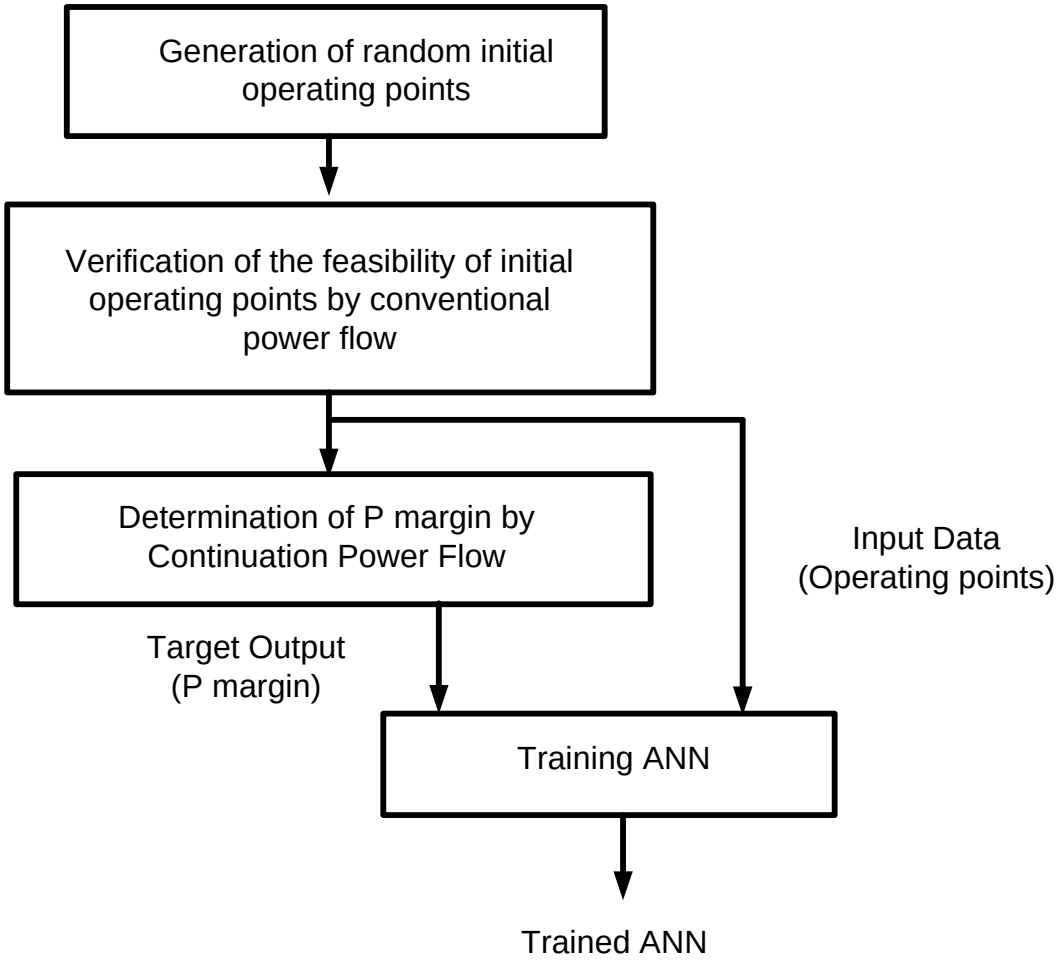

Figure 3.3: ANN training process flow chart

- For Generator Buses

$$P_G^i(k) = P_{G0}^i \left(1 + 2\Delta_{PG} \left[0.5 - \varepsilon_{PG}^i(k) \right] \right) \tag{3.4}$$

$$V_G^i(k) = V_{G0}^i \left(1 + 2\Delta_{VG} \left[0.5 - \varepsilon_{VG}^i(k) \right] \right) \tag{3.5}$$

Where, $P_L^i(k)$, $Q_L^i(k)$, $P_G^i(k)$, and $V_G^i(k)$ are the load active power, load reactive power, generator active power, and the generator voltage magnitude setting at the i^{th} bus for the k^{th} randomly generated case. P_{L0}^i, Q_{L0}^i, P_{G0}^i and V_{G0}^i are the base case

values of the corresponding variables. Δ_{PL}, Δ_{QL}, Δ_{PG}, and Δ_{VG} are the maximum fractional perturbation of the load active power, load reactive power, generator active power and the generator voltage magnitude respectively. In this study, Δ_{PL}, Δ_{QL}, and Δ_{PG}, were set to $\pm 30\%$, and Δ_{VG} of all generator and load buses was set to $\pm$ 3%. ε is a uniform independent random variables between 0 and 1.

If the expected variation of load on a particular bus is over 30%, the random disturbance range can be adjusted to accommodate that. In this thesis, we consider $\pm$ 30% range of load variation to train the ANN. If the load variation in a 24 hours period is within this range, a single ANN is sufficient to cover the 24 hour period. If the variation is higher, say $\pm$ 60%, then two or three ANNs would be needed for different times of the day, depending on the load forecast.

The randomly generated sets of initial operating points using the above model should be verified by a power flow program to make sure that each of the cases has a feasible power flow solution. The cases that passed through this screening process are stored and used as input vectors for training the ANN. Target outputs of the ANN, the voltage stability margin values corresponding to each case, were generated using the CPF program. Starting from an initial operating point, the CPF program traces $P - V$ curve along a specified load direction up to the voltage collapse point, and calculates the margin. After training an ANN, the trained ANN has the capability to predict the voltage stability margin even when it encounters an unseen operating point.

3.2.4 Performance Measures

Two performance measures are used in this thesis to evaluate the performance of the testing data, Mean Absolute Error (MAE) in (3.6) and Maximum Error in (3.7):

$$MeanError\% = \frac{1}{M}\sum_{i=1}^{M}\frac{|y_i - y_0|}{y_0} * 100\% \tag{3.6}$$

$$MaxError\% = \frac{max|y_i - y_0|}{y_0} * 100\% \tag{3.7}$$

Here, y_0 is the target voltage stability margin obtained from the CPF program and y_i is the voltage stability margin estimated by the ANN. M is the number of unseen cases.

3.3 Selection of Input Features

Generally, ANN works as a black box model that relates inputs X and outputs Y, which represents a mathematical relationship, $f : X \rightarrow Y$. It is crucial that we use key physical parameters X contributing to the output Y in ANN models. Some different sets of input variables to the ANN based on a heuristic understanding and knowledge of the voltage stability problem are tested.

3.3.1 Comparison of Four Sets of Input Features

The input vector X of ANN is composed of the variables that represent a base operating point. The voltage stability margin can be expressed as a function of any two (or more) variables of V, θ, P, and Q that define a system operating point. The selection of representative input features is important for the success of ANN application. In [56], real and reactive power injections at all load buses are used as the inputs to ANN. In [57], an input vector is formed by real power, reactive power and voltage magnitude at generator and load buses. In [58], voltages, characteristic impedances of load PQ buses and the total reactive power consumption are used as input variables. The ANN input vector in [59] is formed by voltage magnitudes, active/reactive load and generation, reactive reserve and OLTCs tap positions. The energy method for voltage security assessment and P, Q, and V_g was adopted as input variables in [60]. [61] used generator terminal voltages, real/reactive power of the generators, reactive power reserve of the generators and real/reactive power of the loads. However, none of these methods consider phase angles as input variables. Phase angles are generally thought of as less related to voltage stability.

In order to identify the best combination of inputs to the ANN, four different input data combinations were tried out. These include

1. Voltage magnitudes
2. Net active and reactive power injections
3. Voltage magnitudes and reactive power
4. Voltage magnitudes and phase angles

The fourth set of input features includes voltage phase angles, which is generally not considered as an important parameter in the voltage stability research reported earlier. It will be shown later; however, that the voltage phase angle is an important feature. For on-line applications, the phase angles can be obtained through Phasor Measurement Units (PMUs).

In order to train the ANNs, 3000 random operating points were generated using the model described in Section 3.2.3 and verified by a power flow program. Another 100 cases were created and verified through the same method to be used as the testing data to validate the performance of the trained ANN .

Figure 3.4 compares the accuracy of the estimated voltage stability margin (P Margin) by the ANNs trained with different input data combinations. The graphs plot the 'Target P margin' against the 'Forecasted P margin' by the ANN, for the 100 unseen test cases. If the target P margin completely matches with the forecasted P margin, all points should lie on the diagonal line. Table 3.1 lists the Maximum Error % and Mean Absolute Error % for the 100 unseen test cases.

Table 3.1: ANN performance with different input feature sets

Feature Set	1	2	3	4
Max Error %	4.8370	3.3119	1.5177	0.6566
Mean Error %	1.1068	0.6400	0.3416	0.1205

Figure 3.4 and Table 3.1 show that the ANN that uses Feature Set 4, which includes voltage magnitudes and phase angles of all buses, performs the best. This result indicates that voltage magnitudes and angles are the most appropriate features for ANN model. It is because phase angle is a good predictor of power flow and voltage

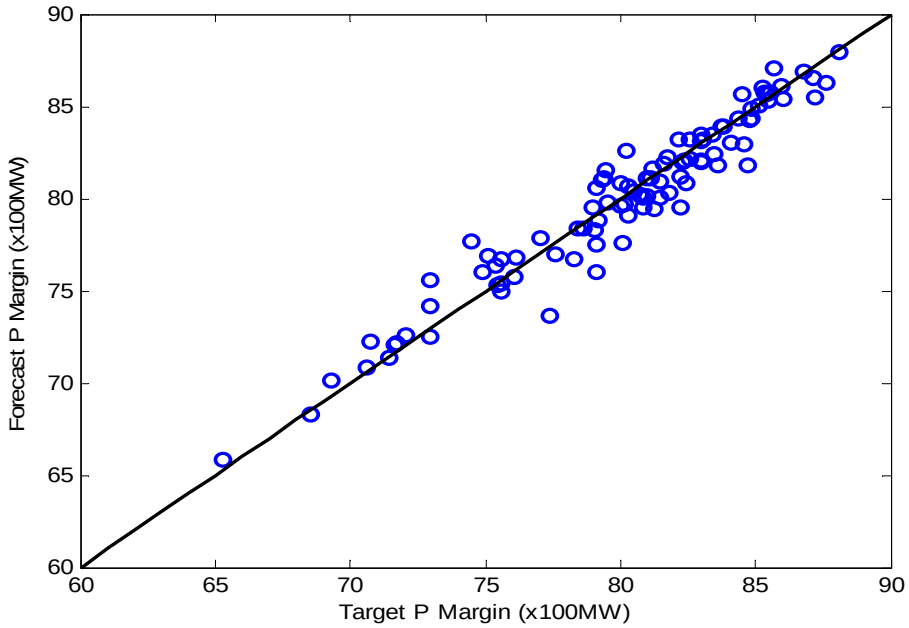

(a) Features Set 1: All bus voltage magnitudes

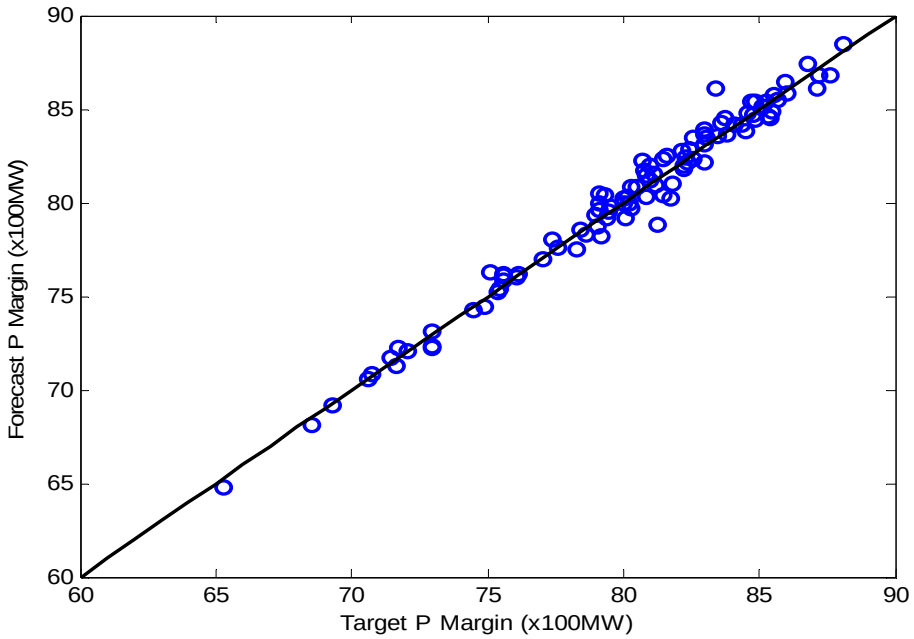

(b) Features Set 2: All bus net active
and reactive power injections

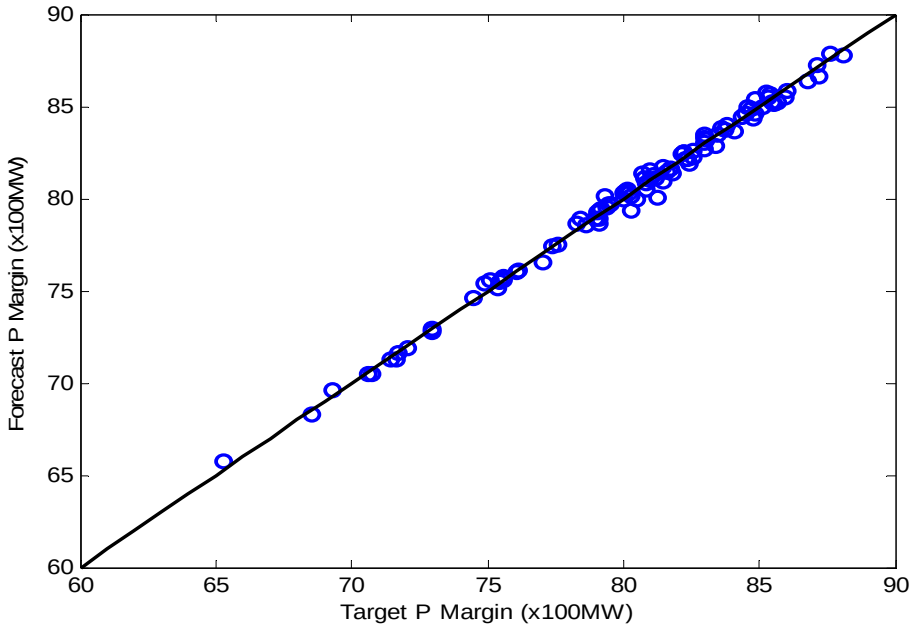

(c) Features Set 3: All bus voltage magnitudes and reactive generation

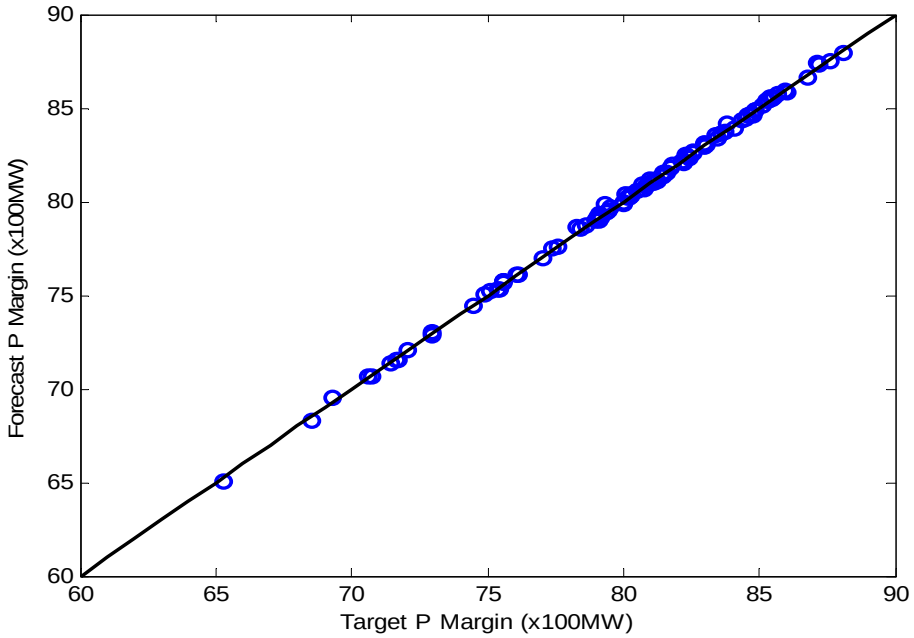

(d) Features Set 4: All bus voltage magnitudes and phase angle

Figure 3.4: The estimation of voltage stability margin with different input feature sets for ANN

is a good predictor of proximity to voltage collapse. Therefore, the ANN used for predicting the voltage stability margin represents the following nonlinear relationship:

$$\begin{pmatrix} V_0 \\ \theta_0 \end{pmatrix} \rightarrow P_{margin}$$

3.3.2 Discussion of the Suitability of V and θ

Although the test results of four sets of input features have shown that voltage magnitudes and phase angles are the most appropriate inputs of ANN to predict voltage stability margin, it is important to analyze this further to ascertain the reason.

From equation (2.1), we know that there are four quantities associated with power flow formulation: active power P, reactive power Q, voltage magnitude V, and voltage angle θ. Once either two variables are known, the other two variables can be obtained by solving equation (2.1). Any two variables of V, θ, P, and Q are sufficient to define the operating point and are necessary to be inputs of ANN.

There are six different ways to solve two quantities by knowing the other two quantities as shown in Table 3.2. If voltage magnitude V and voltage angle θ are known, active power P and reactive power Q can be directly computed by equation (2.1), which is one-to-one mapping. If active power P and reactive power Q are known, magnitude V and voltage angle θ can only be obtained by solving nonlinear equations using iterative methods. As equation (2.1) is a quadratic equation of V, there exist two real roots if the equation has real solutions. So, there are two V solutions for the same P and Q, but only one is a feasible solution. That is to say, obtaining V

and θ from known P and Q is one-to-many mapping. In addition, equation (2.1) has trigonometric function of θ, the solution of which is not straightforward.

Table 3.2: Methods of solving two quantities by knowing the other two quantities

Known quantities	Unknown quantities	Solving Method
V and θ	P and Q	directly calculation by equation (2.1)
P and Q	V and θ	iterative method
P and θ	V and Q	2nd order nonlinear equations
P and V	Q and θ	trigonometric nonlinear equations
Q and V	P and θ	trigonometric nonlinear equations
Q and θ	P and V	2nd order nonlinear equations

The above description shows that variables V and θ uniquely define the operating point so that they govern the voltage stability margin of a power system. Therefore, V and θ are chosen as input features to the ANN.

3.4 Discussion of ANN Training

The designing and optimizing process of a neural network could be very complex. As it is not the main focus of this research it will be given limited discussion. However, some major concerns in designing and building an efficient neural network model are discussed here.

3.4.1 Normalization

The input variables of an ANN are often of different types with different orders of magnitude, such as voltage magnitude (p.u.) and voltage angle (degree/radian). This is similar to the outputs such as voltage stability margin. It is necessary to normalize

the inputs and outputs based on their different data ranges so that they always fall within a specified range. For example, setting minimum -1 and the maximum +1 so that all the data fall within the interval [-1, 1]. Assuming the continuous interval of original variables is $[a, b]$, the data is transformed to [-1,1] by the one to one mapping:

$$x^* = \frac{2(x-a)}{(b-a)} - 1 \tag{3.8}$$

After training and testing, the neural networks convert the outcome back into the same units that are used for the original variables.

3.4.2 Overfitting or Underfitting

One purpose of ANN training is to exhibit good generalization, that is, to make good predictions for new inputs that are not seen in the training phase. This highlights the need to optimize the complexity of the ANN model in order to achieve the best generalization [54]. The complexity can be varied by changing the number of hidden neurons and layers in the network. Selecting too few hidden units may result in underfitting and selecting too many hidden units may result in overfitting [62].

In order to select an optimum ANN model, five models having different numbers of hidden neurons or layers are compared. For example, 77-3-1 means 77 elements in the input layer, 3 neurons having sigmoidal activation functions in one hidden layer, and an output layer with 1 neuron [63]. The rest may be deduced by the same analogy. Five types of multilayer feed-forward networks are implemented for 39-bus system,

namely 77-3-1, 77-5-1, 77-10-1, 77-2-2-1, 77-3-3-1. Each model includes the same input layer and output layer but different hidden layers.

Table 3.3: Various neural network models

		77-3-1	77-5-1	77-10-1	77-2-2-1	77-3-3-1
3000 Training Data	MSE	0.0164	0.0130	0.0060	0.1786	0.0471
	Time (s)	51.5345	73.4790	107.1339	37.0557	42.5802
100 Testing Data	Max Error %	0.4826	0.7633	0.3004	2.1846	1.1258
	Mean Error %	0.1269	0.1079	0.0749	0.3809	0.1953
	Time (s)	0.2312	0.3532	0.4808	0.2423	0.3229

Table 3.3 shows the performance for the 5 configurations of ANN models. It is observed that the more neurons there are in one hidden layer, the better the performance it achieves. For example, the model with five neurons in the hidden layer has better performance than the one with three neurons. The model with ten neurons in a hidden layer has better performance than the one with three or five neurons. On the other hand, once the networks have more hidden layers and turn to more complexity, poor generalization capability happens. For the studied 39-bus system, a model with two hidden layers does not perform well on the unseen data set due to the fact that the system is overfitting. In the 39-bus study system, 77-10-1 results in the best performance but its training time costs twice the time of 77-3-1 and 50% times more than 77-5-1. When the ANN method is applied into a power systems of practical size, it is necessary to balance between the performance and time in order to choose the proper model for practical usage.

3.4.3 Sampling Data Size

A common question in neural networks is "How much sample data do I need to train the network?". There are no simple rules to answer this question. It does definitely need sufficiently large and representative data for the neural network to learn. However, the sampling data size is dependent on many factors related to the problem being investigated such as feature selection and the neural network model.

Table 3.4: Sample size affect performance

Number of Samples	Training Data		Testing Data	
	Time (s)	MSE	Max Error %	Mean Error %
500	41.7825	0.0707	1.0792	0.2011
1000	44.0347	0.029	0.5734	0.1493
1500	47.4860	0.0241	0.5480	0.1448
2000	49.0616	0.0227	0.6499	0.1390
2500	50.0683	0.0173	0.4946	0.1276
3000	51.5345	0.0164	0.4826	0.1269
3500	59.0836	0.0189	0.5041	0.1303
4000	143.7961	0.0186	0.5012	0.1302
4500	219.0792	0.0187	0.5039	0.1310
5000	390.8599	0.0227	0.4195	0.1408
5500	429.1512	0.0233	0.4408	0.1424
6000	469.3999	0.0234	0.4433	0.1427
6500	507.5562	0.0224	0.4200	0.1420
7000	549.0818	0.0232	0.4712	0.1423
7500	584.6677	0.0233	0.5016	0.1422
8000	620.0798	0.0232	0.4803	0.1424
8500	656.5283	0.0228	0.4526	0.1422
9000	697.0825	0.0227	0.4240	0.1422
9500	730.8148	0.0186	0.5328	0.1301
10000	762.3145	0.0183	0.5274	0.1293

Assuming the feature selection and the neural network's algorithm and/or architecture are specified, different amounts of sample data are used to train the ANN and then tested on 100 unseen cases. The amounts of sample data was chosen from 500

to 10000 input vectors. The result is shown in Table 3.4. Only the training performance MSE is plotted in Figure 3.5 as the other performance measures are similar. From Figure 3.5 one can conclude that 3000 sampling data is enough for this neural network's training.

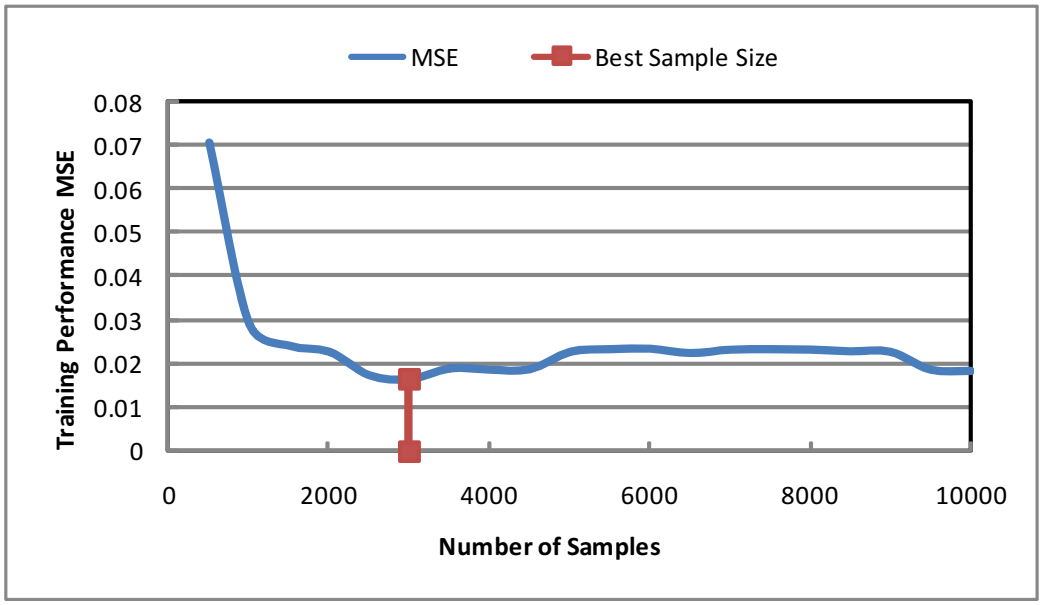

Figure 3.5: Training performance MSE for various sampling size

3.4.4 PMU Measurement Error

Voltage magnitudes and phase angles, which are found to be the best predictors of the voltage stability margin, are obtained by PMU measurements. Although the PMUs are precision level measurement units, there is a possibility that the signal processing may introduce some errors in the phasor calculations. According to IEEE Standard for Synchrophasors for Power Systems 2005 [64], the Total Vector Error (TVE) is an important criteria that must be <1% under steady state conditions. The TVE is

the "vector" difference between the exact applied signal and the measuring one. For example, an exact input is defined precisely by its phasor representation, $x = x_r + jx_i$; and its measuring representation is $x^* = x_r^* + jx_i^*$. The expression of TVE can be represented as [64]:

$$TVE = \sqrt{\frac{(x_r^* - x_r)^2 + (x_i^* - x_i)^2}{x_r^2 + x_i^2}} \tag{3.9}$$

This PMU measurement induces voltage magnitude error Δ_{Vi} and phase angle error $\Delta_{\theta i}$ into real values. Errors in magnitude Δ_{Vi} directly correlate to TVE and 1% magnitude error without angle difference is 1% TVE. If the vectors have identical unit magnitude then 0.57 degrees phase angle error is 1% TVE. The values of Δ_{Vi} and $\Delta_{\theta i}$ were randomly selected such that TVE $\leq$ 1%. The new inputs x_i^* with measurement error can be represented as equation (3.10) and are fed into the ANN.

$$\begin{aligned} V_i^* &= V_i(1 + \Delta_{Vi}) \\ \theta_i^* &= \theta_i + \Delta_{\theta i} \end{aligned} \tag{3.10}$$

Table 3.5 depicts the Maximum Error % and Mean Error % for the unseen cases. The results show that the ANN is still able to accurately estimate voltage stability margins in the presence of PMU errors.

Table 3.5: Impact of PMU measurement error to voltage stability margin estimation

	No measurement error	With measurement error
Max Error %	0.6566	1.1222
Mean Error %	0.1205	0.2559

3.5 A Case Study for a Large System

The proposed ANN based approach for voltage stability margin estimation is also applied to the Alberta Interconnected Electric System which was acquired from the Alberta Electric System Operator (AESO) website. The system consists of 1844 buses of which 746 are load buses and 302 are generator buses. The base load capacity is 7151 MW and generation is 7529 MW. The initial operating points are computed by PSAT [50], a commercial power flow analysis tool within Powertech's DSATools^{TM} suite. The voltage stability margin is computed by the voltage security assessment tool VSAT [30], which is also a key part of Powertech's DSATools^{TM} suite.

The random disturbance range uses the same pattern as described in Section 3.2.3 where the range of active and reactive power of load/generation are set to $\pm 30\%$ and the range of generator voltage is set to $\pm 3\%$. Among a number of random operating points generated by the pattern, 3000 initial operating points pass verification of feasibility by PSAT. These verified 3000 cases are selected to perform the voltage stability analysis in VSAT. In VSAT, the direction of the load increase is to scale all the load of the whole system together to voltage stability margin. At the same time, the generation of the whole system is dispatched to satisfy the increased load demand.

The credible operating points and their corresponding voltage stability margins of the 3000 cases need to be fed into an ANN as inputs and outputs for training the ANN. The Alberta system has 1844 buses or 3688 voltage magnitudes and phase angles that could be used as input features for the ANN. We selected only the buses whose voltage levels are equal or higher than 138KV as input features. In total, 723 buses are selected. Hence, 1446 (723x2=1446) voltage magnitudes and phase angles are

used as inputs in the ANN. One hundred test cases generated by the same method as the training cases are applied after training the ANN. The results of the voltage stability margin estimation performance are shown in Figure 3.6.

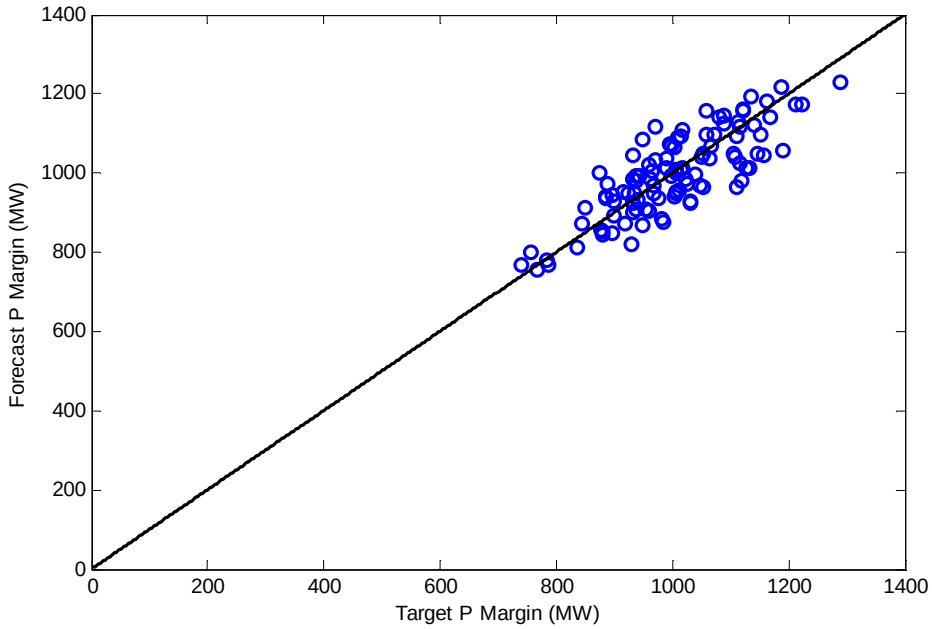

Figure 3.6: Voltage stability margin estimation for Alberta system

The mean error of the unseen cases for the AESO system is 5%, and is larger than that for the 39-bus system (mean error <1%). The result shows that the ANN based approach is feasible to be applied for a practical and large size power system. However, the accuracy of estimation for the practical system still needs to be improved. There are three main reasons for the increased error. First, we have not tried to optimize the ANN for the practical system. The same structure of ANN used for the 39-bus system is used for AESO system. A possible way to improve the accuracy is to optimize the structure of the ANN. Second, the practical power system requires a large number of inputs to properly represent them in voltage stability margin es-

timation. We used only 723 buses out of 1844 buses as inputs for training an ANN, which may account for the increase in the mean error. Third, the larger the system is, the larger the size of training set that is required. For comparison, the practical system uses the same size of training set (3000 cases) as the 39-bus system. If new cases are added to the training set, the accuracy would be improved.

3.5.1 Computational Speed

An artificial neural network is a learning system in which the network is trained by providing it with information of a specific system. Usually this training step requires significantly higher processing time than what is needed to assess the system using a single simulation.

The training time of both the 39-bus system and the Alberta system is recorded in Table 3.6. For both systems, 3000 training sample data is employed for training ANNs. All the computations are executed using a desktop PC, Intel Pentium Dual CPU E2200 @ 2.20GHz. Table 3.6 shows that the practical system requires more training and testing time than 39-bus system as the practical system has many more inputs.

Table 3.6: ANN training CPU time

	New England 39-bus System	Alberta 1844-bus System
Training CPU Time (s)	146	4082

There is always a concern when applying ANN method into a practical system. The major advantage of applying computational intelligence technique to replace the con-

ventional analytical algorithms for voltage stability analysis is its feasibility of real-time operation. ANN is able to sufficiently abstract what it learns in training and extend this to produce reasonable outputs for those inputs not encountered during training. Once trained, an ANN can predict the stability margin for a given set of inputs very quickly as the calculations in the ANN do not involve any iteration as in the case of using analytical methods. Therefore, practical utilization of the neural network model should consider the computational speed after training.

The comparison of the computational speed of the analytical methods (continuation power flow) and computational intelligence (ANN) has been studied as shown in Table 3.7. This Table demonstrates that using neural networks to estimate voltage stability margin is much faster than the continuation power flow method. To predict margin for a certain operating point, the computation time of neural networks is only 1% of that required by the continuation power flow program. For the practical Alberta system, the computation time of neural networks is 2.75% of that required by the analytical method.

Table 3.7: Comparison of the computation time cost by CPF vs. trained ANN

	Analytical Method		Trained ANN	
	39-bus	1844-bus	39-bus	1844-bus
CPU Time (s)	3.53	4.0	0.04	0.11

Chapter 4

Further Applications of ANN

In this chapter, the applications of the ANN approach are further explored. First, an ANN based approach to determine the best locations for PMUs is presented. Second, the ANN approach is used to predict post-contingency voltage stability margin. Finally, the preventive control for power system operating in alert state where the voltage stability margin is not sufficient is investigated. In this application, the sensitivity of the ANN approach is employed to reschedule generation for improving the voltage stability margin.

4.1 Optimal Placement of PMUs

Real-time measurement of voltage magnitudes and phase angles requires the use of PMUs and telecommunication infrastructure to support the data acquisition. The gathered voltage magnitudes and phase angles from the monitoring system are the inputs of the ANN for predicting the on-line voltage stability. If the ANN approach requires voltage magnitudes and phase angles of all the buses over the power system,

PMUs have to be installed on every bus. For example, the 39-bus system has 77 original input variables. It requires PMUs to be placed on every bus of the system to obtain the 77 input features. However, installation of PMUs at all buses in a power system is not economically justifiable. When only a limited number of PMUs are used, it is important to locate them at most effective positions in the network.

4.1.1 Optimal PMU Location Algorithm

Selection of PMU locations can be viewed as the selection of a reduced set of input features of the ANN while the prediction performance is not significantly degraded. In selecting a subset of d features from a set of n total features, the only search strategy that guarantees the optimum selection is an exhaustive search that tries all possible combinations of variables. The number of possible combinations is given by $C_n^d = \frac{n!}{d!(n-d)!}$. For example, if we want to select 5 PMU locations in the 39-bus system, we need to try $C_{39}^5 = \frac{39!}{5!(39-5)!} = 575757$ combinations. Any real power system is much larger than the 39-bus system and therefore, such an exhaustive search is unrealistic. As a solution we propose to use less cumbersome "sequential forward/backward selection (SFS/SBS)" algorithm [53] to determine the optimal input feature set. The sequential forward selection (SFS) is used more often due to the lower number of calculations involved.

SFS algorithm selects a best feature based on the quality criterion function from a pool of candidate variables at the beginning of search. The best one is stored for next selection. SFS obtains a chain of nested subsets of features by adding the locally

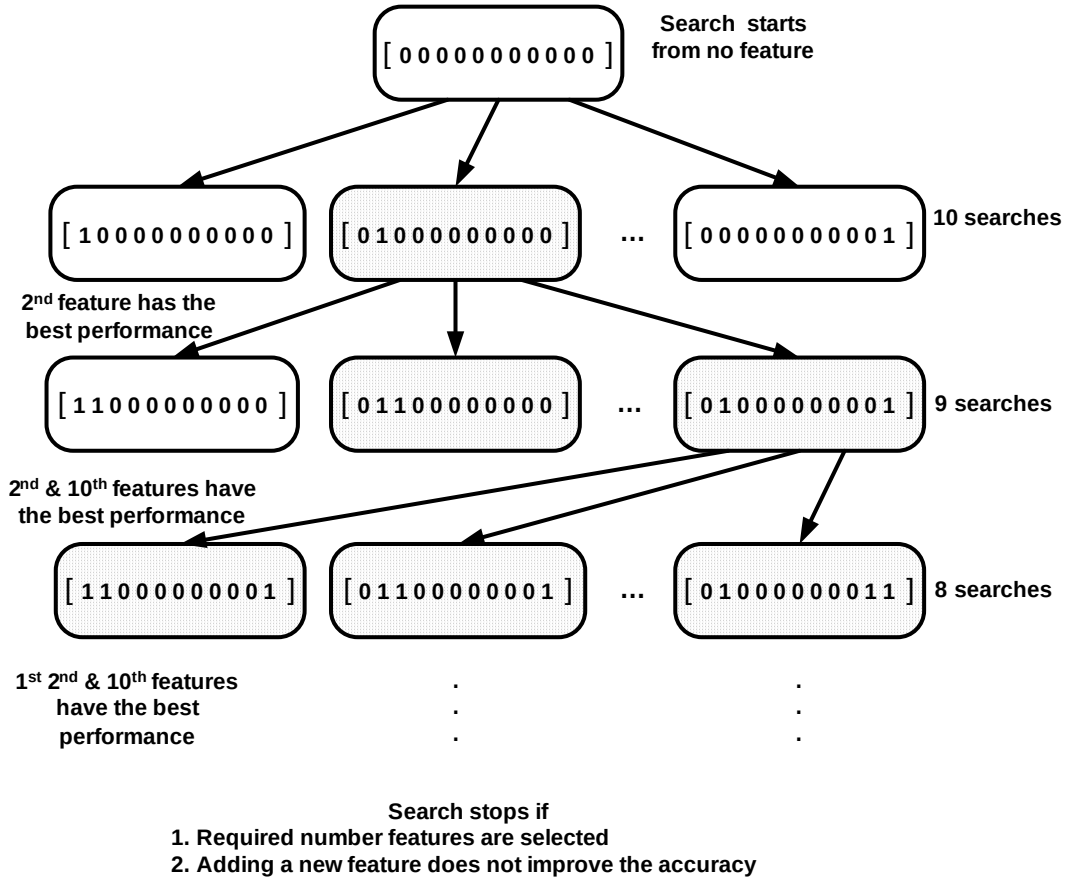

Figure 4.1: The flow chart of Sequential Forward Selection (SFS)

best feature in the set [65]. The algorithm is shown in Figure 4.1 with a total of 10 features as a sample but it can be extended to any number of features.

In sequential forward selection (SFS) algorithm, an ANN with only one input is considered at the beginning. An input feature from a pool of candidate features is selected and the trained ANN is evaluated using a "quality criterion function". The feature that gives the best value for the quality criterion function is retained for the next round of selection where the combinations of two input features are tried. The SFS algorithm obtains a chain of nested subsets of features by adding the locally best feature in the set.

When the required number of features d is known, the total number of searches required in selecting d features from a set of n is $n+(n-1)+(n-2)+...+(n-d+1)$. Thus for selecting 5 PMU locations from 39 possibilities, it needs $39+38+37+36+35 = 185$ searches to find the optimal combinations of features. In comparison to 575757 evaluations required in exhaustive search, SFS requires only 185 evaluations. The quality criterion function used in this thesis was the "minimum of the maximum error in predicting voltage stability margin for 100 test cases". The SFS algorithm is suboptimal, as the optimal feature subset that provides the best performance needs not contain the single best feature obtained earlier [66]. Although the selected combination of features may not be the global optimum, the SFS algorithm always selects a set of good input features.

4.1.2 Margin Estimation with Five PMUs

In the example presented here, it was assumed that only five PMUs are allowed in the 39-bus system. Application of the SFS algorithm described above resulted in the selection of buses 5, 10, 11, 30, and 35 as the optimal locations for installation of PMUs. Limiting of the number of PMUs reduced the number of inputs to the ANN from 77 to 10 (five voltage magnitudes and five phase angles). The performance of estimating the voltage stability margin with a reduced set of input features is shown in Figure 4.2.

The difference of P margin between neural network output and target values is shown in Figure 4.2. Compared to Figure 3.4 (d) which used 77 features, the performance is reduced. Hence, a trade-off between costs and accuracy has to be made.

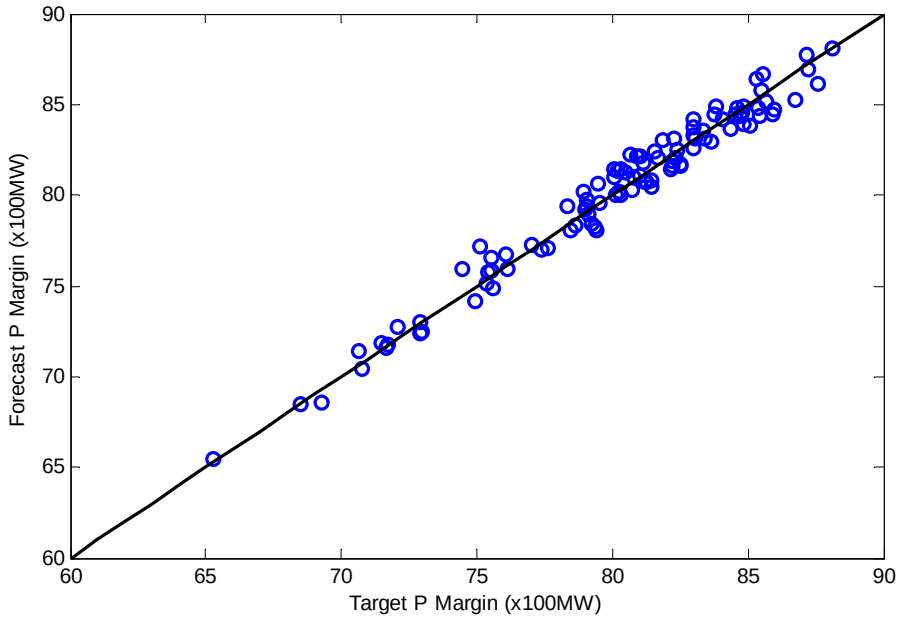

Figure 4.2: Voltage stability margin estimation with optimally located five PMUs

4.1.3 Comparison of Different Approaches of Locating PMUs

Several other approaches to place the PMUs in the power system were also tested. One approach is to place the PMUs in five buses with the largest load. It is clear that the heavily loaded buses play an important role in system voltage stability. Another option is to choose three heavily loaded buses and two buses with largest generation. The third option is to choose the buses which are corresponding to the larger values in the singular vector of Jacobian matrix.

Singular value (or eigenvalue) is a well known index to predict proximity to voltage collapse problems. Its derivative vectors can be used to pinpoint critical buses in the power system [36]. So the measurements at these locations are likely to carry more

information on voltage stability. The detailed computation of singular value and singular vector can be found in Appendix D. In voltage stability assessment, the most critical singular vector of Jacobian matrix is the one corresponding to the voltage stability limit on the $P-V$ curve. In power flow computation, when Jacobian matrix reaches the singular point, both the singular value and its corresponding singular vector are obtained. Ranking the singular vector is to rank the critical buses. The top five buses corresponding to the entry in the singular vector were 7, 8, 12, 4, 15. Therefore five PMUs were located on these five places.

Summarizing the above, four sets of PMU positions are chosen based on the above mentioned four methods:

- SFS selects PMUs position: Bus 5, 10, 11, 30, 35.
- Five largest load buses (listed from largest to smallest MW): Bus 20, 8, 4, 16, 2 (or 3). Since Bus 2 and Bus 3 had the same amount of load, either was used.
- Three largest load buses: Bus 20, 8, 4; and two largest generator buses: Bus 39, 38.
- Larger value in the singular vector: Bus 7, 8, 12, 4, 15.

The results of the different PMU placement approaches are listed in Table 4.1. These results show that the optimum locations obtained using SFS result in smaller error measures compared with those locations obtained using other methods.

Table 4.1: Comparison of PMUs location methods

	MSE	Max Error %	Mean Error %
SFS Bus 5, 10, 11, 30, 35	0.6074	3.2726	0.7485
5 Largest Load Bus 2(/3), 4, 8, 16, 20	2.6624/2.7088	4.8062/4.7278	1.6485/1.7016
Largest 3 load and 2 GEN Bus 4, 8, 20, 38, 39	2.6689	6.7030	1.6217
Sigular Vector Bus 7, 8, 12, 4, 15	0.8899	3.7995	0.9135

4.1.4 Number of Measurements

Compared to the results shown in Figure 3.4 (d), which were obtained using the voltage magnitudes and phase angles of all buses as inputs, the performance shown in Figure 4.2 is somewhat less accurate. Since the number of PMUs in the power systems is limited, is it possible that we use the existing measurement signals along with the PMU measurements? The following test is carried out to see if the prediction error can be reduced by adding more PMUs or by adding traditionally available measurements, such as voltage magnitudes V and reactive power Q. Table 4.2 compares the results of voltage stability margin estimation for the 39-bus system with different sets of inputs:

1. Five voltage magnitude and angle measurements at the optimal locations,
2. Voltage magnitude and angle measurements at the 5 optimal locations plus voltage magnitude and reactive power measurements at 5 additional locations,
3. Voltage magnitude and angle measurements at 10 locations which include the 5 optimal locations,
4. Voltage magnitude and angle measurements at all buses.

Table 4.2: Comparison of P margin estimation with different number of measurements

	5PMUs	5PMUs +5V+5Q	10PMUs	PMUs at all buses
No. of features	10	20	20	77
Max Error %	2.2614	1.5906	1.0779	0.6566
Mean Error %	0.6528	0.5816	0.4009	0.1205

Compared to the results of full features with PMUs at all buses, the performance obtained with only five PMUs is somewhat less accurate. The prediction error can be reduced by adding more PMUs or by adding traditionally available measurements, such as voltage magnitudes V and reactive power Q as inputs to the ANN. Two tests were carried out: (i) with V and Q measurements from buses 3, 4, 9, 13 and 37 in addition to the five optimal locations mentioned above, and (ii) with PMU measurements at all the locations considered in (i). The prediction errors with the full feature set and the reduced feature sets are compared in Table 4.2. The results indicate that a trade-off between the costs and the accuracy needs to be made in deciding the number of PMUs used. For the locations without PMUs, the traditional signals such as reactive power can be used to enhance the prediction accuracy. Although the effect of these conventional signals is not as good as the PMUs, they are better than none.

4.2 Post-Contingency Margin Estimation

The voltage stability margin estimation by ANN approach is not sufficient to help the operator to determine the system security. Security of power system supposes that the robustness of the system can be guaranteed in case of credible contingencies. It is particularly important for the proposed ANN system to be able to estimate the voltage stability margin after a system disturbance or contingency [32]. The standard

procedure in many utilities is to consider N-1 contingencies [67], which means the normal system minus one element. The system restoration after a contingency often requires removal of the faulted element, resulting in a new network configuration. Traditionally, the N-1 contingency analysis has been used for on-line stability assessment.

4.2.1 Approach for Post-Contingency Voltage Stability Margin Estimation

There are two possible approaches for handling the issue of predicting voltage stability margin under different network configurations: (i) to train an ANN for each network configuration, or (ii) to train a single ANN that can estimate the voltage stability margin under all credible post-contingency network configurations. The second approach clearly has the advantage of not requiring a knowledge of the exact nature of the contingency among a set of credible contingencies before estimating the voltage stability margin. Here, the second approach is used, although training of an ANN capable of handling all contingencies is challenging.

The procedures for generating the training data of the ANN for post-contingency voltage stability margin estimation is similar to that described in Chapter 3. However, instead of using normal operating points as inputs of ANN, the post-contingency operating points are fed into ANN as inputs. The detailed steps are:

1. For each contingency, random initial operating points are generated using the same procedure that is used under normal operation.

2. Verify the feasibility of these operating points by running a power flow on the

post-contingency network.

3. These verified post-contingency operating points are used as inputs to the ANN.

4. The corresponding voltage stability margin values are computed using the CPF program to be the target outputs for training the ANN.

4.2.2 Case Study

In this case study, the N-1 contingencies considered are the outages of transmission lines. There are 35 transmission lines in the 39-bus system. Including a healthy system, there would be 36 different system configurations. For each system configuration, 400 random operating points are generated. This results in a total of 14,400 cases which need to be verified by power flow. If the post-contingency operating points are obtained, they are fed into the ANN as inputs; the corresponding voltage stability margins are the outputs. There are 360 cases (10 cases from each configuration) which have been reserved as the testing data. The rest of the data are used for training an ANN.

Figure 4.3 shows the voltage stability margin estimation performance for the unseen testing cases. It shows that a single ANN can successfully estimate the voltage stability margin under post-contingency situations, if the relevant N-1 contingencies were considered in generating the training data.

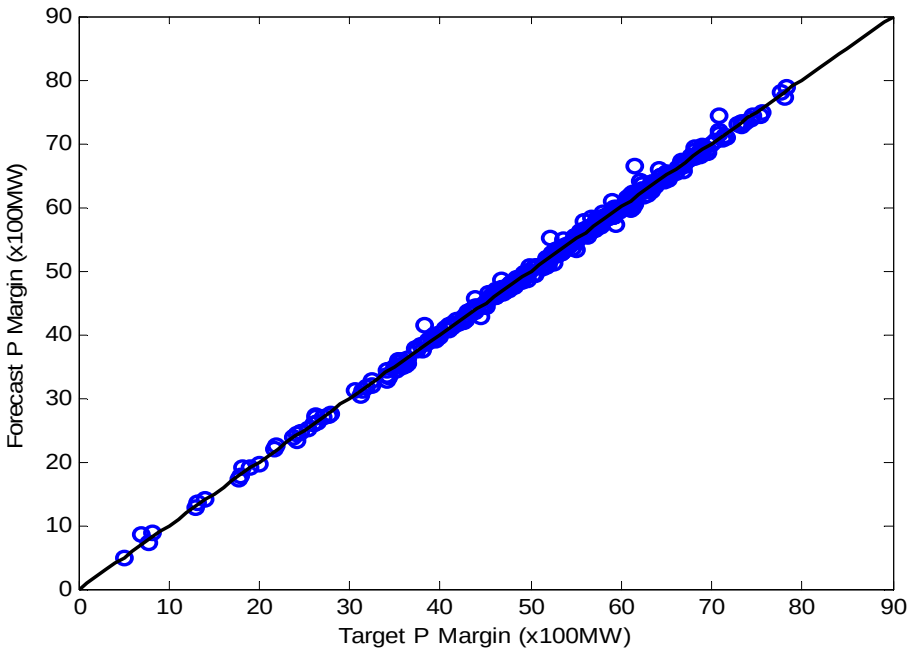

Figure 4.3: Voltage stability margin estimation under N-1 contingencies

4.3 Generation Rescheduling for Improving Voltage Stability

When the voltage stability margin is dropped below a comfortable level, especially after some disturbances, some preventive and corrective control actions need to be taken to mitigate a possible future voltage instability scenario. One possible control action is the rescheduling of real power of generators. The generation dispatch schedule divides the required generation capacity optimally among the available generators considering various operating conditions [68]. If an unexpected event drives the system close to voltage instability, the original generation dispatch may be modified to enhance the voltage stability margin. However, it is required to select the best way to change the generation output so that the voltage stability margin is improved.

The proposed method is to examine the sensitivity of the voltage stability margin to

shifting of the real power output from one generator to another. Different pairs of generators can be considered for shifting the power output and rank the pairs according to the sensitivity. The sensitivity of the voltage stability margin to shifting of real power generation can be quickly estimated using the ANN based voltage stability margin estimator. Therefore, if the changes in real power output are within the range of perturbations applied in generating the ANN training database, the already trained ANN is able to give a good estimate of the voltage stability margin after shifting the power output of a generator by a small amount. The change in voltage stability margin due to shifting of 1.0 MW of real power is taken as the sensitivity, which is used for ranking the control alternatives.

4.3.1 Application Example

In order to illustrate the application of the proposed use of ANN based scheme for selecting the generation rescheduling to improve the voltage stability, the post-contingency 39-bus system was used. In the N-1 contingency screen presented in Figure 4.3, there are several cases which have low voltage stability margins after the contingency. The worst case, that is the case with the least voltage stability margin, was selected for this example. It was found that the worst case occurs when one of the parallel lines between the buses 4 and 5 is removed. Meanwhile the closest generator to the removed line is G31 and its real power output is high under the base case generation dispatch.

The control actions considered are therefore shifting 50 MW of real power from Generator 31 to other generators. The voltage stability margin after shifting 50 MW

was estimated by using the trained ANN. The results are shown in Table 4.3. The voltage stability margins estimated by ANN are close to the actual voltage stability margins (calculated by using CPF). The sensitivities are calculated by dividing the corresponding changes in voltage stability margins by the amount of power shifted, in this case by 50 MW.

Table 4.3: Sensitivity of voltage stability margin to generator rescheduling

Generator Bus	Margin by CPF (p.u.)	Margin by ANN (p.u.)	Sensitivity by CPF	Sensitivity by ANN
Base Case	5.0627	4.9408		
30	7.9337	7.8612	0.0574	0.0584
32	7.4146	7.0624	0.0470	0.0424
33	7.9081	7.7616	0.0569	0.0564
34	7.9209	7.7458	0.0572	0.0561
35	7.9337	7.7989	0.0574	0.0572
36	7.9209	7.7600	0.0572	0.0564
37	7.8184	7.6779	0.0551	0.0547
38	7.8376	7.7295	0.0555	0.0558
39	7.9581	7.8906	0.0579	0.0590

From Table 4.3, the sensitivity is highest for the case of shifting the real power output from Generator 31 to Generator 39. Shifting 50 MW of generation would increase the voltage stability margin by approximately 290 MW. Once the control actions are ranked according to the sensitivity, other secondary considerations such as cost of generation can be taken into account when making the final decision on the voltage stability control action. The important fact to note is that the already trained ANN is used to quickly determine the impact of control actions on improving the voltage stability margin.

Chapter 5

An ANN for Assessment of Large-disturbance Voltage Stability

In the previous chapters, the neural network method has been successfully applied to small-disturbance voltage stability. Beginning in this chapter, the focus of the research moves to large-disturbance voltage stability. The ANN based algorithm is applied to predict a large-disturbance voltage stability index, i.e., transient voltage dip. The ANN approach is combined with a commercial time-domain simulation program to calculate transient voltage dip for given contingencies.

5.1 Overview

Large-disturbance voltage stability refers to the ability of a system to maintain steady voltages following large disturbances such as system faults, loss of generation, or circuit contingencies [11]. The time frame of interest for this kind of voltage stability is in the order of several seconds, and analysis requires solutions of appropriate system

differential equations. In some literature, the term *transient voltage stability* is also used to define the same situation. [11] recommended the term *transient voltage stability* not be used. Hence, large-disturbance voltage stability or short-term voltage stability are used interchangeably in this thesis.

Determination of large-disturbance voltage stability requires the examination of the nonlinear response of the power system over a period of time sufficient to capture the performance and interactions of such devices as motors, underload transformer tap changers, and generator field-current limiters. Traditionally, the large-disturbance voltage stability analysis requires the use of time-domain simulation software, such as Transient Security Assessment Tool (TSAT) [34]. TSAT is a software tool within Powertechs $DSATools^{TM}$ suite which includes a nonlinear time-domain simulation engine that gives accurate dynamic responses of a power system. When using a simulation program for short-term voltage stability simulations, appropriate portions of the loads need to be represented with dynamic load models (i.e., induction motors) since dynamic modelings of loads are often essential to assessing voltage stability. In addition, generators, excitation system, governors, and reactive compensation should be provided with detailed dynamic models as well for dynamic analysis to be performed. After simulation, the transient voltage dip can be obtained as a quantifying index.

Since a time-domain simulation program is very time consuming, the ANN based method is employed to be an alternative to simulation because of its advantage of fast computation speed. The selected simulation data is fed to a designed ANN to train the neural network and to form a trained ANN. Once trained off-line, ANN can

effectively predict the dynamic voltage stability index using less computational time.

5.2 Large-disturbance Voltage Stability Index

Different indices are available to quantify the voltage stability of a power system [36]. Most of them are applied for small-disturbance (or named as steady state) voltage stability as introduced in Chapter 2. A survey [69] on large-disturbance voltage stability indices currently applied or considered by various utilities, operating regions, and countries indicated that transient voltage dip/sag criteria following fault clearing is the most common used indicator. This criteria is currently applied by many utilities/organizations such as the NERC/WECC Planning Standards document [70]. NERC is the North American Electric Reliability Council, and WECC is the Western Electricity Coordinating Council. This thesis employs transient voltage dip criteria as a quantifiable index from the NERC-WECC planning standard to assess short-term voltage stability.

Figure 5.1 illustrates the definition of transient voltage dip that was taken from the NERC/WECC Planning Standards document [70]. In a large interconnection power network, voltage dip criteria is more convenient to use than power margin based criteria [69]. The transient voltage dip is defined as the percentage of maximum deviation of short-term voltage after voltage recovery following fault clearing over initial voltage of each individual bus. The initial voltage is the pre-fault voltage, labeled "V_0" in Figure 5.1. Different buses of the system have different voltage trajectories so that their transient voltage dips are also different. Figure 5.1 only demonstrates one bus voltage. Among all the transient voltage dips of buses, the largest dip represents the

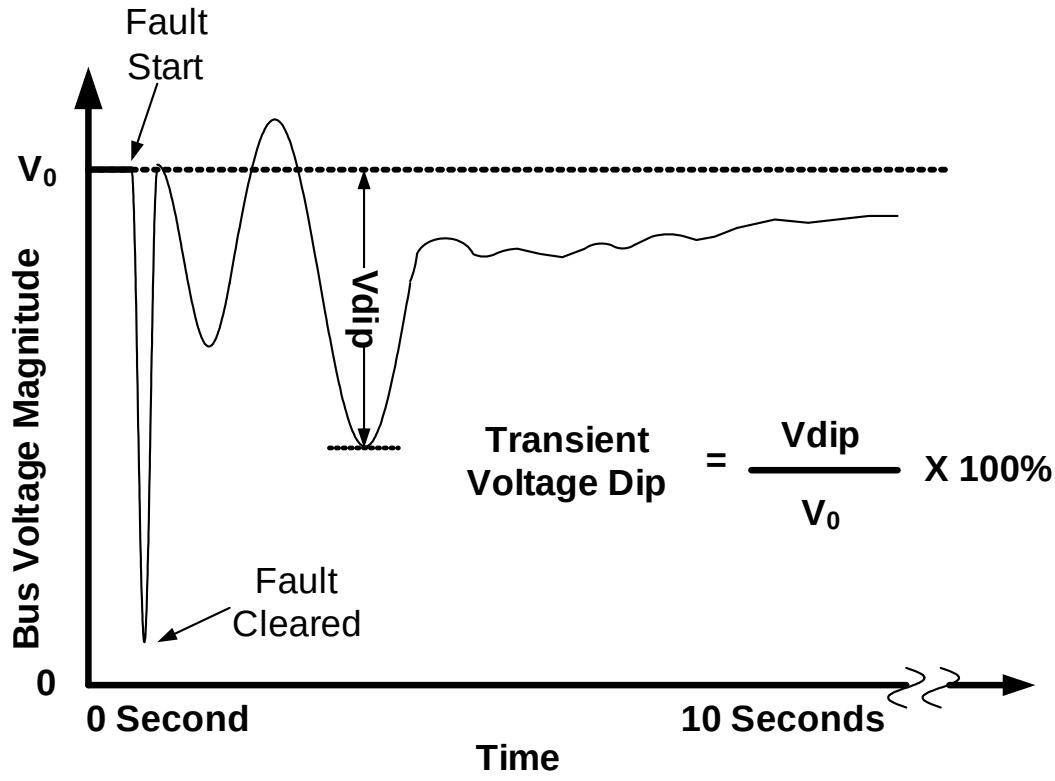

Figure 5.1: WECC voltage performance parameters

severity of the post-contingency behavior. In this thesis, the largest transient voltage dip among buses serves as the short-term voltage stability index. This is referred to as "transient voltage dip" hereafter in this thesis.

According to the definition by the NERC-WECC planning standard, disturbances are categorized into four performance levels: (A) no contingency, (B) an event resulting in the loss of a single element, (C) events resulting in the loss of two or more elements, and (D) an extreme event resulting in two or multiple elements removed or cascading out of service conditions. The following is an abstract of the standard related to voltage stability criteria.

- Category A (No contingency)

  Not applicable.

- Category B (Single Contingency)

  The maximum transient voltage dip should not exceed 25% at load buses or 30% at non-load buses.

  The transient voltage dip should not exceed 20% for more than 20 cycles at load buses.

- Category C (Double Contingencies)

  The maximum transient voltage dip should not exceed 30% at any bus. The transient voltage dip should not exceed 20% for more than 40 cycles at load buses.

- Category D (Multiple Contingencies)

  No specific voltage dip/sag criteria.

According to the NERC/WECC Planning Standards, Category B and Category C are applied for quantitatively assessing short-term voltage stability. However, there is no significant difference for the essential method except that Category B considers single contingency and Category C considers two or more contingencies occurring concurrently. Category B type contingency, the only one considered in this research, is a three phase to ground fault on a transmission line that is cleared after a certain time period by tripping the faulted line. The time-domain simulation is performed for each contingency to simulate system behavior during and post fault periods.

5.3 Data Required for the Simulation

The short-term voltage stability index, which is the transient voltage dip, is evaluated using the time-domain simulation. The following inputs should be provided to the simulation program to determine the transient voltage dip:

1. The steady state operating points, those feasible operating points before the occurrence of a contingency. They are referred to as the initial operating points.

2. The severity of the contingency. The fault location, fault type and fault duration essentially define the severity of the contingency.

3. The system data. The system data includes transmission line data, generator data, and other dynamic device data. The results of simulation depends heavily on the accuracy of the these parameters of the system components.

The transient voltage dip is obtained by examining the voltage trajectories of all the bus voltages in the power network. It is uniquely determined by the time-domain solution and therefore determined by the above data.

Generally, power system simulation can be seen as solving a set of differential and algebraic equations (5.1a, 5.1b). The differential equations (f) describe the dynamic behavior of the generators and their associated control systems, dynamic loads or any dynamic devices. The algebraic equations (g) describe the steady state behavior of the transmission and distribution network and buses.

$$\dot{x} = f(x, y, \mu) \tag{5.1a}$$

$$0 = g(x, y, \mu) \tag{5.1b}$$

Where, x is an n-vector describing the state variables of the system (generators and loads), y is a vector of the algebraic variables (voltage/current magnitude and phase angle) and μ represent the set of control system parameters of interest.

Three types of variables of equations (5.1a, 5.1b), x, y, and μ, are required to define an operating point of a power system. For dynamic stability analysis of a power system, initial operating points (y), state variables of system (x), and control parameters (μ) first need to be determined. Before the occurrence of a contingency, the time derivative of all the state variables ($\dot{x}$) is zero. If the algebraic variables, including the voltage/current magnitude and phase angle, are known, all the initial values of state variables and control variables can be determined. If the voltage magnitudes and phase angles of all the buses of the initial operating point in the network are known, the current of the connected devices can be computed using the nodal admittance matrix. Hence, the voltage magnitudes and phase angles at initial operating points uniquely determine the dynamic system behavior at the starting point of time-domain simulation. In a power system study, we can select a certain number of credible contingencies for the studied network, hence the contingency is known. For a power system for analysis, the dynamic data, is known. Therefore, once we have the information of voltage magnitudes and phase angles at the initial operation point, the short-term voltage stability index (transient voltage dip) can be determined.

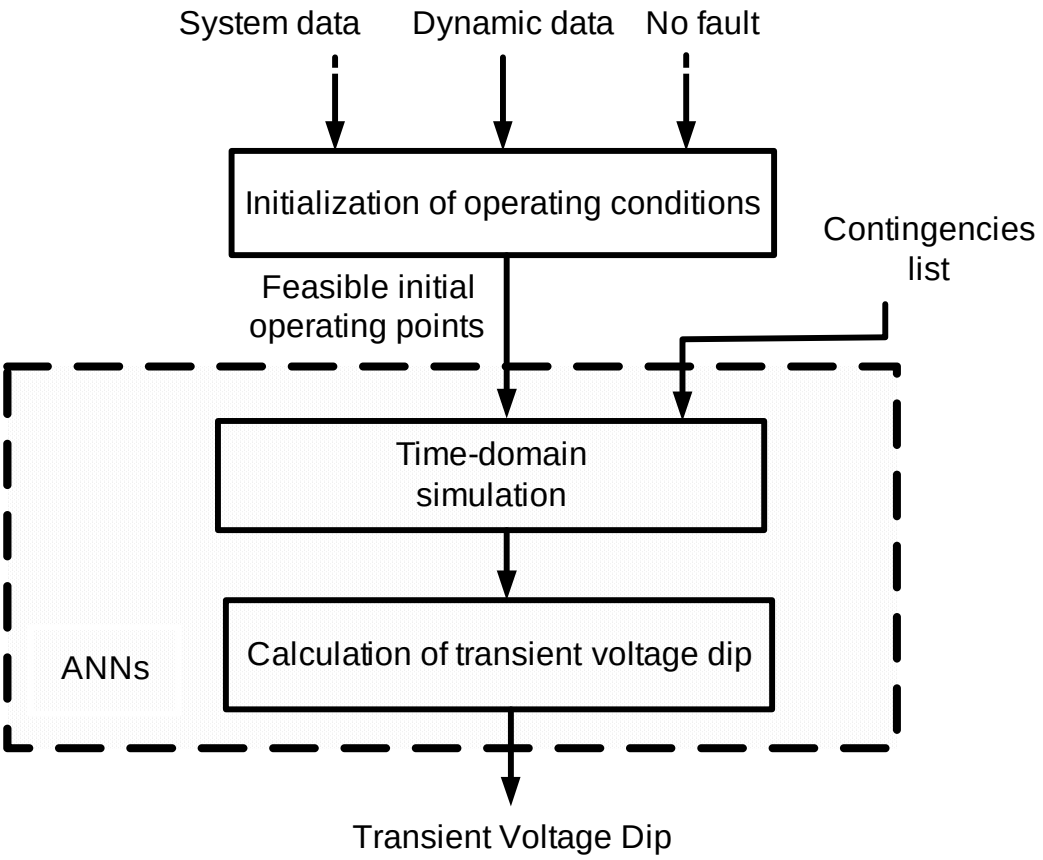

Figure 5.2: Procedure of computing transient voltage dip

5.4 Framework of ANN Approach

Figure 5.2 shows the procedures of computation of transient voltage dip by time-domain simulation. In order to use neural networks to imitate the computation of transient voltage dip, it is essential to understand the process of time-domain simulation and the program that computes transient voltage dip.

Occasionally, a set of system data may or may not be the system real operating point. To obtain the real operating point, it needs to be solved by the overall system equations (5.1a and 5.1b). After a time-domain simulation program successfully solves

the equations, a balanced steady-state representation of operating point is obtained. Later, this operating point is subjected to a contingency. The simulation program determines the system response to this contingency within a period of time. After simulation, a developed program in Matlab traces the trajectories of all of the bus voltages to calculate the transient voltage dip for the given contingency.

When applying the ANN approach to determine the transient voltage dip, ANNs should be able to replace all the computations shown in the block area of Figure 5.2. For each given contingency, a corresponding ANN is designed to work as a black box model between input and output of the shadowed area. The voltage magnitudes and phase angles at pre-contingency are adopted as input variables of the ANN. The transient voltage dip at post-contingency is the output of the ANN.

Artificial neural network can be an alternative to time-domain simulation to predict transient voltage dip only after being trained. The upper-part of Figure 5.2 illustrates the procedures of ANN training strategy and generation of the input data. The input variables are generated in two steps:

1. A number of random load and generation patterns are generated to obtain operating point around the base operation points. The pattern uses the same model described in Section 3.2.3.

2. The simulation program TSAT is applied to ensure the random data have acceptable dynamic simulation at steady state.

For the first step, random operating points are generated using the same procedure that is used for long-term voltage stability margin estimation. For the second step,

the verification step is different. A simulation program is applied in short-term voltage stability rather than a power flow program in long-term voltage stability. This is because only verification of feasibility of the power flow data is not sufficient. The dynamic data needs be included. It is important to perform a sanity check of the data in time-domain simulation before doing any further studies.

A power flow should be solved before carrying out the dynamic simulation. The power flow solution is used for the initialization of state variables of generators, excitation system, and governors, as well as all the controlling devices and induction motor loads. Since the TSAT program has a built-in power flow solver by enabling an option of "solve base power flow before simulation", it is applied directly to verify the feasibility of these randomly generated operating points. Furthermore, all the initial conditions are checked for violation of the controller limits.

5.5 Modeling for Time Domain Simulations

There is a vast amount of published technical literature dealing with the modeling of the broad field of system components. Different mathematical representations of power system components apply to different study problems. In order to study large-disturbance voltage stability in the short term time frame, the following fast acting, automatically controlled power system equipment are considered in the simulation:

- Synchronous machine
- Excitation system
- Power system stabilizer (PSS)

- Prime mover
- Voltage-dependent load
- Induction motor

5.5.1 Synchronous Generator

Synchronous generators are the absolute dominating source in power systems. They can generate active and reactive power independently and have an important role in maintaining a good voltage profile across a power system. Therefore, an understanding of their characteristics and accurate modeling of their dynamic performance are of fundamental importance to the study of power system stability [10].

The theory and mathematical modeling of synchronous machines have been covered in a number of books. While there are no nationally or internationally sanctioned standards on the modeling of power system equipment, there are several data file formats that have become quite widely used and recognized as convenient vehicles for mechanizing the burdensome task of building up databases for simulations of interconnected systems. The PSS/E [33] dynamics data file format may reasonably be regarded as one of these widely recognized formats. PSS/E is the premier software tool used by electrical transmission participants world-wide. Since TSAT accepts PSS/E format, the generators' dynamic data are present in PSS/E format.

5.5.2 Excitation System

The basic function of an excitation system is to provide direct current to the synchronous machine field winding. Therefore, the requirement is that the excitation system supply and automatically adjust the field current of synchronous generators to maintain the generator terminal voltage [10].

The primary role of an excitation system is to quickly respond to voltage variations when disturbances occur in a power system. This control is local by nature since it involves generator bus only [12]. Furthermore, the reference voltage setpoints V_0 can be adjusted based on large area control needs so that an appropriate voltage profile can be maintained. Therefore, the appropriate excitation system modeling is important in dynamic voltage stability studies. In this thesis, PSS/E excitation system models are used.

5.5.3 Power System Stabilizer

The power system stabilizer uses auxiliary stabilizing signals to control the excitation system so as to improve power system dynamic performance. Commonly used input signals to the power system stabilizer are the shaft speed, terminal frequency, and power. Power system dynamic performance is improved by the damping of system oscillations. In this thesis, PSS/E power system stabilizer models are used.

5.5.4 Prime Mover

The representation of prime movers, including turbines and speed governors, are sometimes neglected in transient simulation studies. This is based on the assumption that the time constant of prime mover is larger than the study period of interest. It is important to note; however, that the time frame in which dynamic voltage instability occurs is usually in the range of several seconds, so that the prime mover may take action during the length of simulation. Therefore, the prime movers need to be represented using detailed models. In this thesis, PSS/E turbine and speed governor system models are used.

5.5.5 Load Model

Load dynamic response is a key mechanism of power system voltage stability driving the dynamic evolution of voltages and, in extreme cases, leading to voltage collapse [71]. There are two broad categories of load models, namely, static and dynamic. Both static and dynamic load are applied in this thesis.

Voltage Dependent Load

A composite system load can be expressed as exponential load model which reflects the change of active and reactive power according to the change of voltage. The following algebra equation can be used to represent the aggregate effect of different types of load components [12]:

$$
\begin{aligned}
P &= P_0 \cdot [p_1(\frac{V}{V_0})^{n_{p1}} + p_2(\frac{V}{V_0})^{n_{p2}} + p_3(\frac{V}{V_0})^{n_{p3}}] \\
Q &= Q_0 \cdot [q_1(\frac{V}{V_0})^{n_{q1}} + q_2(\frac{V}{V_0})^{n_{q2}} + q_3(\frac{V}{V_0})^{n_{q3}}]
\end{aligned} \tag{5.2}
$$

In this equation (5.2),

P_0/Q_0	= Normal active/reactive power of load when the bus voltage magnitude is V_0
$p_1 - p_3/q_1 - q_3$	= Proportion of each component active/reactive power
$n_{P1} - n_{P3}/n_{Q1} - n_{Q3}$	= Exponent for active/reactive power.

Note that by setting these exponents of equation (5.2) to 0, 1, or 2, the load can be represented by constant power, constant current, or constant impedance models, respectively. This model is sometimes referred to as ZIP load which has been widely used to represent the voltage dependency of loads. ZIP load comprises a large portion of the load in this thesis.

Induction Motor Load

Induction motor loads have a significant impact for dynamic voltage stability studies for the following reasons [12]:

- They are low power factor and consume a lot of reactive power
- They are fast restoring in the time frame of a second
- They are prone to stalling as a result of a reduction in applied voltage.

The motor model uses TSAT format that holds a specified portion of the total load as dynamic motor at a load bus. The initial active power of the induction machine is specified as a percentage ($P\%$) of the total active power at a load bus. For example, assume that a load bus has 100 MW and 30 MVAR of load. A model is added at this bus and holds 30% active power, $P\% = 30$. Thus 30 MW and 9 MVAR of induction motor load is assigned to this bus. The remaining load is to be represented with the static model.

5.6 Software Implementation of Data Generation for ANN

Since the ANN-based approach requires large amounts of data for training an ANN, it should be able to automatically collaborate with the commercial grade simulation software. The flow chart of generation procedures used for the ANN-algorithm to call TSAT simulation program is shown in Figure 5.3.

There are four programs written in MATLAB to call TSAT to complete the generation of input and output data for training an ANN. The main functions of the four programs are:

1. Generate random operating points.
2. Create TSAT case files (with extension name .tsa).
3. Form a DOS (Disk Operating System) batch file to execute all the .tsa files for TSAT batch mode.
4. Read TSAT binary result files to obtain the initial operating points and calculate the transient voltage dip.

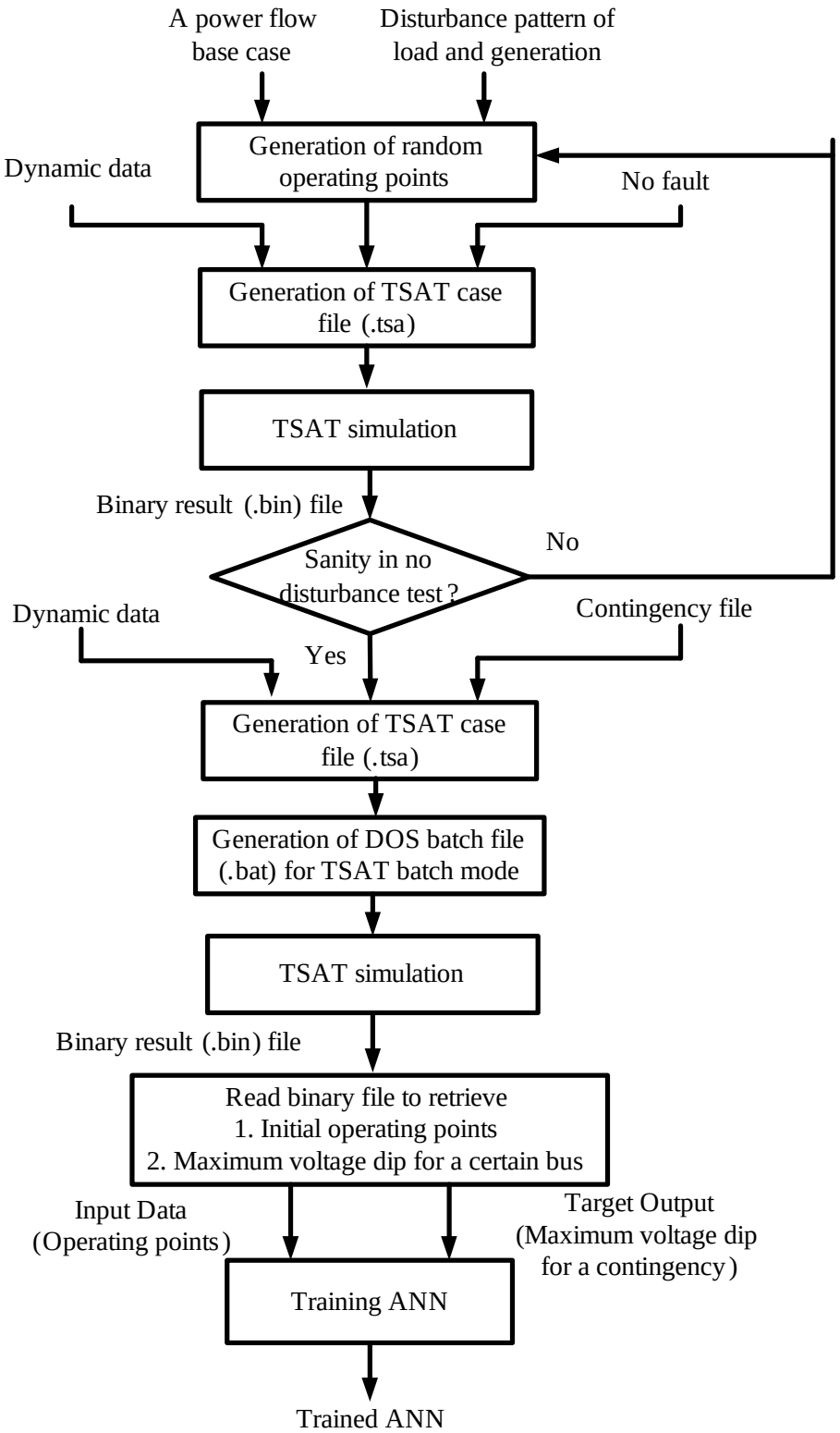

Figure 5.3: Flow chart of generation of data used for the ANN algorithm

A large number of cases with different load/generation levels are created randomly. Random disturbances are added to the base case active and reactive power of the loads and generators. Furthermore, small random disturbances are added to the base case generator voltage magnitudes. This program is the same one used for steady state voltage stability analysis.

A TSAT case is described by a tsa file which is an ASCII text file. A TSAT case file contains the information necessary to run TSAT, includeing [34]:

- Scenario specifications
- Computation parameters
- Input data specifications
- Output files specifications

The *scenario specifications* data section is defined as the base scenario. The *computation parameters* data section is used to specify simulation control parameters, security criteria setting, etc. For detailed data range of each parameter setting, the TSAT manual [34] can be referred to. In the *input data specifications* data section, the randomly generated operating points (power flow data), dynamic data, monitor data, and contingency data, etc., are specified individually. Output location and files need to be specified individually in the *output files specifications* data section.

In this thesis, the TSAT batch version is utilized to deal with the large number of TSAT cases. This version of TSAT has the same computational capabilities as the GUI version, but it runs entirely in a batch mode. Therefore, a DOS batch file including the DOS commands to run each TSAT case one by one in TSAT batch mode

is created.

Basecase analysis simulation results in all scenarios and all contingencies processed by TSAT are stored in the binary result file of the case, an extension ".bin" is always appended to the result file name. For each contingency, TSAT stores simulation results of all monitored quantities specified in the monitor data. Quantities defined as monitored variables are available to be acquired by a number of scripting languages, such as VBScript, JScript and MATLAB. MATLAB is used to retrieve data from the binary result files. The voltage magnitudes and phase angles of all buses at the steady state (pre-fault) are achieved as input data for training the corresponding ANN. For the contingencies simulation, all the bus voltages are scanned after fault clearing and voltage recovery, and the voltage dip of each bus is found. The transient voltage dip is saved as output for training an ANN.

5.7 Case Study

The proposed scheme is implemented in Matlab language with the time-domain simulations performed in TSAT. The New England 39-bus system is taken as the test system. The network consists of 18 load buses, 10 generator buses, and 35 transmission lines. All the generators are modeled using PSS/E salient pole generator 5^{th} order model together with their exciters, stabilizers, and steam turbine governor models. Bus 8 and 16 have 25% of power modeled as TSAT induction motor models and the rest of the power is static ZIP load models. The other load buses are expressed as static ZIP load models.

5.7.1 Different Initial Operating Points

A case study is carried out for three different initial operating points under the same contingency event. The contingency event is:

1. Simulation starts with no fault.
2. A three-phase to ground fault occurs at bus 8.
3. The fault is cleared by tripping line 8-9.
4. Total simulation time is 5 seconds.

The three different initial operating points in the 39-bus system are:

1. A base case
2. All the load and generation increased by 10%
3. All the load and generation increased by 20%

The results of simulation with load and generation at different levels are shown in Figure 5.4. Graph (a) shows the bus voltages for the base case under the specified contingency. Graph (b) shows the bus voltages when the load and generation increased by 10% of base case, under the specified contingency. Graph (c) shows the bus voltages when load and generation increased by 20% of base case, under the specified contingency. It is obvious that voltage instability happens in Graph (c) according to the voltage dip criteria. As can be seen, different initial operating points impact dynamic voltage stability differently under the same contingency.

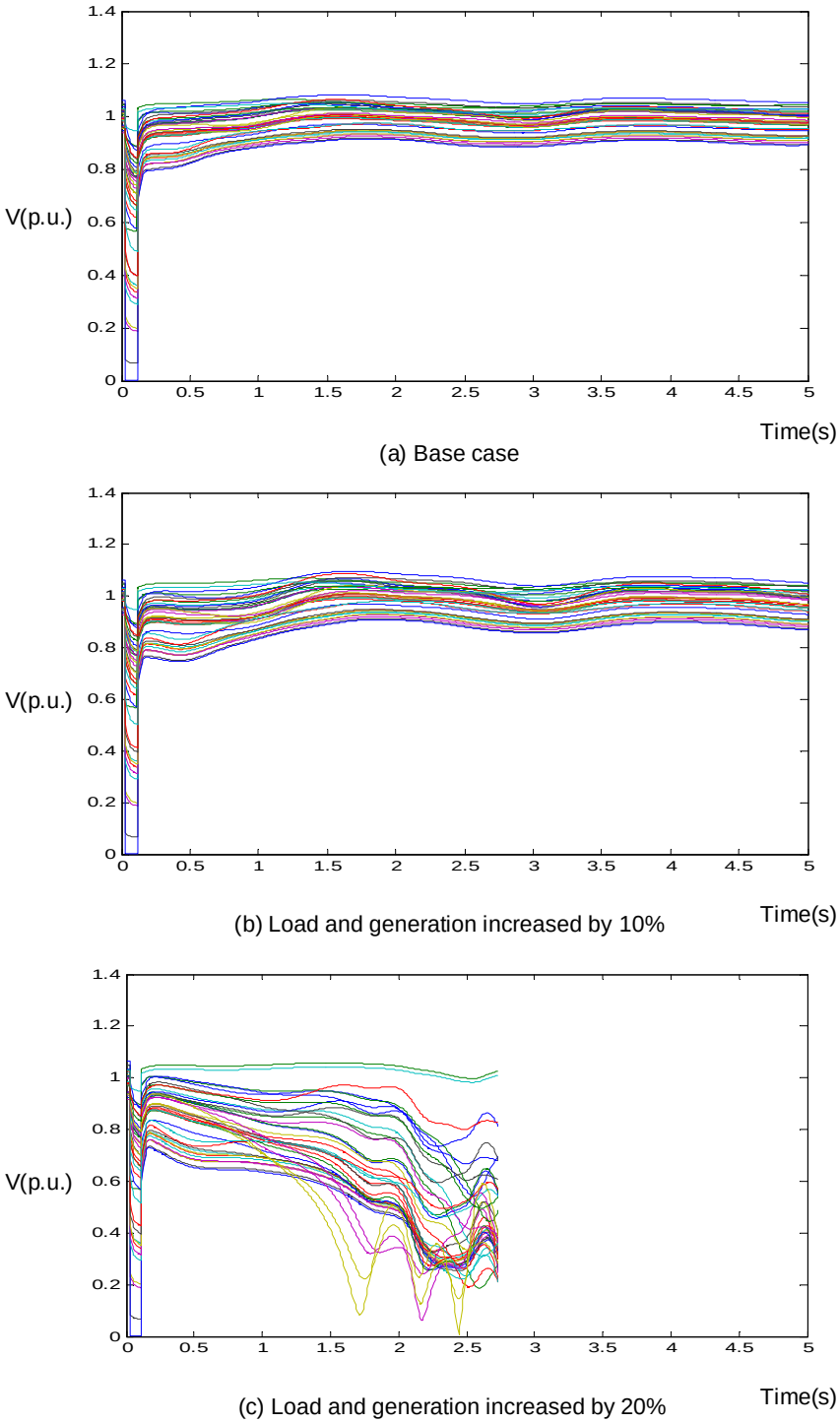

Figure 5.4: Bus voltage simulation at different load level

5.7.2 Different Contingency Locations

The large disturbance considered in this study is a three phase to ground fault on a transmission line, cleared 0.1s after fault inception by tripping the line. The total simulation time period is five seconds. For a given contingency, the voltages of 39 buses vary differently so that they have 39 different voltage trajectories and different transient voltage dips as shown in Figure 5.5. When the transient voltage dip is small and within the voltage stability criteria (25%), the case is marked as healthy for voltage stable. When the largest transient voltage dip is over the voltage stability criteria (25%), the case is marked as voltage unstable.

Figure 5.5 shows the simulation results for the same original operating point, but for different locations of the three phase fault. Graph (a) is the simulation result when three phase fault occurs at bus 3 on line 3-18 and the line 3-18 is tripped. Graph (b) is the simulation result when three phase fault occurs at bus 16 on line 16-17 and the line 16-17 is tripped. Graph (c) is the simulation result when three phase fault occurs at bus 21 on line 21-22 and the line 21-22 is tripped.

The simulation results show that different contingency locations affect significantly the post-contingency voltage behavior. For the same initial operating point, the voltages remain stable for a fault at bus 3. When the fault occurs at bus 16, some transient voltage dips exceed the voltage dip criteria. These cases are classified as voltage instability. When a contingency occurs at bus 21, there is a system voltage collapse. In this thesis, situations (b) or (c) of Figure 5.5 are of the main interest. A corrective action (load shedding) for mitigating the transient voltage dip will be investigated in detail, later in this thesis.

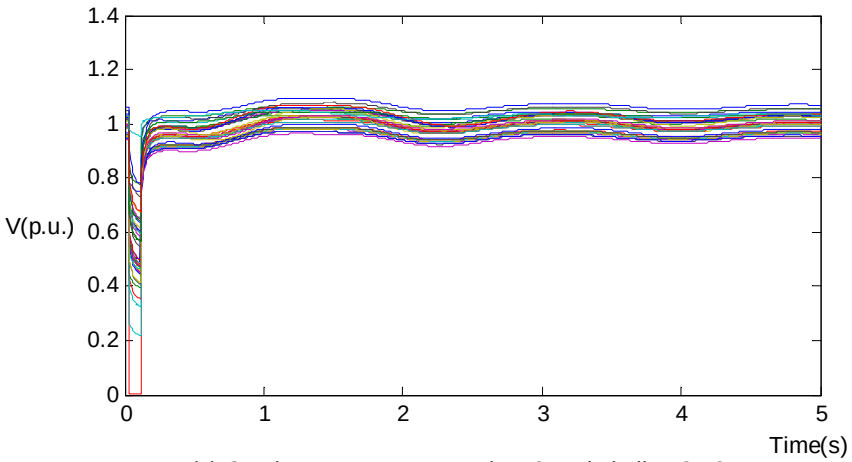

(a) Contingency occurs near bus 3 and trip line 3-18

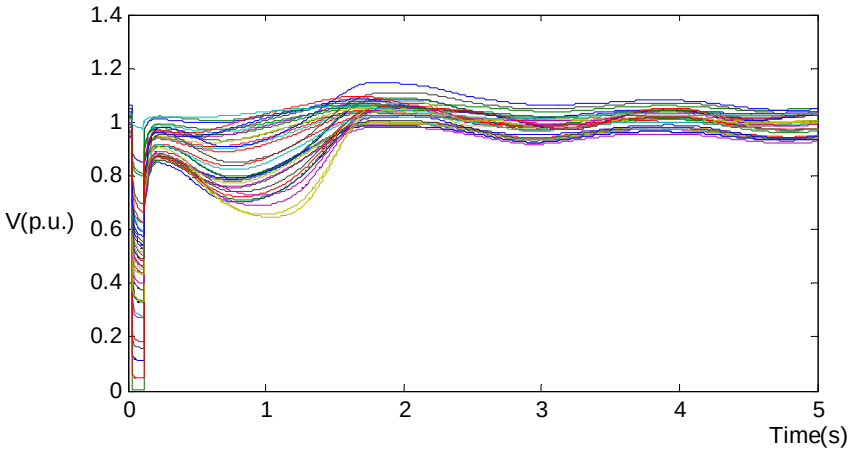

(b) Contingency occurs near bus 16 and trip line 16-17

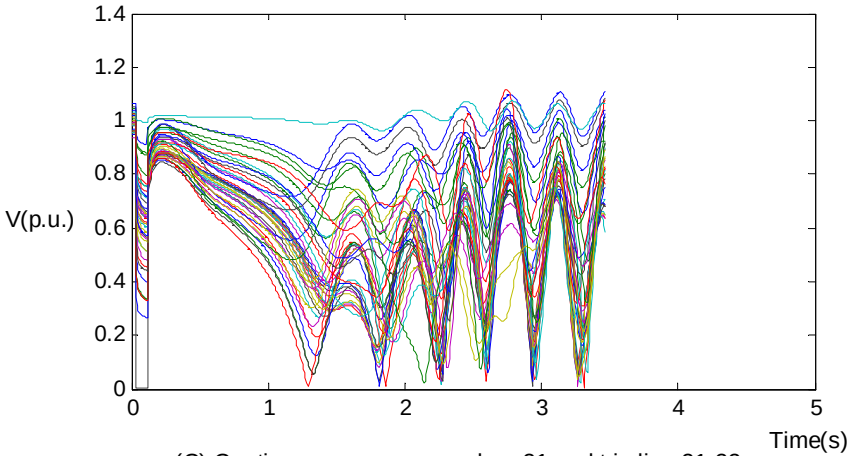

(C) Contingency occurs near bus 21 and trip line 21-22

Figure 5.5: Bus voltage simulation at different contingency locations

5.7.3 Estimation of Transient Voltage Dip by ANN

In order to apply ANN for predicting transient voltage dip, different sets of training-test data need to be generated. A large number of operating points are randomly generated within the range of ± 30% of the base case active and reactive power of both load and generator. These random operating points are verified for valid initial conditions. Therefore, 3,000 cases that pass the sanity verification are saved as initial operating points for the simulation with a series of contingency events. A contingency event is set as follows: a three-phase ground fault occurring at one end of a transmission line, and then is cleared 0.1s after the fault inception by tripping the faulted line. A total of 35 contingencies are considered. All the 3,000 cases are simulated under each contingency in the contingency list and the bus voltage trajectories are recorded. The initial operating points including voltage magnitudes and phase angles are obtained and fed into an ANN as input features. The transient voltage dip is sought on the corresponding voltage trajectories. The transient voltage dip of the system is calculated and kept as the output target for each associated ANN. There are an additional 100 sanity checked cases generated by the above method and used for testing the ANNs.

There are 35 contingencies in the 39-bus study system. The ANN algorithm is used for each contingency separately. Figure 5.6 presents the results of the estimated transient voltage dip by two ANNs. The first ANN is designed for the contingency occurring at the motor load bus 8 and the fault is cleared by tripping line 7 to 8. The second ANN is designed for the contingency occurring at the motor load bus 16 and

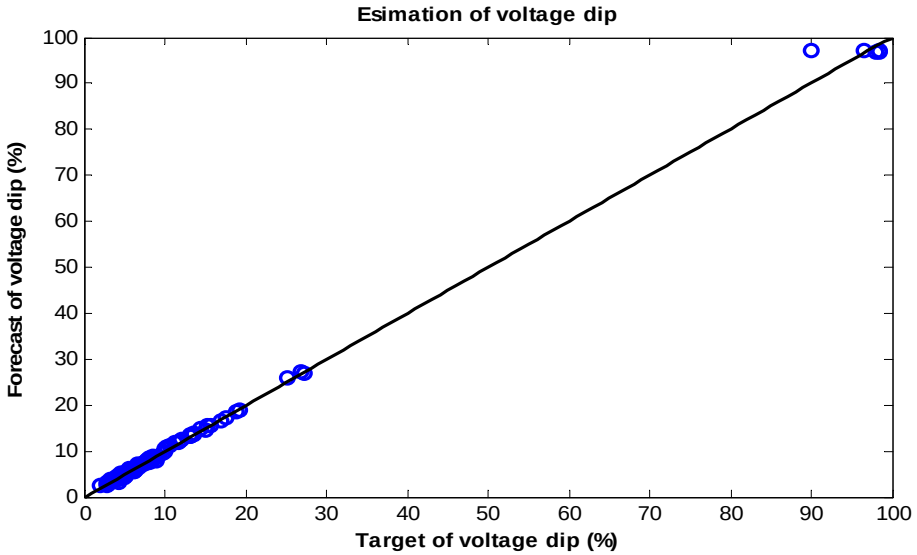

(a) Fault occurs at bus 8, trip line 7-8

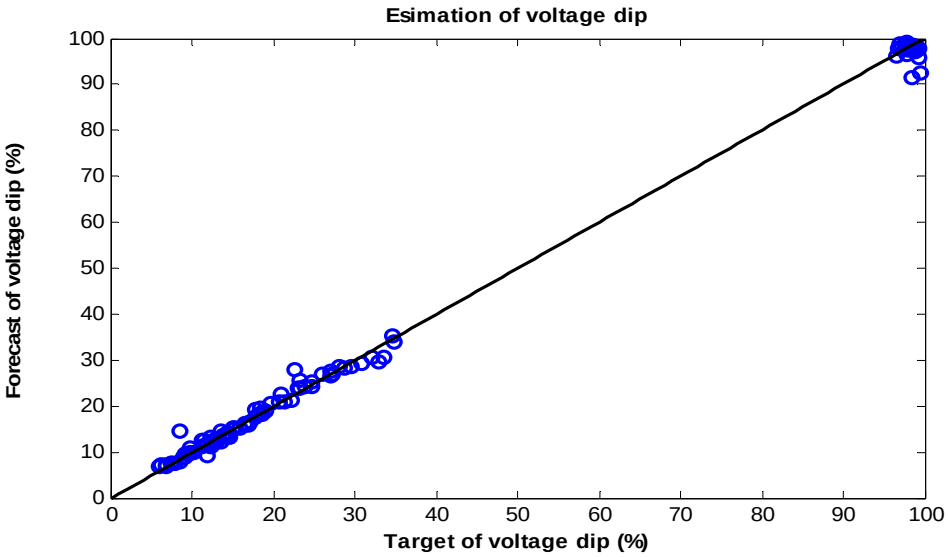

(b) Fault occurs at bus 16, trip line 16-17

Figure 5.6: Transient voltage dip estimation by ANNs

the fault is cleared by tripping line 16 to 17. In the figure, the x-axis represents the maximum transient voltage dips in percentage of all the buses calculated by simulation. The y-axis represents the corresponding forecasted maximum transient voltage dips estimated by the ANNs. There are 100 testing cases in each graph. If the target values completely match with the forecasted one, all points should lie on the diagonal line. Figure 5.6 (a) and (b) show that ANN approach is able to estimate the transient voltage dip accurately.

Chapter 6

On-line Corrective Control of Large-disturbance Voltage Stability

In the last chapter, the neural network method has been successfully applied to predict large-disturbance voltage stability. Upon detection of the imminent voltage instability or voltage collapse, some corrective actions have to be carried out. Load shedding is considered in this chapter as an effective corrective action. In this chapter, two simulation based approaches, particle swarm optimization algorithm and sensitivity based algorithm, are proposed to find the optimal load shedding .

6.1 Overview

Short-term voltage security or voltage collapse studies the system behavior under large disturbances which may lead to a system blackout. Similar to long term voltage security control against the small disturbances, there are two main forms of remedial actions that can be armed for a large-disturbance voltage security control. They are

preventive control and corrective control. Preventive control is applied prior to any contingency occurrence while corrective control is applied after the contingency has occurred. Preventive control is a lot more costly than corrective control. Hence, if the probability of occurrence of the contingency that poses the security threat is very low, utilities prefer to resort to corrective control actions [7].

In large-disturbance voltage security analysis, the occurrence of contingency is uncertain and might remain at very low probability; however, once it happens it may be very severe. It is neither possible nor economical to design any preventive control against a large disturbance. In order to prevent the voltage collapse after a large disturbance, proper corrective actions need to be taken in addition to isolating faulted components to maintain system security. A corrective action for short-term voltage stability then has to be designed to mitigate the consequence of the abnormal condition and provide acceptable system performance following any severe contingencies.

Load shedding is one of the most effective approaches against voltage instability [72]. If the available equipment protection and controls have been exhausted or there are no more fast control actions available, the last but very effective option to prevent voltage collapses will be the emergency load shedding. However, shedding loads means losing revenue to both the utility and the customer; hence, it should only be considered when there is a high risk of system instability. It is therefore important to develop an algorithm to minimize the amount of load shedding. The basic requirement of load shedding needs to answer three fundamental questions [12]:

- When should the load be shed?
- Where should the load be shed?

- How much load should be shed?

Various research studies have proposed solutions to achieve load shedding schemes. [73] proposed that the loads with lower voltage or greater voltage decay be shed sooner so that locations of load shedding become dependent on the location of disturbance. [74] used pre-defined tables that determine loads to shed first for the MW amount at the time of request. [75] proposed a load shedding scheme by solving optimal power flow (OPF) with different objective functions. [76, 77, 78] determined minimal shedding required in a given location and delay, then determined which delay and location yield the smallest MW amount. These existing load shedding schemes only considered long-term voltage stability, neglecting the dynamic behavior of the loads and system during and after disturbances. Hence, they are not designed for the short term voltage stability after large disturbances.

It is important to search for an optimal load shedding scheme which determines the minimal load shedding amount with due consideration for the shedding location and time to stabilize the system after the occurrence of disturbance. For short-term voltage stability, load shedding action needs to be taken immediately after contingency. Therefore, what needs to be determined are (i) the most effective location for load shedding, and (ii) the amount of load to be shed. If a load shedding scheme is to be obtained through the iterations of simulation runs with a series of sequentially or randomly generated parameter sets of locations and shedding amount, the total number of simulations will be too large and will result in unacceptable delays in load shedding.

To address these issues, two algorithms are developed and combined with the time-domain simulation. The first approach is a particle swarm optimization (PSO) algo-

rithm that performs an efficient global optimization search. The second approach is a sensitivity based algorithm that is conducted through the sensitivity index of the load shedding buses. As a result, an optimal load shedding solution makes a decision about (i) where the most effective locations are for load shedding, and (ii) what is the minimal amount of loads to be shed at the known breaker operation time for those selected shedding locations.

6.2 Load Shedding Candidate Matrix

Before running a load shedding algorithm, the representation of the candidate load shedding options must be defined. In our study, each option x_i is a vector with the dimension equal to NL which is the number of available load locations. Each option can be represented as $x_i = (x_{i1}, x_{i2}, ..., x_{in})$. Each element of the vector x_i is the amount of a load to be shed in the specific option. For example, a candidate load shedding scheme is

	Load 1	Load 2	Load 3
Option 1	10	0	30
Option 2	0	40	0
Option 3	0	20	20

The above matrix represents three load shedding options. The first option is to shed Load 1 by 10MW and Load 3 by 30MW. The second option is to shed Load 2 by 40MW. The third option is to shed Load 2 by 20MW and Load 3 by 20MW. The shedding amount of each load (x_{ij}) cannot exceed the load constrain that is the available load to be shed. The load constrain may or may not be the largest power. The load constrain should be pre-defined according to the practical system conditions.

For example, if a 100 MW load is all available to be shed, the relevant load constrain is set to [0,100]; if a 100 MW load only has half the amount available to be shed, the relevant load constrain is set to [0,50].

6.3 Particle Swarm Optimization

Particle swarm optimization (PSO) is an algorithm modelled on swarm intelligence aimed at finding a solution to an optimization problem in a search space. Particle swarm optimization, having been proved to be a competitor to solve nonlinear optimization problems, was introduced by Kennedy and Eberhart in 1995 [21]. A review of the PSO technique [22] presents the basic concepts, different structures and variants, as well as its applications to different optimization problems in power systems. In this thesis, the PSO algorithm explores a problem space of candidate load shedding locations and found the load shedding solutions.

In particle swarm optimization, a swarm consisting of several particles moves in the search space of an optimization problem. Each particle keeps track of its own attribute. The most important attribute of the particles is their current positions, represented by n-dimensional vectors. The position of a particle represents a candidate solution to the optimization problem at hand. Each particle searches for better positions in the search space by changing its velocity according to set of rules. Additionally, each particle also remembers its group's best position, so that potentially good solutions upon termination of the algorithm may serve as the answer of the optimization problem.

6.3.1 PSO Formulation

PSO belongs to the class of direct search methods used to find a solution to non-linear optimization problems in a search space. A population of individuals defined as random solutions in the problem space is initialized. These individuals (particles) are candidate solutions which comprise a swarm. The swarm is typically modelled by particles in hyperspace space (i.e., $\Re^n$) that have a position (denoted by x) and a velocity (denoted by v). These particles fly through hyperspace and adjust two essential capabilities: their memory of their own best position (*pbest*) and knowledge of the global best (*gbest*). Suppose the i-th particle is expressed as $x_i = (x_{i1}, x_{i2}, ..., x_{in})$ in a n-dimensional space. This concept for particle flying can be formulated as:

$$\begin{aligned} v_i^{k+1} &= w_i^k v_i^k + c_1 \cdot rand \cdot (pbest_i - x_i^k) \\ &\quad + c_2 \cdot rand \cdot (gbest_i - x_i^k) \qquad (6.1) \\ x_i^{k+1} &= x_i^k + v_i^{k+1} \qquad (6.2) \end{aligned}$$

where,

v_i^k current velocity of particle i at iteration k,

v_i^{k+1} updated velocity of particle i at iteration k+1,

x_i^k current position of particle i at iteration k,

x_i^{k+1} updated position of particle i at iteration k+1,

$pbest_i$ best position of particle i at iteration k,

$gbest_i$ best position of the group i at iteration k,

w_i inertia weight for velocity,

c_1, c_2 acceleration coefficients,

$rand$ random number between 0 and 1.

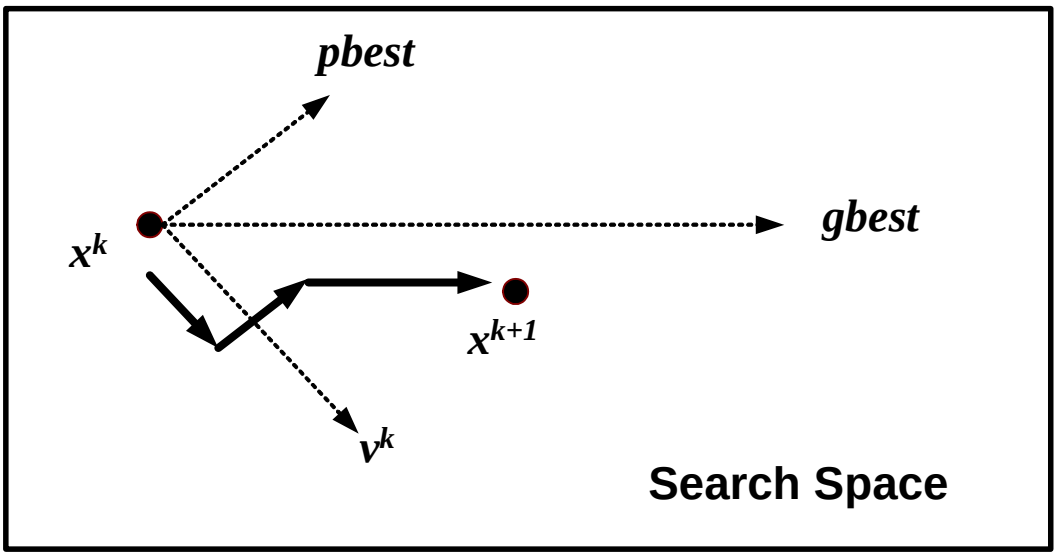

Figure 6.1: A single particle movement within searching space

A single particle movement at iteration k is illustrated in Figure 6.1. A particle movement is determined by three things: its current velocity, its best position and the best position of its group. Inertia weight controls the exploration of the search space and usually can be defined as equation (6.3). The initial large value of the inertia weight (typically 0.9) allows the particles to move freely in order to find the global optimum. Once the optimal region is found, the value of inertial weight can be decreased (say 0.4) in order to narrow the search.

$$w_i^k = w_{max} - \frac{w_{max} - w_{min}}{\text{maximum iterations}} \times k \tag{6.3}$$

In addition, the condition boundary of both velocity and position can be specified according to the characteristics of the problem. The boundary of position is limited by the searching space. The boundary of velocity is determined by the space between the current position and the target position. If velocity is too high, particles might fly past good solutions. If velocity is too low, particles may not explore sufficiently beyond local solutions [79]. In this thesis, the position boundary is set as the available amount for shedding of each potential load bus. The velocity boundary is set as the largest distance from the current position to the available amount for shedding.

6.3.2 Objective Functions

The objective function provides a measure of the performance of each particle in the problem solution. For a load shedding scheme, there are two essential objectives for the short-term voltage stability challenges under a severe contingency: 1. maintain the system stability by shedding some loads after the contingency occurs; and 2. minimize the total amount of load shedding while not losing system stability. The objective function is then expressed in equation (6.4) and (6.5).

When it is at risk of voltage unstable:

$$f1 = min(Vdip(x_1, x_2, ..., x_i, ..., x_n) - 25\%) \tag{6.4}$$

Where, $Vdip(x_1, x_2, ..., x_i, ..., x_n)$ expresses the transient voltage dip when the system employs load shedding scheme $(x_1, x_2, ..., x_i, ..., x_n)$ after contingency occurs.

When it is voltage stable:

$$f2 = min(\sum(x_{i1}, x_{i2}, ..., x_{in})) \tag{6.5}$$

When the power system is moving towards voltage instability or collapse, the target is to bring the system back to voltage stability. The loads with most effective impact on transient voltage dip are selected. Once the system is assessed to be stable, meaning transient voltage dip is smaller than criteria, the target is changed to seek the minimum load shedding amount of the selected loads.

6.3.3 Load Shedding Process with PSO

The PSO algorithm for load shedding, given in Figure 6.2, is to search for the optimal places of load shedding and relevant minimum required amount at the known load shedding time. The initial swarm (candidate load shedding places) are determined by system operators based on their experience or use of the available loads in that area. The procedure of PSO algorithm can be summarized as follows:

1. Initialize the particle swarm $x_i^0 = (x_{i1}^0, x_{i2}^0, ..., x_{in}^0)$ uniformly. The n-dimension corresponds to the number of the candidate loads which are selected by ANN sensitivity. Assign a random and uniform velocity v_i^0 for each particle.

2. For the initial swarm, run TSAT simulation program and calculate the voltage

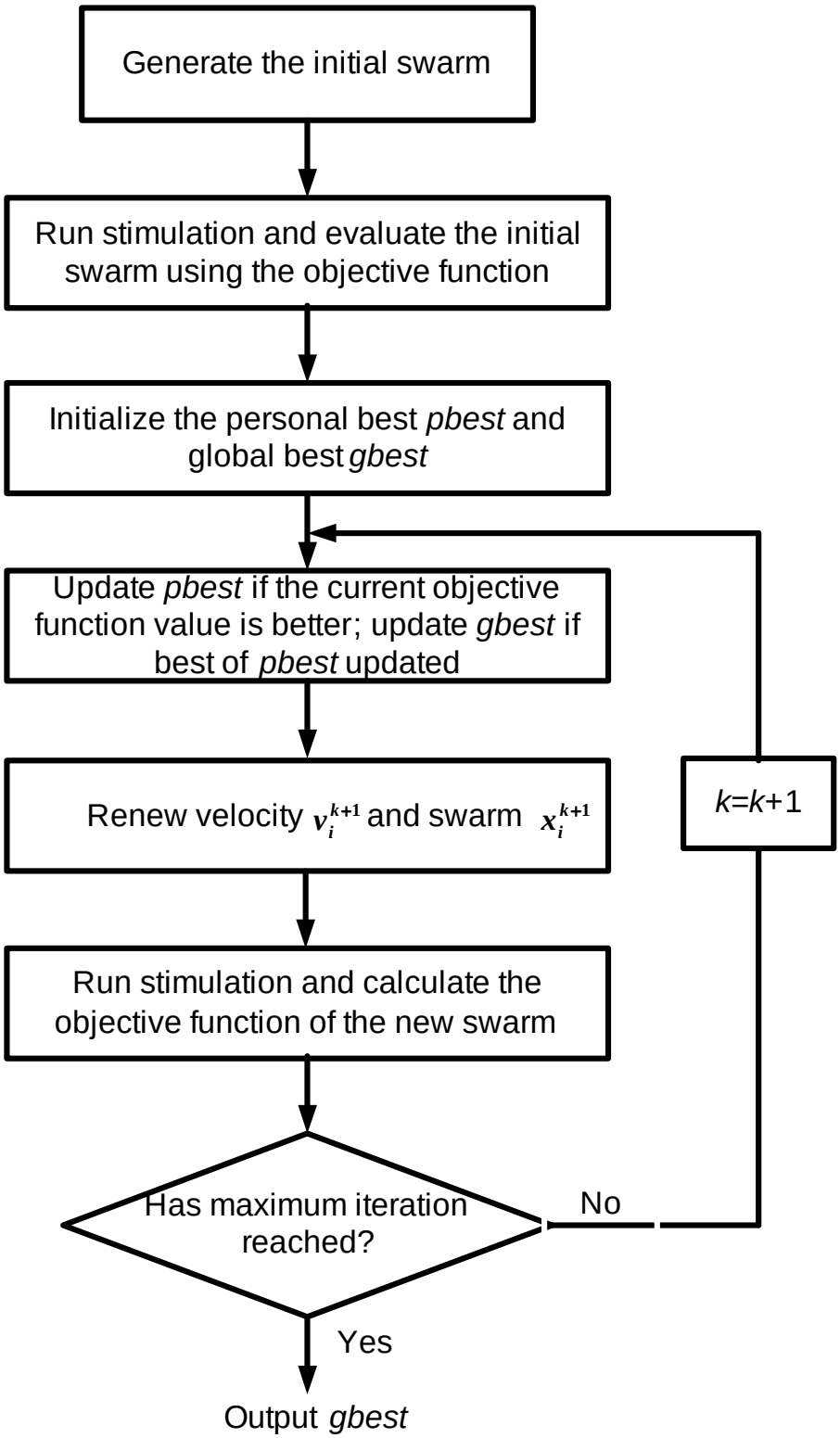

Figure 6.2: The PSO procedures for load shedding

dip, then evaluate the initial swarm using the objective function as given by (6.4) or (6.5).

3. Initialize x_i^0 as the personal best (*pbest*). The initial best x_j^0 is the global best (*gbest*) of the entire swarm.

4. Start iteration $k = 1$.

5. If the objective function value is better than the personal best value (*pbest*) in history, set current value as the new *pbest*. Update global best *gbest* with best *pbest*.

6. Calculate the particle velocity using equation (6.1). If the velocity is beyond the boundary, set it equal to the boundary. Calculate the position of particles using equation (6.2). If the position is beyond the load constrain, limit it to equal to the constrain.

7. Run TSAT simulation program and reevaluate the swarm using the objective function as given by (6.4) or (6.5); go to step 5 if the maximum iterations or minimum error criteria are not attained.

8. Output the global best (*gbest*) of the entire swarm, which is the optimal load shedding scheme.

In the above procedures, once a swarm of load shedding schemes makes the studied power system move from unsafe to safe, the particles of the swarm participating in load shedding do not change anymore and only the value of the particles can change. Then the objective function is moved to equation (6.5).

6.4 Sensitivity Based Algorithm

The sensitivity based algorithm is divided into three sub-processes. In the first step, small-disturbance analysis coupled with time-domain simulation is used to identify sensitivity of the transient voltage dip to the shedding amount of the load. The sensitivity indicates the best shedding location for a given scenario. In the second step, an amount of load shedding obtained by the sensitivity in the first step is applied to the selected load to approach the voltage stability criteria. In the third step, a process of time-domain simulation is used to verify the effect of load shedding. After several iterations of the three-step process, the optimal load shedding scheme can be found.

6.4.1 Sensitivity of Load Shedding Amount

The objective of a load shedding scheme is to restore the transient voltage dip within 25%. The sensitivity of the shedding amount of the load to the change of the transient voltage dip is expressed in (6.6):

$$S_k = \frac{A_k - A_{k-1}}{V_{dip,k} - V_{dip,k-1}} \tag{6.6}$$

After the sensitivity is known, the predicted load shedding amount is calculated

$$A_{k+1} = A_k + S_k * (criteria - V_{dip,k}) \tag{6.7}$$

Where,

$$
\begin{aligned}
S_k &= \text{sensitivity of the leading bus} \\
&\quad \text{at the } k^{th} \text{ iteration,} \\
A_k &= \text{the load shedding amount of the leading bus} \\
&\quad \text{at the } k^{th} \text{ iteration,} \\
V_{dip,k} &= \text{the transient voltage dip at the } k^{th} \text{ iteration,} \\
criteria &= 25\%.
\end{aligned}
$$

6.4.2 Load Shedding Process

A flow chart of the proposed load shedding process is illustrated in Figure 6.3.

This algorithm is based on the simulation and sensitivity of the load shedding amount at each step. The relay time of each load that attends the load shedding scheme is set in the simulation. The sensitivity finds out the best load shedding place at a certain step, and the anticipated amount to be shed can be calculated. This anticipated amount is applied in simulation for the next step. The procedure of algorithm can be summarized as follows:

1. Initialize the load shedding options $x_i^0 = (x_{i1}^0, x_{i2}^0, ..., x_{in}^0)$ with small amount of shedding at each load. The n-dimension corresponds to the number of the candidate loads which attend load shedding scheme.

2. For all the options, run simulation program and calculate the transient voltage

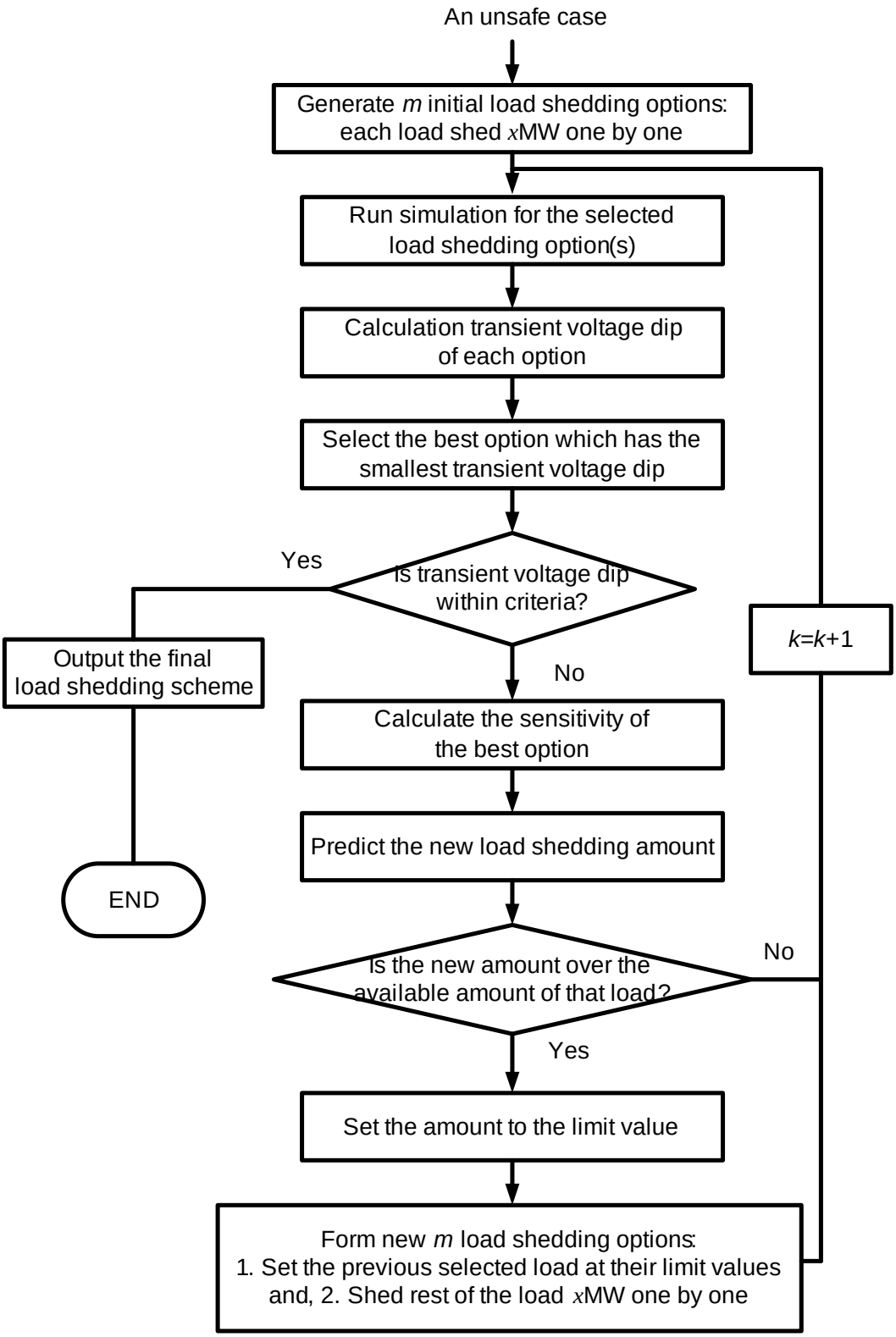

Figure 6.3: The sensitivity based algorithm combines with simulation

dips, then select the best option which brings the smallest transient voltage dip.

3. If the best transient voltage dip is over the short-term voltage stability criteria, the computation continues. Otherwise, the final load shedding scheme is found and program ends.

4. For the best option selected in the last step, calculate the sensitivity by (6.6) for the leading load. Predict the new load shedding amount of the leading load by (6.7) for the next step. As long as the leading load has more power to be shed, the other loads keep their current status in the option.

5. If the new shedding amount of the leading load is within its available amount limit, the best option is kept and only the amount of the leading load is changed. Then, only one load shedding option returns to step 2. The iteration continues.

6. If the new shedding amount of the leading load is over the available amount limit of that load, two things are done: (i) set the load amount to the limit value, and (ii) form a series of new load shedding options for the next step. The new load shedding options have the same format: all the previous leading loads employ their load constrains and the rest of load shed xMW one by one. Then, go back to the step 2, the iteration continues.

In the above procedures, once a leading load having more power to be shed, only one option including the leading load is used in the simulation. When the leading load reaches its amount boundary and short-term voltage stability is still not achieved, the rest of the loads have to combine with the previous leading loads respectively to form a series of new options. This method greatly reduces the candidate options for simulation, resulting in large savings in the number of simulations.

6.5 Impact of Load Shedding Places

The load shedding place significantly affects the post-contingency transient voltage dip. A voltage instability case, shown in Figure 5.5(b), is used as a sample. In this case, the contingency occurs on line 16 to 17 and close to Bus 16. The load shedding is activated 0.15s after fault happening on all the available load buses one by one. If the same amount of power at different loads is shed, the results are different. Figure 6.4 shows a few results of transient voltage dips, which include the one without shedding load and shedding load at different buses. If shedding Bus 4, the lowest voltage is brought back to 0.75 and the transient voltage dip is smaller than criteria. If shedding Bus 8, the transient voltage dip is 26% which is close to criteria but right out of criteria. If shedding Bus 16, the result is almost exactly the same as the one of no load shedding. From this specific case, the good load shedding place may not be the load buses close to the fault location. In this example, although the fault occurs near Bus 16 and on line 16 to 17, shedding load on Bus 16 does not help to recover voltage stability.

6.6 Load Shedding Case I

6.6.1 PSO Algorithm

The proposed load shedding algorithms (PSO and sensitivity based method) have been implemented respectively on a voltage instability case predicted by ANN, shown in Figure 3.2 (b). The case is an incident with the transient voltage dip 36.2% when a three-phase ground fault occurs close to motor load Bus 16 and trip line 16 to 17. It supposes that the relays of all the load buses can be activated 0.15s after fault

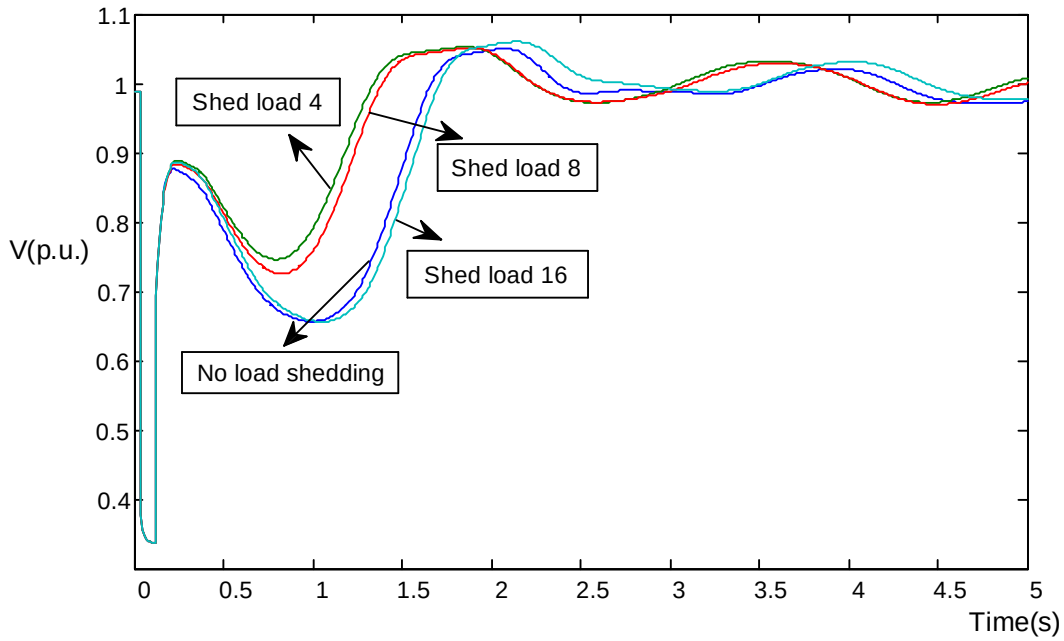

Figure 6.4: Impact of load shedding at different locations for a given contingency

happening if necessary. There are a total of 18 load buses and their bus numbers are: 3, 4, 7, 8, 12, 15, 16, 18, 20, 21, 23, 24, 25, 26, 27, 28, 29, 39. In addition, it assumes that all the 18 load buses are available to be shed till their maximum power limit. The relevant load shedding boundaries are set to [0, maximum_amount_(i)]. Here, i denotes any load bus.

Table 6.1 describes the detailed procedures of iteration by PSO algorithm. As a result, the combination shedding plan on four load buses (4, 7, 12, and 28) forms a load shedding scheme. Bus 12 is a small load with a maximum of 7.5 MW. It is the most effective load shedding place at the beginning of iteration. However, Bus 12 does not have sufficient load amount to be shed to stabilize the whole system under the contingency. The PSO algorithm selects loads 4, 7, and 28 in the sequential procedures. At the ninth iteration, the transient voltage dip changes from 25.48% to

24.72% with 117.2MW total shedding amount so that the load shedding scheme at the ninth iteration can restore the system from unsafe to reach the voltage stability criteria. At this time, the objective function is changed to reduce the total load shedding amount while still keeping voltage stability. At the 14^{th} iteration, the total load shedding amount reduces from 117.2MW to 107.9MW while the transient voltage dip is still within voltage stability criteria. After the 14^{th} iteration, the PSO algorithm cannot find a better shedding scheme with less total load shedding amount but keep the transient voltage dip within the criteria.

Table 6.1: Iteration of load shedding scheme for Case I by PSO

Iteration	Shedding Places (Bus No.)	Shedding Amount (MW)	Total Amt. (MW)	Trans. Vdip (%)
0	0	0	0	36.2113
1	12	5.0	5.0	32.5288
2	12	7.5	7.5	31.0556
3	4,12	31.5,7.5	39.0	28.5285
4	4,7,12	6.2,41.2,7.5	54.9	27.8410
5	4,7,12,28	25.5,2.0,7.5,48.6	83.6	27.1272
6	4,7,12,28	29.1,28.3,7.5,6.5	71.4	26.8974
7	4,7,12,28	29.1,28.3,7.5,6.5	71.4	26.8974
8	4,7,12,28	39.0,42.4,7.5,12.6	101.5	25.4829
9	4,7,12,28	53.0,42.4,7.5,14.3	117.2	**24.7208**
10	4,7,12,28	46.1,57.1,7.5,0.0	110.7	24.8167
11	4,7,12,28	46.1,57.1,7.5,0.0	110.7	24.8167
12	4,7,12,28	46.1,57.1,7.5,0.0	110.7	24.8167
13	4,7,12,28	46.1,57.1,7.5,0.0	110.7	24.8167
14	4,7,12,28	44.2,55.4,7.5,0.8	**107.9**	24.9634
15	4,7,12,28	44.2,55.4,7.5,0.8	107.9	24.9634
16	4,7,12,28	44.2,55.4,7.5,0.8	107.9	24.9634
17	4,7,12,28	44.2,55.4,7.5,0.8	107.9	24.9634
18	4,7,12,28	44.2,55.4,7.5,0.8	107.9	24.9634
19	4,7,12,28	44.2,55.4,7.5,0.8	107.9	24.9634
20	4,7,12,28	44.2,55.4,7.5,0.8	107.9	24.9634

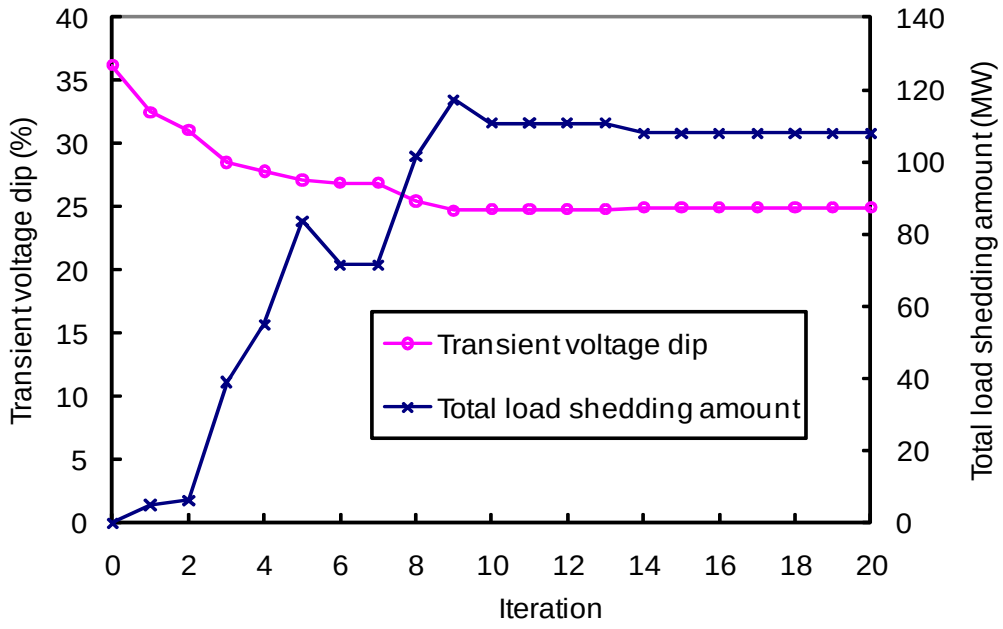

Figure 6.5: Load shedding convergence characteristic for Case I by PSO

The objective functions of the PSO algorithm are plotted in Figure 6.5. The figure has two y-axes. The left y-axis is the first objective function (6.4) and the right y-axis is the second objective function (6.5). In the case study, the iteration runs up to 20 times. The transient voltage dip recovers within criteria at the ninth iteration. After that, the algorithm switch from the first objective function to the second objective function. It reduces the total amount of load shedding and maintain the transient voltage dip within criteria. The load shedding amount does not change much after the tenth iteration. In order to effectively execute the procedures of iteration, an early stop criteria can be set in the iteration.

6.6.2 Sensitivity Based Algorithm

Similar to the PSO algorithm, the sensitivity based algorithm is applied on the same case. Table 6.2 shows the load shedding options and relative amount of the chosen loads during each iteration. The initial amount of load shedding is 5MW of active power and corresponding reactive power to keep the power factor unchanged for that load. Bus 12 is the most effective load shedding place at first but it has only 7.5MW power which can be shed. When a leading bus hits its load constrain, the other loads shed 5MW each to form the new candidate options of load shedding for the next iteration. After Bus 12 is totally shed (7.5MW), Bus 15 becomes the leading bus. After shedding Bus 12 by 7.5MW and Bus 15 by 97.5MW, the transient voltage dip reduced from 36.21% to 24.84% that restores the system to voltage stability.

Table 6.2: Iteration of load shedding scheme for Case I by sensitivity method

Iteration	Shedding Places (Bus No.)	Shedding Amount (MW)	Total Amt. (MW)	Trans. Vdip (%)
0	0	0	0	36.2113
1	12	5.0	5.0	32.5288
2	12	7.5	7.5	31.0556
3	12, 15	7.5, 5.0	12.5	30.6301
4	12, 15	7.5, 71.2	78.7	26.2613
5	12, 15	7.5, 90.3	97.8	25.2734
6	12, 15	7.5, 97.5	**105.0**	**24.8425**

The total amount to be shed and the relative transient voltage dip of each iteration are plotted in Figure 6.6. As can be seen, the transient voltage dip is reduced within criteria at the sixth iteration. Hence, the case is restored to be voltage stable if performing the load shedding scheme on Bus 12 by 7.5MW and Bus 15 by 97.5MW, total load shedding 105MW, at 0.15s after the fault happening. A bus voltage trajectory of pre- and post- load shedding in simulation is plotted in Figure

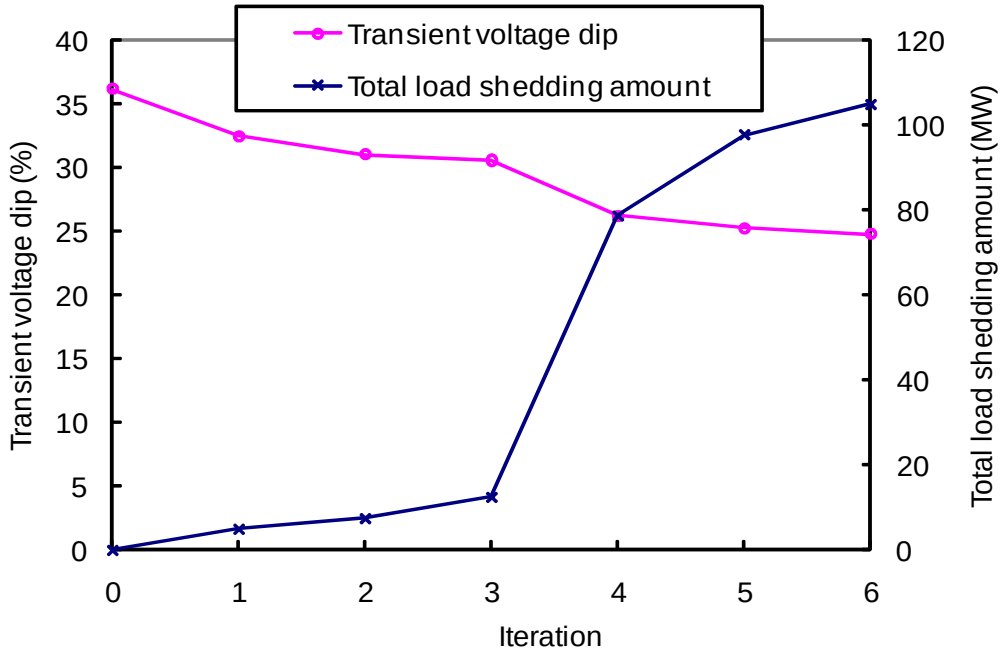

Figure 6.6: Load shedding convergence characteristic for Case I by sensitivty method

6.7. The graph shows the load shedding scheme after the occurrence of contingency can successfully and effectively prevent the system from tending to voltage instability.

6.7 Load Shedding Case II

6.7.1 PSO Algorithm

The proposed load shedding algorithms (PSO and sensitivity based method) have been implemented respectively on another case predicted by ANN, shown in Figure 3.2 (a). The case is a voltage collapse incident with the transient voltage dip 99.3% when a three-phase ground fault occurs close to motor load Bus 8 and trip line 8 to 9. In this case study, we still suppose all of the 18 loads can be shed. However, as the initial operating points are different between Case I and Case II, the maximum

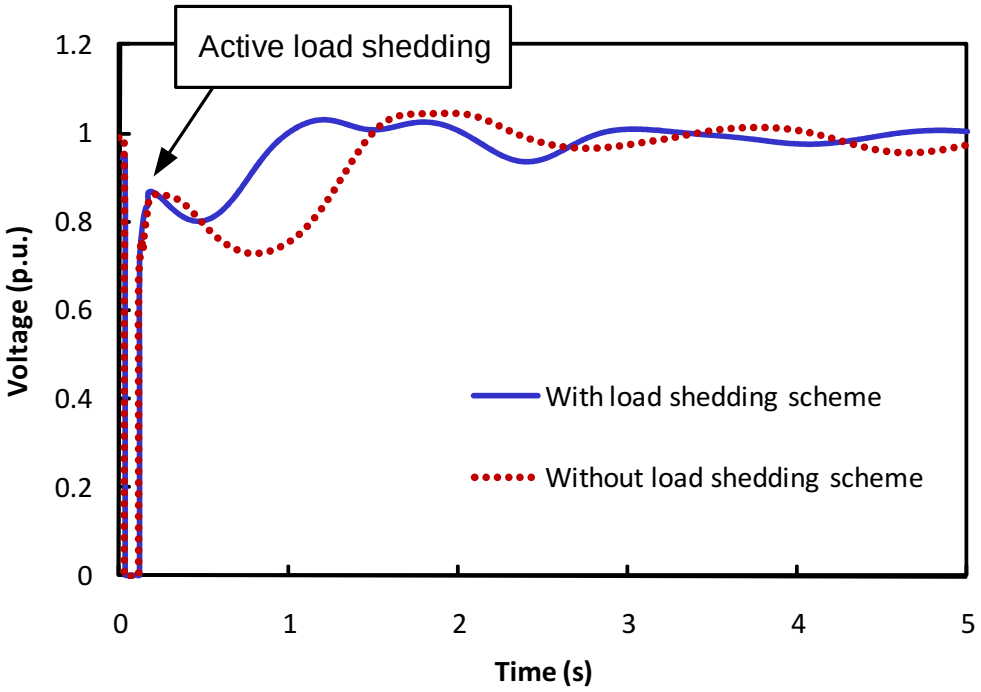

Figure 6.7: The effect of load shedding scheme for Case I

amounts of 18 loads in Case II are different from those in Case I. The load shedding relay time is still set at 0.15s after fault happening on all the candidate load buses.

Table 6.3 describes detailed procedures of iteration by the PSO algorithm. As can be seen, the combination shedding plan on seven buses (8, 12, 16, 20, 25, 26, and 39) forms a load shedding scheme. At the 13^{th} iteration, the transient voltage dip changes from 25.09% to 24.93% with total shedding amount 376.5MW so that the load shedding scheme at this iteration can restore the system from unsafe to voltage stability. At this time, the objective function is changed to reduce the total load shedding amount while still keeping voltage stability. At the 20^{th} iteration, the total load shedding amount is reduced from 376.5MW to 362.5MW while the transient voltage dip is still within criteria.

Table 6.3: Iteration of load shedding scheme for Case II by PSO

Iteration	Shedding Places (Bus No.)	Shedding Amount (MW)	Total Amt. (MW)	Trans. Vdip (%)
0	0	0	0	99.2608
1	26	5.0	5.0	98.3500
2	26	5.0	5.0	98.3500
3	26	5.0	5.0	98.3500
4	26,39	6.8,91.0	97.8	98.3169
5	26,39	8.5,106.0	114.5	97.8458
6	12,26,39	8.6,7.5,30.1	46.2	95.9743
7	8,12,26,39	66.4,8.6,7.7,62.6	145.3	32.8908
8	8,12,26,39	88.4,8.6,8.3,74.1	179.4	31.4234
9	8,12,16,26,39	82.5,8.6,37.2,5.9,142.4	276.6	30.2154
10	8,12,16,25,26,39	118.0,8.6,6.3,39.1,7.8,126.7	306.5	27.7867
11	8,12,16,25,26,39	147.2,8.6,10.9,41.1,8.0,128.5	334.3	26.1410
12	8,12,16,25,26,39	168.2,8.6,14.3,42.5,8.2,129.7	371.5	25.0865
13	8,12,16,20,25,26,39	171.9,8.6,13.9,8.0,35.9,7.8,130.4	376.5	**24.9251**
14	8,12,16,20,25,26,39	171.9,8.6,13.9,8.0,35.9,7.8,130.4	376.5	24.9251
15	8,12,16,20,25,26,39	171.9,8.6,13.9,8.0,35.9,7.8,130.4	376.5	24.9251
16	8,12,16,20,25,26,39	171.9,8.6,13.9,8.0,35.9,7.8,130.4	376.5	24.9251
17	8,12,16,20,25,26,39	178.6,8.6,5.0,5.7,38.3,7.7,121.7	365.7	24.8800
18	8,12,16,20,25,26,39	178.6,8.6,5.0,5.7,38.3,7.7,121.7	365.7	24.8800
19	8,12,16,20,25,26,39	178.6,8.6,5.0,5.7,38.3,7.7,121.7	365.7	24.8800
20	8,12,16,20,25,26,39	176.4,8.6,5.4,5.3,37.8,7.6,119.9	**362.5**	24.9604

The objective functions of the PSO algorithm can be plotted in Figure 6.8. The figure has two y-axes. The left y-axis is the first objective function (6.4) and the right y-axis is the second objective function (6.5). To clearly show the procedures, we do not abort the iteration and have the iteration runs up to 20 times. The transient voltage dip recovers within criteria at the 13^{th} iteration. After that, the algorithm switches from the first objective function to the second objective function. It reduces the total amount of load shedding and maintains the transient voltage dip within criteria.

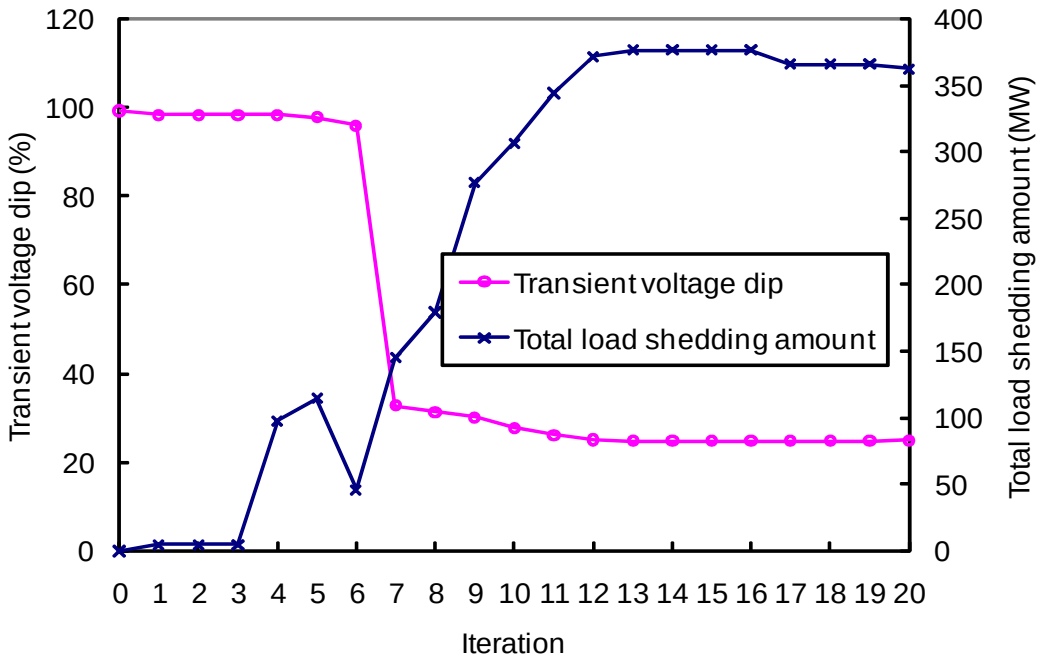

Figure 6.8: Load shedding convergence characteristic for Case II by PSO

6.7.2 Sensitivity Based Algorithm

Table 6.4 shows the load shedding options and relative amount of each iteration. The initial amount of load shedding is 5MW of active power and corresponding reactive power to keep the power factor unchanged of that load. When the leading buses hit their load limits, these buses are completely shed. At the same time, the other loads shed 5MW each to form the new candidate options of load shedding. Bus 26 is the most effective load shedding place at the beginning. After completely shedding Bus 26 (153.5MW), Bus 12 becomes the leading bus. However, Bus 12 only has 8.6MW to be shed which is not enough. After both Bus 26 and Bus 12 are completely shed, Bus 7 is selected as the leading bus. After continually shedding 105.4MW at Bus 7, the transient voltage dip is reduced within criteria with 24.99% dip. The final load shedding scheme is obtained by shedding a total of 267.5MW which includes Bus 7

(105.4MW), completely shedding Bus 12 (8.6MW) and Bus 26 (153.5MW).

Table 6.4: Optimal load shedding scheme during iteration for Case II by sensitivity method

Iteration	Shedding Places (Bus No.)	Shedding Amount after limit (MW)	Trans. Vol. Dip (%)
0			99.2608
1	26	5.0	98.3500
2	26	153.5	98.1549
3	26, 12	153.5, 5.0	35.5570
4	26, 12	153.5, 5.9	34.5824
5	26, 12	153.5, 8.6	32.1422
6	26, 12, 7	153.5, 8.6, 5	31.7686
7	26, 12, 7	153.5, 8.6, 96.9	25.4781
8	26, 12, 7	153.5, 8.6, 105.4	24.9889

The total load shedding amount is 267.5 MW of the final scheme that brings 24.99% transient voltage dip. The total amount to be shed and the relative transient voltage dip at each iteration are plotted in Figure 6.9. The figure has two y-axes. The left y-axis is the transient voltage dip and the right y-axis is the total amount of load shedding. The transient voltage dip is reduced within criteria at the end of the eighth iteration. The case is restored to be voltage stable by activating the load shedding scheme after the fault happening. A bus voltage trajectory of pre- and post- load shedding in simulation is plotted in Figure 6.10. The graph shows the load shedding scheme obtained from the sensitivity based method can successfully and effectively prevent the system from tending to collapse after the contingency occurs.

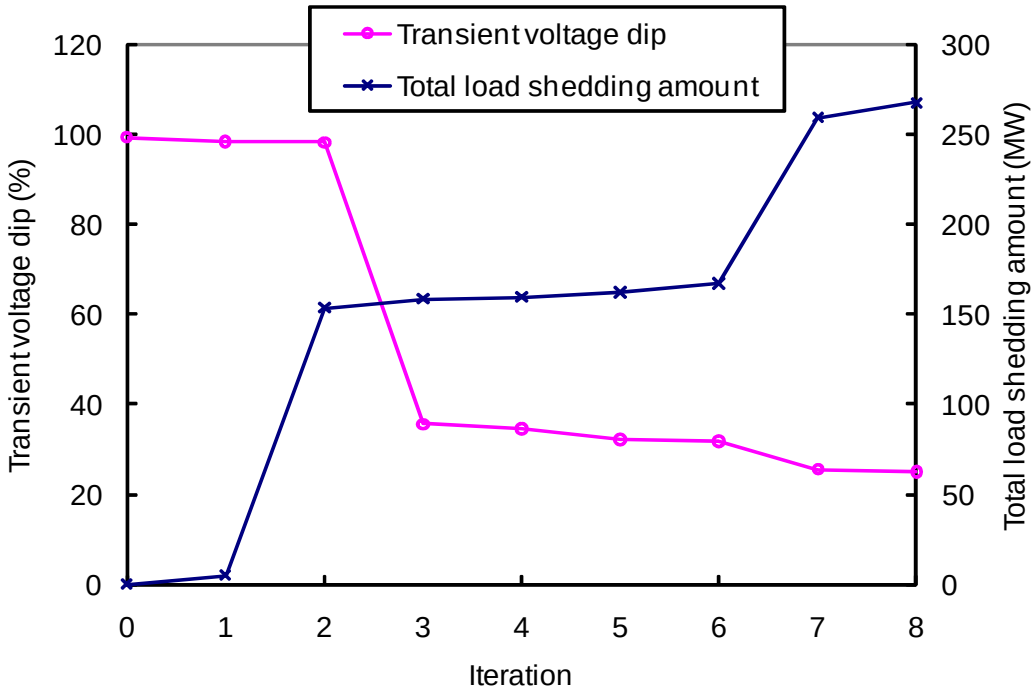

Figure 6.9: Load shedding convergence characteristic for Case II by sensitivity method

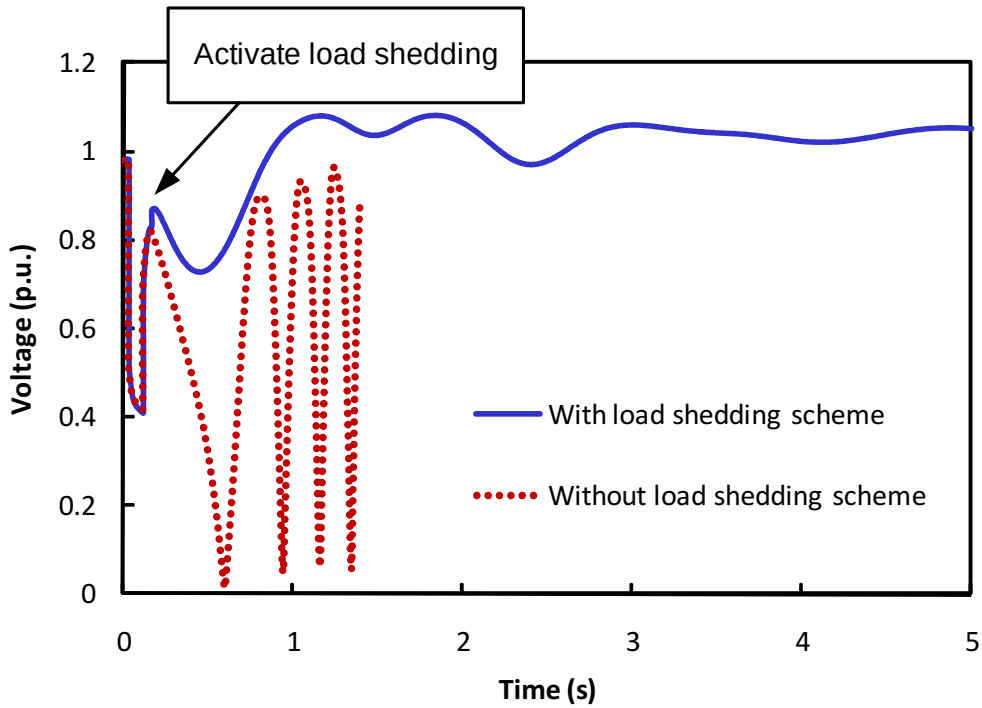

Figure 6.10: The effect of load shedding scheme for Case II

6.8 Comparison of Two Algorithms

Both particle swarm optimization algorithm (PSO) and sensitivity based algorithm are able to find a load shedding scheme that can restore the system from emergency state to safe state after a severe contingency. However, the results of the load shedding schemes are different. Table 6.5 presents some key factors that evaluate the effect of the load shedding algorithm. **Iteration** is an incremental index to execute each algorithm. **No. of simulation** defines the times of running time-domain simulation. Each iteration can include one or several potential load shedding plans that need to be verified by simulation. For the PSO algorithm, each iteration includes 18 load shedding plans. For the sensitivity based algorithm, whenever selecting a new leading bus, it needs 18 times of simulation. If the leading bus still has an available amount to be shed, it only needs one simulation. The No. of simulation determines most of the time to execute each algorithm. For example, if one simulation takes 2 seconds, 100 simulations need 200 seconds. If the algorithm requires 100 simulations, it takes around 200 seconds to obtain the load shedding scheme with this algorithm. **Total shedding Amt.(MW)** and **Trans. vol. dip (%)** are two main objectives for the load shedding algorithms. **No. of shed loads** represent the number of loads that attend the final load shedding scheme.

Table 6.5 indicates the following difference of PSO and sensitivity based algorithms:

1. The PSO algorithm usually uses fixed iteration steps. In the first few iteration steps, the objective function of the PSO algorithm is to restore the system from emergency state to safe state. After reaching this aim, the objective function is changed to minimize the total load shedding amount in the later iteration steps. The sensitivity based algorithm uses early stop rule that stops the iteration when

Table 6.5: Comparison of PSO and sensitivity based algorithms

		PSO	Sensitivity
Case I	Iteration	20	6
	No. of simulation	360	40
	Total shedding Amt.(MW)	107.9	105.0
	Trans. vol. dip (%)	24.96	24.84
	No. of shed loads	4	2
Case II	Iteration	20	8
	No. of simulation	360	59
	Total shedding Amt.(MW)	362.5	267.5
	Trans. vol. dip (%)	24.96	24.99
	No. of shed loads	7	3

the sensitivity based algorithm finds a load shedding scheme that satisfies the voltage stability criteria. The PSO algorithm needs more iterations than the sensitivity based algorithm.

2. The PSO algorithm conducts more simulations than the sensitivity based algorithm. Therefore, PSO takes more time to find the solution of load shedding scheme than the sensitivity based algorithm. The PSO algorithm sets a certain number of particles which are candidate solutions in the searching space. PSO then conducts a simulation for each particle in each iteration. The sensitivity based algorithm uses a variable number of simulations for each iteration. In order to find a leading bus to shed load, the sensitivity based algorithm sheds small amount for each candidate load that takes n (n = candidate loads) times of simulation. Once the leading bus still has an available amount to be shed, the sensitivity based algorithm only needs one simulation for shedding more on that leading bus. Hence, even if the PSO algorithm uses the same iteration as the sensitivity based algorithm, the PSO algorithm needs a higher number of simulations.

3. The PSO algorithm sheds higher load amount than the sensitivity based algorithm in order to restore the system to maintain voltage stability after contingency.

4. The PSO algorithm selects more loads to shed than the sensitivity based algorithm in the final load shedding scheme.

Based on the above comparison, the sensitivity based algorithm has a faster and more effective performance than the particle swarm optimization algorithm (PSO). The sensitivity based algorithm uses less computation time to find the minimum load shedding amount to maintain system voltage stability after the occurrence of contingency.

Chapter 7

Conclusions

This chapter concludes the work carried out, discusses main contributions, and presents thoughts for future research in the area of power systems security assessment and control.

7.1 General conclusions

In the thesis, two specific areas of research have been investigated under the power system voltage stability enhancement. The two areas are small disturbance voltage stability and large disturbance voltage stability. The small disturbance voltage stability has been discussed in Chapter 2 to Chapter 4 and the large disturbance voltage stability has been discussed in Chapter 5 to Chapter 6. For each area of voltage stability, a combination algorithm of computational intelligence techniques and conventional voltage stability assessment has been proposed. The reason for using computational intelligence techniques is that they have the advantage at computational speed and are suitable for online application.

The proposed combination algorithms not only predict how far the system is from insecure, but also provide approaches to carry out actions of voltage stability controls. The artificial neural network as the representative of computational intelligence techniques is combined with continuation power flow to perform small disturbance voltage stability assessment. Furthermore, the applications of combinational algorithm is applied in preventive control, such as generation reschedule, of small disturbance voltage stability. Similarly, the artificial neural network technique is combined with time domain simulation to perform large disturbance voltage stability assessment. Furthermore, a load shedding algorithm is combined with time-domain simulation to perform corrective control to prevent large disturbance voltage instability.

Continuation power flow, the method of assessing small-disturbance voltage stability, is discussed in Chapter 2. Small-disturbance voltage stability is concerned with a system's stability to a progressive drop in voltage when increasing gradually in load demand. The voltage stability margin is quite straightforward and an easily understood index for this kind of voltage stability. The conventional power flow algorithms are prone to convergence problems in calculating the voltage stability margin. The continuation power flow overcomes this problem by reformulating the power flow equations so that they remain well-conditioned at all possible loading conditions. The equations are introduced and Continuation Power Flow (CPF) program is developed in Matlab language. The CPF uses an iterative predictor-corrector scheme to find the solution path and to determine the small-disturbance voltage stability limit for a certain load increase pattern. The program can handle various types of constraints and models which can have a significant impact on the voltage stability phenomenon. A commercial power flow program, PSAT, is used to validate the correctness of CPF

based on a 12-bus test system.

Since the continuation power flow is time consuming for large-scale power systems, an online application requires faster tools. In Chapter 3, the previous developed CPF program is used to generate training patterns for training an ANN to calculate the voltage stability margin which serves as a voltage stability index. A major advantage of the ANN approach is that ANN is able to sufficiently abstract what it learns in training and extend this to produce reasonable outputs for those inputs not encountered during training. Once trained, an ANN can predict the stability margin for a given set of inputs very quickly, as the calculations in the ANN do not involve any iteration as in the case of using analytical methods. Therefore, the thesis proposes the framework of ANN strategy including a complete process of training and testing an ANN to predict voltage stability margin.

Generally, ANN works as a black box between inputs X and outputs Y, which represents a mathematical relationship: $f : X \rightarrow Y$. It is crucial that we use key physical parameters contributing to voltage stability in ANN models. Some different sets of input variables to the ANN models based on a heuristic understanding and knowledge of the problem are tested in ANN. Bus voltage magnitudes and phase angles of individual buses are found to be the best input variables to predict voltage stability margin in ANN. Phase angles are generally thought of as less related to voltage stability. However, this research proposes to adopt voltage magnitudes and phase angles as input features of ANN. In the test of different sets of inputs on the New England 39-bus system, it significantly improves the accuracy of the estimation of voltage stability margin.

In Chapter 3, it was found that voltage magnitudes and phase angles are the proper input variables for ANN. In addition to the tests, the importance of why voltage magnitudes and phase angles as input features of ANN to predict real power margin was analyzed. Besides input variables selection, some important aspects of ANN application were discussed based on the study system (the New England 39-bus system). These were sample data size, overfitting or underfitting, computation speed and accuracy measure. The proposed ANN based approach for voltage stability margin estimation was also applied to an Alberta Interconnected Electric System which was acquired from the Alberta Electric System Operator (AESO) website. The system consists of 1844 buses. We used the AESO system as an application example to demonstrate the feasibility of the proposed method to predict the voltage stability index of a large practical system.

In Chapter 4, several extended applications of the proposed ANN approach for small-disturbance voltage stability and control were presented. The first application was optimal placement of PMUs. The input variables for the proposed ANN based online voltage stability monitoring system were the voltage magnitudes and the phase angles. Real-time measurement of phase angles requires the use of Phasor Measurement Units (PMUs) and telecommunication infrastructure to support the data acquisition. When only a limited number of PMUs are used, it is important to locate them at the most effective positions in the network. Selection of PMU locations can be viewed as the selection of a reduced set of input features to the ANN while the prediction error is not increased significantly. As sequential forward selection (SFS) algorithm is proposed to determine the optimal input feature set. In comparison to exhaustive

search, SFS largely reduces the number of searches and always selects a good input feature set.

The second application is N-1 contingency scanning. Since disturbances are inevitable in a power system, it is particularly important for the proposed ANN approach to be able to estimate the voltage stability margin after a contingency. The system restoration after a contingency often requires removal of the faulted element, resulting in a new network configuration. Usually separate ANNs are used for different contingencies in order to achieve good performance of ANN. This thesis tackles this drawback and deals with a single ANN for all the contingencies. The input variables of post-contingency power flow are used to feed to ANN, which results in this compact and efficient ANN approach.

The third ANN application of Chapter 4 is for generation rescheduling. Generation rescheduling is applied as a preventive action to enhance voltage stability margin. The method proposed is to examine the sensitivity of the voltage stability margin to shifting of the real power output of one selected generator to another. The sensitivity of the voltage stability margin to shifting of real power generation is calculated by the already trained ANN. Therefore, it quickly selects the best way to change the generation output that maximizes the voltage stability margin under a given condition.

Large-disturbance voltage stability is an increasing, but often overlooked, industry concern. Moreover, few studies have reported on how to execute corrective control action after the contingency occurs if the system is short-term voltage instability. Chapter 5 and Chapter 6 concentrate on analyzing the power system for short-term

voltage stability and control under large-disturbances (contingencies).

In a large interconnection power network, transient voltage dip criteria is more convenient to use than power margin based criteria. Short-term voltage stability assessment needs to consider the fast acting and automatically controlled dynamic power system equipments. Generally speaking, time domain simulation is the most essential approach to provide insight into the dynamic behavior of those equipments and calculate transient voltage dip after a contingency. However, time domain simulation has been computationally challenging for online application. In Chapter 5, the combination of the ANN method and a commercial time-domain simulation program is developed to calculate transient voltage dip. The voltage magnitudes and phase angles of pre-contingency operation conditions are used as input features to the ANN. The transient voltage dip is the output of ANN. It has been shown that the proposed ANN method for large-disturbance voltage stability assessment is promising.

When an ANN method predicts that the system may indeed move toward voltage instability under a large disturbance, some remedial actions such as load shedding need to be undertaken to preserve the system integrity. In order to carry out the remedial action, two load shedding algorithms are developed in Chapter 6 to calculate the optimal load shedding locations and the associated minimum load shedding amount at the known relay time of these loads. The first approach is a particle swarm optimization (PSO) algorithm that performs an optimization search in the search space of an optimization problem. The second approach is a sensitivity based algorithm that is conducted through the sensitivity index of the load shedding buses. The sensitivity is used to seek the leading bus. The anticipated load shedding amount of the leading

bus is then calculated by sensitivity and verified in simulation aiming at approaching the voltage stability criteria. As a result, both algorithms have provided a load shedding scheme providing two important elements of load shedding: the load shedding locations, and minimum shedding amount when the relay time is known. Both algorithms are based on simulation so that all the dynamic behavior of the system before and after subjecting it to large disturbances are considered. The simulation results show that the load shedding algorithm leads to a satisfactory result which can recover the potential unsafe system to voltage stability after the occurrence of contingencies.

7.2 Contributions

The goal for this thesis research is to develop a comprehensive on-line strategy for voltage stability analysis, and for voltage stability preventive and corrective control, through application of wide area measurements. The contributions of this thesis, with respect to this goal, include the following:

1. Identifying the performance indices which predict proximity to voltage instability problems for small-disturbance voltage stability analysis and large-disturbance voltage stability analysis individually.

2. Developing a continuation load flow program to calculate the small-disturbance voltage stability margin. The program considers continuous techniques to overcome the singularity of Jacobian matrix when the system is approaching stressful conditions. The continuation load flow program includes the features: generator reactive power capability limits; transformer tap changing; static load

models; reactive compensation devices; and HVDC converters.

3. Developing a framework of artificial neural network method to calculate voltage stability margin that can replace the continuation load flow program at on-line application.

4. Proposing to use the voltage magnitudes and phase angles measured by PMUs as the inputs for ANN. The selection of inputs is tested on the study system and analyzed theoretically.

5. Implementing and testing the ANN approach on a practical power system with over 1800 buses to evaluate the feasibility and reliability of the proposed approach in a real and large size system.

6. Applying the ANN based approach to determine the voltage stability margin under the different N-1 contingency scenarios. According to the output of evaluation of voltage stability under N-1 contingency, the proper preventive control, such as generation reschedule and generator second voltage control, are carried out to enhance voltage stability based on sensitivity.

7. Proposing a sequential forward selection approach based on ANN to determine the best locations for PMUs since only a limited number of PMUs can be installed. The proposed algorithm significantly reduces the searching times as compared to the exhausted searching algorithm.

8. Developing an ANN approach that involves the initial system operating points measured by PMUs to predict transient voltage dip that is calculated by the time-domain simulation. Since the simulation program is a commercial software, the data exchange and simulation is incorporated in the developed ANN

approach.

9. Developing two simulation based algorithms to find the load shedding scheme as a corrective control for on-line large-disturbance voltage stability. Both of the algorithms are executed based on time-domain simulation so that they are able to investigate the dynamic behavior of the system before and after subjecting it to large disturbances, in depth with all the dynamic devices and voltage-dependant loads taking part in the short-term voltage instability.

These contributions have led to the following publications.

- Debbie Q. Zhou, U. D. Annakkage, and A. D. Rajapakse, "Online Monitoring of Voltage Stability Margin Using an Artificial Neural Network", Accepted for publication in IEEE Transactions on Power Systems.
- Debbie Q. Zhou, Udaya D. Annakkage, and Athula Rajapakse, "Combination of Computational Intelligence and Simulation for Online Prediction and Control of Large-disturbance Voltage Stability", to be submitted to IEEE Transaction on Power Systems.
- Debbie Q. Zhou, Udaya D. Annakkage, and Athula Rajapakse, "An Online Load Shedding Approach for Voltage Stability Enhancement," CIGRE Canada Conference on Power Systems, Toronto, October, 2009.
- Debbie Q. Zhou, Udaya D. Annakkage, and Athula Rajapakse, "Optimal Placement of PMUs in a Wide Area Monitoring System Using an Artificial Neural Network Based Technique", CIGRE Canada Conference on Power Systems, Winnipeg, October, 2008.

- Debbie Q. Zhou and Udaya D. Annakkage, "Investigation of a Criterion for Load Shedding Based on voltage stability indices", CIGRE Canada Conference on Power Systems, Calgary, August, 2007.

7.3 Suggestions for Future Research

The area of research presented in this thesis offers a wide range of projects that the author would like to suggest for future studies.

The success of application of the artificial neural network for predicting voltage stability indices is dependent on choosing voltage magnitudes and phase angles as inputs of the ANN. The wide-area or global signals of voltage magnitudes and phase angles are essentially based on synchronized data acquisition technology, e.g. Phasor Measurement Units (PMUs). In this thesis, the input variables, voltage magnitudes and phase angles, are computed by power flow program under different operating conditions. In order to implement this ANN algorithm for real-time application, it is suggested to use real-time data which are gathered by PMUs and the SCADA system. Such a system can be tested on Real Time Digital Simulator (RTDS) before using in the real power system. The power system with wide area measurement can be simulated on RTDS and the signals can be sampled from the I/O of RTDS and fed to the ANN to perform voltage stability assessment.

The artificial neural network is an adaptive system that is able to learn the complex relationships based on external or internal information during the training phase. Accurate training of a neural network algorithm requires a great computational effort. A practical power system usually consists of hundreds and thousands of nodes.

Therefore, there are hundreds and thousands of nodes whose data are associated with each operating condition. Faced with numerous input data, training an ANN is a big challenge because the computer may not have enough memory available to run this ANN training program. In addition as the training time increases, it becomes an obstacle for on-line training. Hence, more research is necessary to deal with large scale computing capabilities and for reducing the training time. One possible area to explore is parallel computing which is a form of computation in which many calculations are carried out simultaneously. Large problems can often be divided into smaller ones, which are then solved in parallel.

When discussing the corrective control of the short-term voltage stability under large disturbance, load shedding is employed as one of the important control actions. There are new control actions that can be carried out at the emergency state. For example, FACTS devices and multiterminal HVDC transmission have significant growth with the development of the power industry. FACTS control devices provide new control systems for existing transmission lines. HVDC systems have the ability to rapidly control the transmitted power. Therefore, they have a significant impact on the stability of the associated ac power systems [10]. These trends become a challenge for the proper coordination of protection and control systems. It is interesting to compare the different control actions and select the most effective and fast control action to secure the system state of operation.

Appendix A

12-bus System Network

This appendix provides complete steady state data for a system.

Figure A.1 shows the 12-bus system network with some of the main data at base case condition [51]. Table A.1 to Table A.3 are the system data.

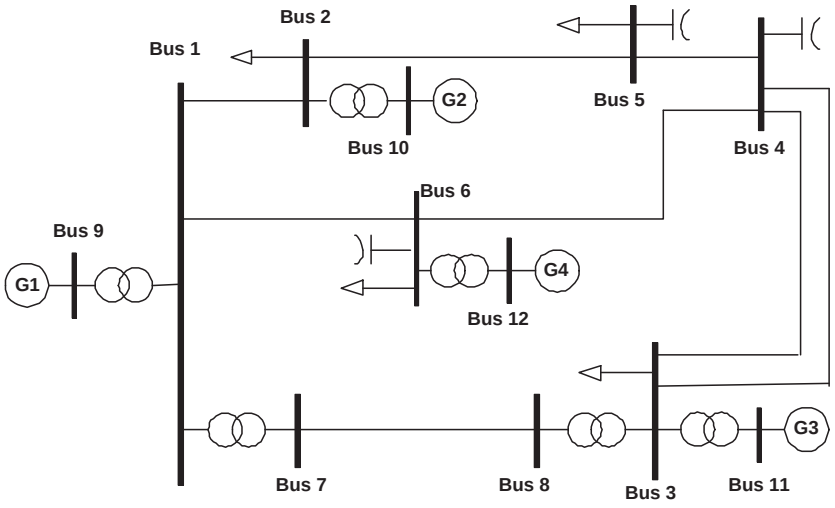

Figure A.1: 12 Bus Single Line Diagram

Bus Number	P_{gen} (MW)	Q_{gen}^{max} (MVar)	Q_{gen}^{min} (MVar)	MBASE (MW)	V_{set} (p.u.)
9	509.123	330	-1100	800	1.04
10	500	300	-1000	700	1.02
11	200	440	-800	500	1.04
12	300	240	-600	500	1.02

Table A.1: Generation Data

Bus	$P_{load}(MW)$	$Q_{load}(MVar)$
2	280	200
3	320	240
4	320	240
5	100	60
6	440	300

Table A.2: Load Data

Bus	Shunt Q (MVar)	Step Size
4	200	40
5	80	40
6	200	40

Table A.3: Switched Shunt Data

Bus Number		R	X	B/2
From	To	(p.u.)	(p.u.)	(p.u.)
1	2	0.01144	0.09111	0.18261
1	6	0.03356	0.26656	0.55477
2	5	0.03356	0.26656	0.55477
3	4	0.01144	0.09111	0.18261
3	4	0.01144	0.09111	0.18261
4	5	0.03356	0.26656	0.55477
4	6	0.03356	0.26656	0.55477
7	8	0.01595	0.17214	3.28530

Table A.4: Transmission Line Data

Bus Number		R	X	Transformer Tap Settings (p.u.)			
From	To	(p.u.)	(p.u.)	Initial	Max	Min	Step Size
1	7	0.0	0.01	1.0	1.1	0.9	0.00625
1	9	0.0	0.01	1.0	1.1	0.9	0.00625
2	10	0.0	0.01	1.0	1.1	0.9	0.00625
3	8	0.0	0.01	1.0	1.1	0.9	0.00625
3	11	0.0	0.01	1.0	1.1	0.9	0.00625
6	12	0.0	0.02	1.0	1.1	0.9	0.00625

Table A.5: Transformer Data

Appendix B

New England 39-bus System Network

This appendix provides complete steady state data for the New England 39-bus system [80].

Figure B.1 shows the system network with some of the main data at base case conditions. Table B.1 to Table B.4 are system data.

Bus Number	P_{gen} (MW)	Q_{gen}^{max} (MVar)	Q_{gen}^{min} (MVar)	MBASE (MW)	V_{set} (p.u.)
30	250.000	500	-9999	300.000	1.04750
31	898.805	9999	-9999	612.000	0.98200
32	650.000	9999	-9999	765.000	0.98310
33	632.000	9999	-9999	700.000	0.99720
34	508.000	9999	-9999	613.000	1.01230
35	650.000	300	-9999	798.000	1.04930
36	560.000	9999	-9999	660.000	1.06350
37	540.000	9999	-9999	660.000	1.02780
38	830.000	9999	-9999	1151.000	1.02650
39	1000.000	9999	-9999	1200.000	1.03000

Table B.1: Generation Data

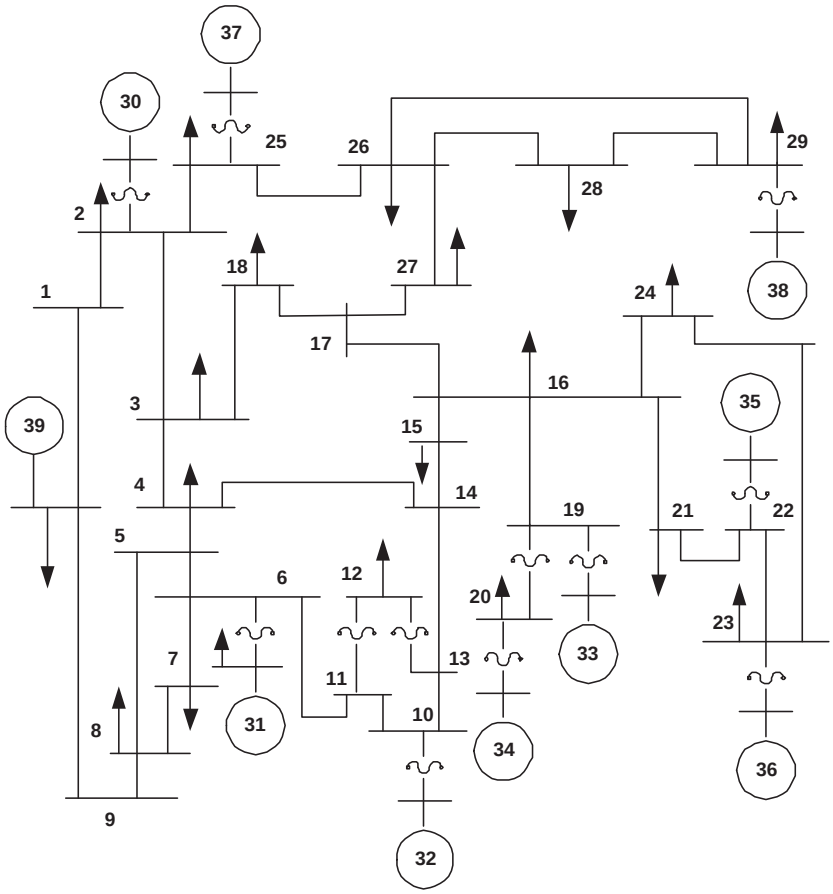

Figure B.1: 39 Bus Single Line Diagram

Bus Number	$P_{load}(MW)$	$Q_{load}(MVar)$	Bus Number	$P_{load}(MW)$	$Q_{load}(MVar)$
2	322.0	2.4	21	274.0	115.0
3	322.0	2.4	23	247.5	84.6
4	500.0	184.0	24	308.6	-92.2
7	233.8	84.0	25	224.0	47.2
8	522.0	176.0	26	139.0	17.0
12	8.5	88.0	27	281.0	75.5
15	320.0	153.0	28	206.0	27.6
16	329.4	32.3	29	283.5	26.9
18	158.0	30.0	31	9.2	4.6
20	680.0	103.0	39	1004.0	117.0

Table B.2: Load Data

Bus Number		R	X	B/2	Bus Number		R	X	B/2
From	To	(p.u.)	(p.u.)	(p.u.)	From	To	(p.u.)	(p.u.)	(p.u.)
1	2	0.0035	0.0411	0.6987	14	15	0.0018	0.0217	0.3660
1	39	0.0010	0.0250	0.7500	15	16	0.0009	0.0094	0.1710
2	3	0.0013	0.0151	0.2572	16	17	0.0007	0.0089	0.1342
2	25	0.0070	0.0086	0.1460	16	19	0.0016	0.0195	0.3040
3	4	0.0013	0.0213	0.2214	16	21	0.0008	0.0135	0.2548
3	18	0.0011	0.0133	0.2138	16	24	0.0003	0.0059	0.0680
4	5	0.0008	0.0128	0.1342	17	18	0.0007	0.0082	0.1319
4	14	0.0008	0.0129	0.1382	17	27	0.0013	0.0173	0.3216
5	6	0.0002	0.0026	0.0434	19	20	0.0007	0.0138	0.2548
5	8	0.0008	0.0112	0.1476	21	22	0.0008	0.0140	0.2565
6	7	0.0006	0.0092	0.1130	22	23	0.0006	0.0096	0.1846
6	11	0.0007	0.0082	0.1389	23	24	0.0022	0.0350	0.3610
7	8	0.0004	0.0046	0.0780	25	26	0.0032	0.0323	0.5130
8	9	0.0023	0.0363	0.3804	26	27	0.0014	0.0147	0.2396
9	39	0.0010	0.0250	1.2000	26	28	0.0043	0.0474	0.7802
10	11	0.0004	0.0043	0.0729	26	29	0.0057	0.0625	1.0290
10	13	0.0004	0.0043	0.0729	28	29	0.0014	0.0151	0.2490
13	14	0.0009	0.0101	0.1723					

Table B.3: Transmission Line Data

Bus Number		R	X	Transformer Tap Settings (p.u.)			
From	To	(p.u.)	(p.u.)	Initial	Max	Min	Step Size
2	30	0.0000	0.0181	1.0	1.1	0.9	0.00625
6	31	0.0000	0.0250	1.0	1.1	0.9	0.00625
10	32	0.0000	0.0200	1.0	1.1	0.9	0.00625
12	11	0.0016	0.0435	1.0	1.1	0.9	0.00625
12	13	0.0016	0.0435	1.0	1.1	0.9	0.00625
19	33	0.0007	0.0142	1.0	1.1	0.9	0.00625
20	34	0.0009	0.0180	1.0	1.1	0.9	0.00625
22	35	0.0000	0.0143	1.0	1.1	0.9	0.00625
23	36	0.0005	0.0272	1.0	1.1	0.9	0.00625
25	37	0.0006	0.0232	1.0	1.1	0.9	0.00625
29	38	0.0008	0.0156	1.0	1.1	0.9	0.00625

Table B.4: Transformer Data

Appendix C

Voltage Stability in Simple Radial Network

Figure C.1 presents a simple radial network. This network has a constant voltage source, which imitates a synchronous machine with sufficient exciter supporting, go through a transmission line and On-load Tap Changing transformer (OLTC) to supply a load. Voltage source is E_s, the off-normal radio of the transformer is k, the impedance of the transmission line is $Z_L\angle\theta$; load impedance is $Z_D\angle\phi$.

The expression for current $\dot{I}$ is

$$\dot{I} = \frac{\dot{E}_s}{\dot{Z}_L + \dot{Z}_D} = \frac{E_s}{Z_L\angle\theta + \frac{1}{k^2}Z_D\angle\phi} \tag{C.1}$$

The magnitude of the current $\dot{I}$ is

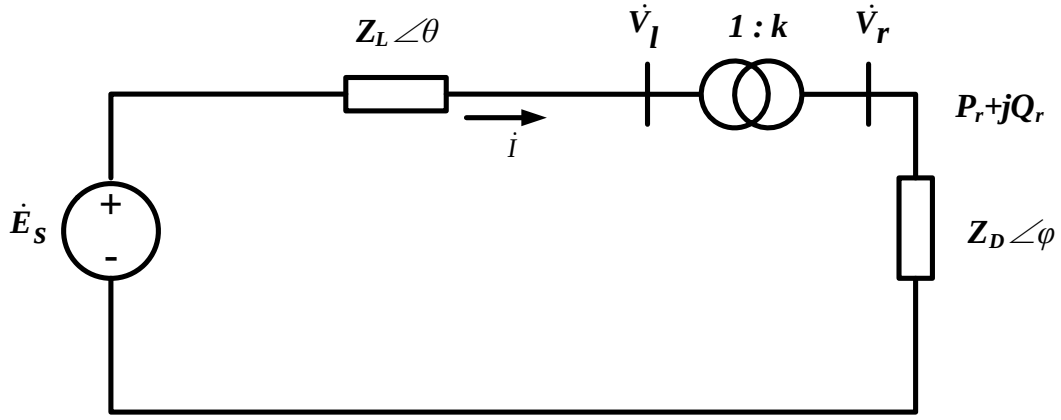

Figure C.1: A simple radial network with transformer

$$I = \frac{k^2 E_s}{\sqrt{k^4 {Z_L}^2 + 2k^2 Z_L Z_D \cos(\theta - \phi) + {Z_D}^2}} \tag{C.2}$$

The per unit of the current $\dot{I}$ is given by

$$I/I_{SC} = \frac{k^2 Z_{LD}}{\sqrt{1 + \left[\ 2k^2 \cos(\theta - \phi) Z_{LD} + k^4 Z_{LD}^2\ \right]}} \tag{C.3}$$

Where,

$$Z_{LD} = \frac{Z_L}{Z_D}, \qquad I_{SC} = \frac{E_S}{Z_L} \tag{C.4}$$

The receiving end voltage is expressed as,

$$\dot{V}_R = \dot{I} \frac{Z_D \angle\phi}{k} \tag{C.5}$$

The voltage of the first side of the tap change transformer is expressed as

$$\dot{V_P} = \dot{E_s} - \dot{I} Z_L \angle\theta \tag{C.6}$$

The per unit of the receiving end voltage is given by

$$V_R/E_S = \frac{k}{\sqrt{1 + \left[\ 2k^2 \cos(\theta - \phi) Z_{LD} + k^4 Z_{LD}^2\ \right]}} \tag{C.7}$$

The per unit of the first side voltage is given by

$$V_P/E_S = \frac{1}{\sqrt{1 + \left[\ 2k^2 \cos(\theta - \phi) Z_{LD} + k^4 Z_{LD}^2\ \right]}} \tag{C.8}$$

The transferring power in the transmission line is

$$P_R + jQ_R = \dot{V_R} \frac{\hat{\dot{I}}}{k} = \frac{I^2 Z_D}{k^2} (\cos\phi + j \sin\phi) \tag{C.9}$$

Substitute equation (C.2) to equation (C.9), get

$$\begin{aligned} P_R &= \frac{k^2 E_S \cos\phi}{Z_L} \frac{Z_{LD}}{1 + \left[\ 2k^2 \cos(\theta - \phi) Z_{LD} + k^4 Z_{LD}^2\ \right]} \\ Q_R &= P_R \tan\phi \end{aligned} \tag{C.10}$$

If setting $\dfrac{dP_R}{dZ_{LD}} = 0$, the maximum value of power can be calculated. When $Z_{LD} = \dfrac{1}{k^2}$,

means $Z_D = k^2 Z_L$

$$\begin{aligned} P_{Rmax} &= \frac{E_S^2 \cos\phi}{2Z_L \left[\ 1 + \cos(\theta - \phi) \ \right]} \\ Q_{Rmax} &= P_{Rmax} \tan\phi \end{aligned} \tag{C.11}$$

P_{Rmax} of equation (C.11) is the maximum power which is transmitted from generator to load. Normalizing P_R and Q_R as below

$$P_R/P_{Rmax} = Q_R/Q_{Rmax} = \frac{2k^2 Z_{LD} \left[\ 1 + \cos(\theta - \phi) \ \right]}{1 + \left[\ 2k^2 \cos(\theta - \phi) Z_{LD} + k^4 Z_{LD}^2 \ \right]} \tag{C.12}$$

The receiving end power for the load with $k = 1$ can be expressed,

$$P_R + jQ_R = \dot{V}_R \hat{\dot{I}}_R = \dot{V}_R \frac{E_S - \hat{\dot{V}}_R}{Z_L \angle -\theta} = \frac{V_R E_S \cos\theta_R - V_R^2 + jV_R E_S sin\theta_R}{\frac{X_L}{\tan\theta - jX_L}} \tag{C.13}$$

To normalize active power, reactive power and load voltage, set,

$$p = \frac{P_R X_L}{E_S^2}, \qquad q = \frac{Q_R X_L}{E_S^2}, \qquad v = \frac{V_R}{E_S} \tag{C.14}$$

Substituting to equation (C.13) get,

$$v\cos\theta_R = v^2 + \frac{p}{\tan\theta} + q$$

$$v\sin\theta_R = \frac{q}{\tan\theta} - q \tag{C.15}$$

Eliminating θ_R from equation (C.15) obtain the following equation,

$$v^4 + \left(\frac{2}{\tan\theta}p + 2q - 1 \right) v^2 + \left(1 + \frac{1}{\tan^2\theta} \right) \left(p^2 + q^2 \right) = 0 \tag{C.16}$$

Solve equation (C.16) and replace q by $q = p\tan\phi$, the relationship of voltage and active power is,

$$v^2 = \frac{1}{2} - \left(\frac{1}{\tan\theta} + \tan\phi \right) p \pm \sqrt{\frac{1}{4} - \left(\frac{1}{\tan\theta} + \tan\phi \right) p - \left(1 - \frac{\tan\phi}{\tan\theta} \right)^2 p^2} \tag{C.17}$$

Appendix D

Eigenvalue and Singular-value Decomposition

In the conventional power flow, the power flow equation by using the Newton-Raphson technique has a linearized model around the given operating point which can be expressed as equation (D.1),

$$\begin{bmatrix} \Delta P \\ \Delta Q \end{bmatrix} = \begin{bmatrix} \frac{\partial P}{\partial \theta} & \frac{\partial P}{\partial V} \\ \frac{\partial Q}{\partial \theta} & \frac{\partial Q}{\partial V} \end{bmatrix} \begin{bmatrix} \Delta \theta \\ \Delta V \end{bmatrix} = [J] \begin{bmatrix} \Delta \theta \\ \Delta V \end{bmatrix} \tag{D.1}$$

Where J is Jacobian matrix which is a linear transformation of space of $[\Delta\theta \ \Delta V]$ into space of $[\Delta P \ \Delta Q]$. ΔP, ΔQ, ΔV and $\Delta\theta$ represent incremental change in bus active power, reactive power, voltage magnitude and phase angle respectively.

Letting J be a kxk square matrix

$$J = \begin{bmatrix} J_{11} & J_{12} & \cdots & J_{1k} \\ J_{21} & J_{22} & \cdots & J_{1k} \\ \cdots & \cdots & \ddots & \cdots \\ J_{k1} & J_{k2} & \cdots & J_{kk} \end{bmatrix} \tag{D.2}$$

with eigenvalue λ, then the corresponding eigenvectors satisfy

$$J = \begin{bmatrix} J_{11} & J_{12} & \cdots & J_{1k} \\ J_{21} & J_{22} & \cdots & J_{1k} \\ \cdots & \cdots & \ddots & \cdots \\ J_{k1} & J_{k2} & \cdots & J_{kk} \end{bmatrix} \begin{bmatrix} x_1 \\ x_2 \\ \cdots \\ x_k \end{bmatrix} = \lambda \begin{bmatrix} x_1 \\ x_2 \\ \cdots \\ x_k \end{bmatrix} \tag{D.3}$$

which can be written compactly as

$$\begin{aligned} JX &= \lambda X \\ or, \qquad J &= X^{-1}\lambda X \end{aligned} \tag{D.4}$$

x_i is the i^{th} column right eigenvector which corresponding to eigenvalue λ_i.

Singular value decomposition takes a rectangular matrix (defined as A, where A is a n x p matrix). The SVD theorem states:

$$A_{n\times p} = U_{n\times n} S_{n\times p} V^T_{p\times p} \tag{D.5}$$

Where

$$\begin{aligned} U^T U &= I_{n\times n} \\ V^T V &= I_{p\times p} \end{aligned} \tag{D.6}$$

Where the columns of U are the left singular vectors; S (the same dimensions as A) has singular values; and V^T has rows that are the right singular vectors.

The singular values are always real numbers. If the matrix A is a real matrix, then U and V are also real.

Appendix E

Multilayer Percetron Networks

This appendix provides a basic concept of Multilayer Percetron Networks which is applied in this report [81].

E.1 Model

Among the numerous artificial neural networks which have been proposed recently, the most widely used type of neural network is the Multilayer Perceptron (MLP) Networks, also known as the multilayer feed-forward network. This type of network consists of the input, the hidden, and the output layers of neurons. A circle represents a neuron. The line between two neurons represents the weight relationships. The output layer is compared to a target teacher and the error of them is applied in a backpropagation process to adjust the weights. The graphical composition of the neural network is shown in Figure E.1.

Each neuron performs two computations shown in Figure E.2: one is the weighted

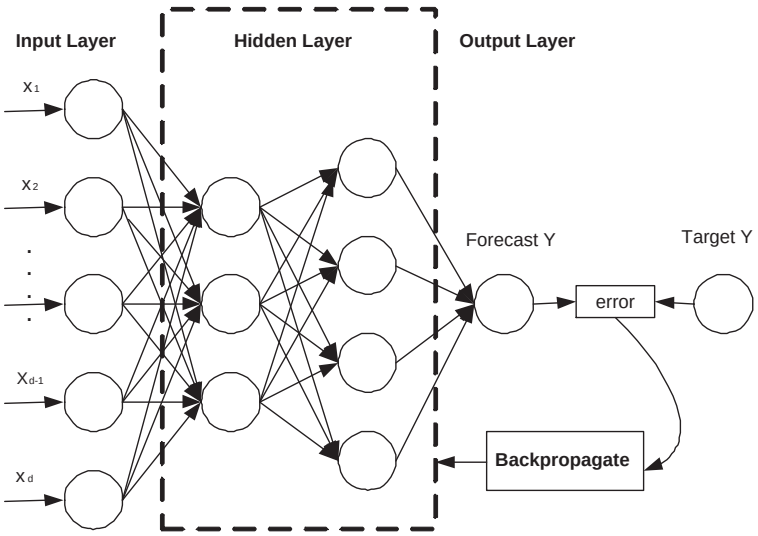

Figure E.1: Multilayer Neural Network Architecture

sum of its inputs which can be expressed as

$$net_j = \sum_{i=1}^{d} x_i w_{ji} + w_{j0} \tag{E.1}$$

where the subscript i indexes units on the input layer or the upstream hidden layer, j for the downstream successive hidden layer; w_{ji} denotes the weights at the hidden unit j from input-to-hidden layer or up-level hidden layer to down-level hidden layer. $w0$ is a single bias unit.

The other computation neuron performs, emitting an output that is a nonlinear function of its activation, $f(net)$ as equation (E.2), where y_j denotes the output layer or the downstream successive hidden layer j.

$$y_j = f(net_j) \tag{E.2}$$

The widely used activation function $f(net)$ which is also applied in this thesis is

Sigmoidal function. It is given as

$$y_j = \frac{1}{1 + e^{-net_j}} \tag{E.3}$$

where y_i is the output of the neuron and v_j is the weighted sum of all inputs and the bias of neuron j.

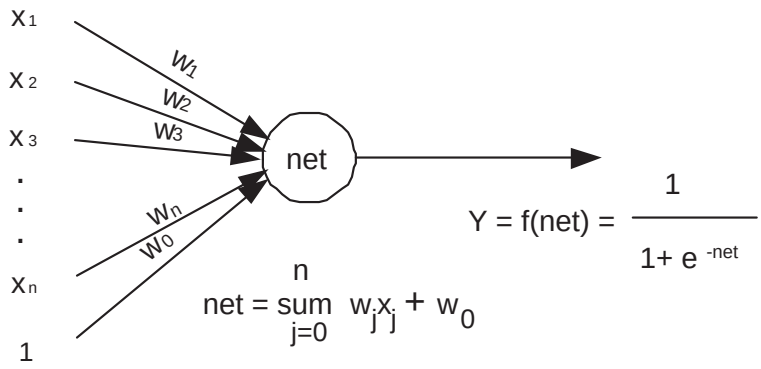

Figure E.2: Two computational steps in each neuron

E.2 Learning

A neural network learns about its objects through an iterative variation of connection weights based on training patterns and desired output. Learning will be based on the definition of a suitable error function, which is then minimized with respect to the weights and biases. Usually a backpropagation algorithm is one of the simplest and most general methods for evaluating the error function.

The back-propagation learning consists of a forward and a backward pass through the different layers of the network. The algorithm is represented in the following steps:

1. Initialize the weights in the network (often randomly)

2. Begin an iterative process

   for each example set e in the training data

   - forward pass
     - Y = activation function is applied to the network, layer by layer, until an output is produced in the network
     - T = desired response or target output for e
     - Calculate training error $J = 1/2(T - Y)^2$ at the output units
   - backward pass
     - Compute Δw for all weights from hidden layer based on gradient descent $\Delta w = -\eta \frac{\partial J}{\partial w}$. Coefficient η is the learning rate; it affects network teaching speed.
     - Update the weights in the network $w' = w + \Delta w$

   end

3. Repeat until all examples are trained correctly or criteria to stop the program are satisfied

References

[1] U.S.-Canada Power System Outage Task Force, "Final Report on the August 14, 2003 Blackout in the United States and Canada: Causes and Recommendations", April 2004.

[2] Carson W. Taylor, *Power System Voltage Stability*, Mcgraw-Hill (Tx), 1993.

[3] G. Andersson, P. Donalek, R. Farmer, N. Hatziargyriou, I. Kamwa, P. Kundur, N. Martins, J. Paserba, P. Pourbeik, J. Sanchez-Gasca, R. Schulz, A. Stankovic, C. Taylor, and V. Vittal, "Causes of the 2003 Major Grid Blackouts in North America and Europe, and Recommended Means to Improve System Dynamic Performance", *IEEE Transactions on Power Systems*, vol. 20, no. 4, pp. 1922–1928, November 2005.

[4] D.N. Kosterev, C.W. Taylor, and W.A. Mittelstadt, "Model validation for the August 10, 1996 WSCC system outage", *IEEE Transactions on Power Systems*, vol. 14, no. 3, pp. 967–979, August 1999.

[5] Working Group 01 of Advisory Group 6 of Study Committee C4, "Review of On-line Dynamic Security Assessment Tools and Techniques", *CIGRE Technical Brochure No. 325*, December 2006.

[6] Michele Di Santo, Alfredo Vaccaro, Domenico Villacci, and Eugenio Zimeo, "A Distribuited Architecture for Online Power Systems Security Analysis", *IEEE Transactions on Industrical Electronics*, vol. 51, no. 6, pp. 1238–1248, December 2004.

[7] N. Balu, T. Bertram, A. Bose, V. Brandwajn, G. Cauley, D. Curtice, A. Fouad, L. Fink, M.G. Lauby, B.F. Wollenberg, and J.N. Wrubel, "On-line Power System

Security Analysis", Proceedings of the IEEE, Feburary 1992, vol. 80, pp. 262–282.

[8] T. E. DyLiacco, "The Adaptive Realiability Control Systems", *IEEE Transactions on Power Appratus and Systems*, vol. 86, pp. 517–531, May 1967.

[9] L. H. Fink and K. Carlsen, "Operating Under Stress and Strain", IEEE spectrum, March 1978, vol. 15, pp. 48–53.

[10] P. Kundur, *Power System Stability and Control*, McGrew-Hill Inc., 1994.

[11] P. Kundur, J. Paserba, V. Ajjarapu, G. Andersson, A. Bose, C. Canizares, N. Hatziargyriou, D. Hill, A. Stankovic, C. Taylor, T. Van Cutsem, and V. Vittal, "Definition and Classification of Power System Stability", *IEEE Transactions on Power Systems*, vol. 19, no. 2, pp. 1387–1401, May 2004.

[12] Thierry Van Cutsem and Costas Vournas, *Voltage Stability of Electric Power Systems*, Kluwer Academic Publishers, 1998.

[13] Jan Machowski, Janusz W. Bialek, and James R. Bumby, *Power System Dynamics: Stability and Control*, John Wiley and Sons, Ltd, 2008.

[14] Wikipedia, *Computational Intelligence*, Wikimedia Foundation, Inc, July, 2009.

[15] David B. Fogel, *Evolutionary Computation: Toward a New Philosophy of Machine Intelligence*, Wiley-IEEE Press, December, 2005.

[16] Russell C. Eberhart and Yuhui Shi, *Computational Intelligence: Concepts to Implementations*, Morgan Kaufmann, August, 2007.

[17] Narendranath Udapa A., D. Thukaram, and K. Parthasarathy, "An ANN Based Approach for Voltage Stability Assessment", International Conf. on Computer Applications in Electrical Engineering, September 1997, vol. 8, pp. 666–670.

[18] Nitin Malik, "Artificial Neural Networks and Their Applications", National Conference on Unearthing Technological Developments & their Transfer for Serving Masses, April 2005, pp. 17–18.

[19] G. Peter Zhang, *Neural Networks in Business Forecasting*, Idea Group Inc, 2003.

[20] Vidya Sagar, S. Vankayala, and Nutakki D. Rao, "Artificial Neural Networks and Their Applications to Power Systems- A Bibliographical Survey", Electrical Power Systems Research, 1993, vol. 28, pp. 66–67.

[21] J. Kennedy and R.C. Eberhart, "Particle Swarm Optimization", IEEE Proceedings International Conference on Neural Networks, November 1995, vol. 4, pp. 1942–1948.

[22] Yamille del Valle, Ganesh Kumar Venayagamoorthy, Salman Mohagheghi, Jean-Carlos Hernandez, and Ronald G. Harley, "Particle Swarm Optimization: Basic Concepts, Variants and Applications in Power Systems", *IEEE Transactions on Evolutionary Computation*, vol. 12, no. 2, pp. 171–195, April 2008.

[23] Zhihong Yu, Xiaoxin Zhou, and Zhongxi Wu, "Design of a Fast Transient Stability Control Scheme in Power System", IEEE Power Engineering Society General Meeting, 2006, pp. 8–15.

[24] G.K. Venayagamoorthy and S. Ray, "A Neural Network Based Optimal Wide Area Control Scheme for A Power System", Industry Applications Conference, Fourtieth IAS Annual Meeting, October 2005, vol. 1, pp. 700–706.

[25] Hui Ni, G.T. Heydt, and L. Mili, "Power System Stability Agents Using Robust Wide Area Control", *IEEE Transactions on Power Systems*, vol. 17, no. 4, pp. 1123–1131, November 2002.

[26] K. Srivastava T. Jonsson P. Holmberg Jiuping Pan, R. Nuqui and Y.-J. Hafner, "Ac grid with embedded vsc-hvdc for secure and efficient power delivery", IEEE Energy 2030 Conference, ENERGY 2008, November 2008, pp. 1–6.

[27] J. Bertsch, C. Carnal, D. Karlson, J. McDaniel, and K. Vu, "Wide-Area Protection and Power System Utilization", *Proceedings of the IEEE*, vol. 93, no. 5, pp. 997–1003, May 2005.

[28] R.F. Nuqui, A.G. Phadke, R.P. Schulz, , and N. Bhatt, "Fast On-line Voltage Security Monitoring Using Synchronized Phasor Measurements and Decision Trees", 2001, vol. 3.

[29] G. Benmouyal, E.O. Schweitzer, and A. Guzman, "Synchronized Phasor Measurement in Protective Relays for Protection", 29^{th} Annual Western Protective Relay Conference, Washinton, USA, October 2002.

[30] Powertech Labs Inc., *Voltage Security Assessment Tool (VSAT) User Manual*, April, 2008.

[31] Hsiao-Dong Chiang, A.J. Flueck, K.S. Shah, and N. Balu, "CPFLOW: A Practical Tool for Tracing Power System Steady-state Stationary Behavior due to Load and Generation Variations", *IEEE Transactions on Power Systems*, vol. 10, no. 2, pp. 623–634, May 1995.

[32] T. Van Cutsem and C.D. Vournas, "Voltage Stability Analysis in Transient and Midterm Time Scales", *IEEE Transactions on Power Systems*, vol. 11, pp. 146–154, 1996.

[33] Power Technologies Inc., *Online Documentation PSS/E-28*, November, 2001.

[34] Powertech Labs Inc., *Transient Security Assessment Tool (TSAT) User Manual*, April, 2008.

[35] V. Ajjarapu and C. Christy, "The Continuation Power Flow: A Tool for Steady State Voltage Stability Analysis", *IEEE Transactions on Power Systems*, vol. 7, no. 1, pp. 416–423, February 1992.

[36] IEEE Power Engineering Society, *Voltage Stability Assessment: Concepts, Practices and Tools*, Power System Stability Subcommittee Special Publication, Product number: SP101PSS, ISDN:0780378695.

[37] P-A Lof, G Andersson, and D. J. Hill, "Voltage Stability Indices for Stressed Power Systems", *IEEE Transactions on Power Systems*, vol. 8, no. 1, pp. 326–335, February 1993.

[38] P-A. Lof, T. Smed, G. Andersson, and D.J. Hill, "Fast Calculation of a Voltage Stability Index", *IEEE Transactions on Power Systems*, vol. 7, no. 1, pp. 54–64, February 1992.

[39] E.H. Abed, J.C. Alexander, H. Wang, A.M.A. Hamdan, and H.C. Lee, "Dynamic Bifurcations in a Power System Model Exhibiting Voltage Collapse", IEEE International Symposium on Circuits and Systems, ISCAS '92 Proceedings, May 1992, vol. 5, pp. 2509–2512.

[40] R.J. Avalos, C.A. Canizares, F. Milano, and A.J. Conejo, "Equivalency of Continuation and Optimization Methods to Determine Saddle-Node and Limit-Induced Bifurcations in Power Systems", *IEEE Transactions on Circuits and Systems I: Regular Papers*, vol. 56, no. 1, pp. 210–223, January 2009.

[41] A.C.Z. de Souza, C.A. Canizaresa, and V.H. Quintana, "New Techniques to Speed Up Voltage Collapse Computations Using Tangent Vectors", *IEEE Transactions on Power Systems*, vol. 12, no. 3, pp. 1380–1387, August 1997.

[42] S. Greene, I. Dobson, and F.L. Alvarado, "Sensitivity of the Loading Margin to Voltage Collapse With Respect to Arbitrary Parameters", *IEEE Transactions on Power Systems*, vol. 12, no. 1, pp. 262–272, February 1997.

[43] A. Berizzi, P. Finazzi, D. Dosi, P. Marannino, and S. Corsi, "First and Second Order Methods for Voltage Collapse Assessment and Security Enhancement", *IEEE Transactions on Power Systems*, vol. 13, no. 2, pp. 543–551, May 1998.

[44] C.L. DeMarco and C.A. Canizares, "A Vector Energy Function Approach for Security Analysis of AC/DC Systems", *IEEE Transactions on Power Systems*, vol. 7, no. 3, pp. 1001–1011, August 1992.

[45] B. Gao, G. K. Morrison, and P. Kundur, "Voltage Stability Evaluation Using Modal Analysis", *IEEE Transactions on Power Systems*, vol. 7, no. 4, pp. 1529–1542, November 1992.

[46] P. Kessel and H. Glavitsch, "Estimating the Voltage Stability of a Power System", *IEEE Transactions on Power Delivery*, vol. 1, no. 3, pp. 346–354, July 1986.

[47] Badrul H. Chowdhury and Carson W. Taylor, "Voltage Stability Analysis: VQ Power Flow Simulation Versus Dynamic Simulation", *IEEE Transactions on Power System*, vol. 15, no. 4, pp. 1354–1359, November 2000.

[48] Enrico De Tuglie, Maria Dicorato, Massimo La Scala, and Pierangelo Scarpellini, "A Static Optimization Approach to Assess Dynamic Available Transfer Capability", *IEEE Transactions on Power System*, vol. 15, no. 3, pp. 1069–1076, August 2000.

[49] V. Ajjarapu, *Computational Techniques for Voltage Stability Assessment and Control*, Springer US, 2007.

[50] Powertech Labs Inc., *Powerflow and Short-circuit Analysis Tool (PSAT) User Manual*, April, 2008.

[51] Shan Jiang, U.D. Annakkage, and A.M. Gole, "A Platform for Validation of FACTS Models", *IEEE Transactions on Power Delivery*, vol. 21, no. 1, pp. 484–491, January 2006.

[52] A. Sittithumwat and K. Tomsovic, "Dynamic Security Margin Estimation Using Artificial Neural Networks", Power Engineering Society Summer Meeting, July 2002, vol. 3, pp. 25–25.

[53] P. Devijver and J. Kitler, *Pattern Recognition: A Statistical Approach*, Prentice Hall, 1982.

[54] Christopher M. Bishop, *Neural Networks for Pattern Recognition*, Oxford University Press, USA, January, 1996.

[55] Bathiya Jayasekara, *Determination of Transient Stability Boundary in Functional Form with Applications in Optimal Power Flow and Security Control*, PhD thesis, University of Manitoba, 2006.

[56] V.R. Dinavahi and S.C. Srivastava, "ANN Based Voltage Stability Margin Prediction", IEEE Power Engineering Society Summer Meeting, July 2001, vol. 2, pp. 1275–1280.

[57] S. Kamalasadan, A.K. Srivastava, and D. Thukaram, "Novel Algorithm For Online Voltage Stability Assessment Based On Feed Forward Neural Network", IEEE Power Engineering Society General Meeting, 18-22 June 2006.

[58] P.J. Abrao, A.P. Alves da Silva, and A.C. Zambroni de Souza, "Rule Extraction From Artificial Neural Networks For Voltage Security Analysis", Neural Networks, 2002. IJCNN '02. Proceedings of the 2002 International Joint Conference, 12-17 May 2002, vol. 3, pp. 2126–2131.

[59] T.M.L. Assis, A.R. Nunes, and D.M. Falcao, "Mid and Long-Term Voltage Stability Assessment using Neural Networks and Quasi-Steady-State Simulation", Power Engineering, 2007 Large Engineering Systems Conference, 10-12 October 2007, pp. 213–217.

[60] A.A. El-Keib and X. Ma, "Application of Artificial Neural Networks in Voltage Stability Assessment", *IEEE Transactions on Power Systems*, vol. 10, no. 4, pp. 1890–1896, November 1995.

[61] B. Jeyasurya, "Artificial Neural Networks For On-line Voltage Stability Assessment", Power Engineering Society Summer Meeting, 16-20 July 2000, vol. 4, pp. 2014–2018.

[62] Randall Matignon, *Neural Network Modeling Using SAS Enterprise Miner*, AuthorHouse, 2005.

[63] The Math Works Inc., *Neural network toolbox user's guide*, Natick, Massachusetts, MATLAB, 2006.

[64] IEEE Std C37.118-2005, *IEEE Standard for Synchrophasors for Power Systems*, 2005.

[65] S. Piramuthu, "Evaluating Feature Selection Methods for Learning in Data Mining Applications", Proceedings of the Thirty-First Hawaii International Conference on System Sciences, January 1998, vol. 5, pp. 294–301.

[66] Robi Polikar, *Pattern Recognition*, Rowan University, Glassboro, New Jersey, Wiley Encyclopedia of Biomedical Engineering, John Wiley and Sons, Inc., 2006.

[67] S. Chakrabarti and B. Jeyasurya, "On-line Voltage Stability Monitoring Using Artificial Neural Network", Power Engineering, LESCOPE-04. Large Engineering systems Conference, July 2004, pp. 71–75.

[68] Mani Venketasubramanian and Kevin Tomsovic, *The Electrical Engineering handbook Chapter 8*, School and Electrical Engineering and Computer Science, Washington State University, Pullman, Washington, USA, 2005.

[69] D.J. Shoup, J.J. Paserba, and C.W. Taylor, "A survey of current practices for transient voltage dip/sag criteria related to power system stability", Power Systems Conference and Exposition, IEEE PES 10-13, October 2004, vol. 2, pp. 1140–1147.

[70] NERC/WECC, *Planning Standards*, April, 2003.

[71] IEEE Task Force, "Load Representation for Dynamic Performance Analysis [of Power Systems]", *IEEE Transactions on Power Systems*, vol. 8, no. 2, pp. 472–482, May 1993.

[72] Carson W. Taylor, "Concepts of Undervoltage Load Shedding for Voltage Stability", *IEEE Transactions on Power Delivery*, vol. 7, no. 2, pp. 480–488, April 1992.

[73] A. Saffarian, M. Sanaye-pasand, and H. Asadi, "Performance Investigation of New Combinational Load Shedding Schemes", IEEE Joint International Conference on Power System Technology, October 2008, pp. 1–8.

[74] L.A. Finley, T.R. Standish, and R.C. Phillips, "Optimizing System Performance Through Dynamic Load Shed Scheduling", *IEEE Transactions on Power Apparatus and Systems*, vol. PAS-104, no. 6, pp. 1286–1289, June 1985.

[75] Xu Fu and Xifan Wang, "Load Shedding Scheme Ensuring Voltage Stability", IEEE Power Engineering Society General Meeting, June 2007, pp. 1–6.

[76] T. Van Cutsem, C. Moors, and D. Lefebvre, "Design of Load Shedding Schemes Against Voltage Instability Using Combinatorial Optimization", IEEE Power Engineering Society Winter Meeting, January 2002, vol. 2, pp. 848–853.

[77] C. Moors, D. Lefebvre, and T. Van Cutsem, "Design of load shedding schemes against voltage instability", IEEE Power Engineering Society Winter Meeting, January 2000, vol. 2, pp. 1495–1500.

[78] S. Shah and S. M. Shahidehpour, "A Heuristic Approach To Load Shedding Scheme", *IEEE Transactions on Power Systems*, vol. 4, no. 4, pp. 1421–1429, October 1989.

[79] B. Zhao, C.X. Guo, and Y.J. Cao, "A multiagent-based particle swarm optimization approach for optimal reactive power dispatch", *IEEE Transactions on Power Systems*, vol. 20, no. 2, pp. 1070–1078, May 2005.

[80] M. A. Pai, *Energy Function Analysis for Power System Stability*, Kluwer Academic Publishers, Boston, 1989.

[81] Simon Haykin, *Neural Networks: A Comprehensive Foundation*, Prentice Hall, Upper Saddle River, N.J, 1999.